



Title	RESONANCE RAMAN INVESTIGATIONS OF THE OXYGEN BINDING SITES IN HEMOPROTEINS WITH CARBON MONOXIDE AS A PROBE
Author(s)	Tsubaki, Motonari
Citation	大阪大学, 1985, 博士論文
Version Type	VoR
URL	https://hdl.handle.net/11094/27676
rights	
Note	

The University of Osaka Institutional Knowledge Archive : OUKA

<https://ir.library.osaka-u.ac.jp/>

The University of Osaka

RESONANCE RAMAN INVESTIGATIONS OF THE OXYGEN BINDING SITES IN
HEMOPROTEINS WITH CARBON MONOXIDE AS A PROBE

MOTONARI TSUBAKI

Department of Biochemistry, Kagawa Medical School, Miki-cho, Kita-gun,
Kagawa 761-07, Japan

RESONANCE RAMAN INVESTIGATIONS OF THE OXYGEN BINDING SITES IN
HEMOPROTEINS WITH CARBON MONOXIDE AS A PROBE

MOTONARI TSUBAKI

Department of Biochemistry, Kagawa Medical School, Miki-cho, Kita-gun,
Kagawa 761-07, Japan

CONTENTS

Part A. Theoretical and Experimental Backgrounds	5
0. General Introduction and Scope of the Study	5
I. Theoretical Basis of Raman Effect	7
1. Physical Description	7
2. Isotopic Substitution	10
3. Quantum Mechanical Description	11
4. Resonance Raman Theory	16
II. Mechanism of Resonance Raman Enhancement of Metalloporphyrins	20
1. Porphyrin In-Plane Enhancement	20
(a) B-band Scattering	20
(b) Q-band Scattering	21
2. Out-of-Plane Enhancement	23
(a) Porphyrin Out-of-Plane Deformation Modes	23
(b) Axial-Ligand Modes	25
i) $\pi - \pi^*$ Resonance	25
ii) Charge-Transfer Resonance	32
Porphyrin - M Charge-Transfer	32
Ligand - M Charge-Transfer	35
References	40
Part B. Resonance Raman Investigation of Carbon Monoxide Bonding in	
HbCO and MbCO	47
0. Introduction	47

I. Experimental	49
1. Preparation of Proteins	49
2. Preparation of Carbon Monoxide Derivatives	50
3. Measurement of Raman Spectra	50
II. Results	51
1. High-Frequency Region Spectra	51
2. Detection of Bound C-O Stretch	52
3. Detection of Fe-CO Stretch and Fe-C-O Bending Frequencies	53
4. Quaternary Structure Change	56
III. Discussion	58
1. Porphyrin Ring Vibrations	58
2. Fe-CO Stretching Vibration	59
3. Fe-C-O Bending Vibration	61
4. Carp HbCO and Quaternary Structure Change	62
References	65
 Part C. Resonance Raman Detection of a $\nu(\text{Fe-CO})$ Stretching Frequency in Cytochrome P-450 _{scc}	 69
0. Introduction	69
I. Experimental	70
1. Preparation of Cytochrome P-450 _{scc}	70
2. Preparation of Carbon Monoxide Form of Cytochrome P-450 _{scc}	71
3. Measurement of Resonance Raman Spectra	72
II. Results	73
1. Detection of Bound C-O Stretch	73
2. Detection Bound Fe-CO Stretch	74

III. Discussion	74
1. Fe-CO Bonding Geometry	74
2. Effect of Cysteiny1 Axial Ligand on Fe-CO Stretch	77
References	81
 Part D. Effects of Cholesterol and Adrenodoxin on the Heme Moiety of Cytochrome P-450 _{scc} : A Resonance Raman Study	 84
0. Introduction	85
I. Experimental	86
1. Purification of Cytochrome P-450 _{scc}	86
2. Depletion of Emulgen 913 from the Purified Cytochrome P-450 _{scc}	88
3. Measurements of Optical Absorption Spectra	88
4. Measurement of Resonance Raman Spectra	89
II. Results	89
1. Oxidized Form	89
2. Carbon Monoxide Reduced Form and Its Conversion to P-420 Form in the Absence of Cholesterol	92
3. Effects of Cholesterol and Adrenodoxin on the CO-Reduced Form	94
III. Discussion	95
1. Oxidized Form	95
2. CO-Reduced Form	98
References	102
 Conclusions	 105
Acknowledgements	108

Part A. Theoretical and Experimental Background

0. General Introduction and Scope of the Study

The Raman effect is a consequence of inelastic scattering of light by a material molecule. The difference in energy between the incident and Raman scattered photons corresponds to the energy difference between the initial and final states of the scattering molecule. Although the effect is named after Sir. C.V. Raman who observed inelastic light scattering from liquids in 1928 (1,2), the Raman effect was observed almost simultaneously by Landsberg and Mandelstam in the U.S.S.R. in their studies of light scattering from quartz (1,3). However the possibility of inelastic light scattering was envisaged earlier in 1923 by Smekal (1).

The application of Raman spectroscopy to biological compounds is quite recent. Its progress, however, has been remarkable. Because of its potential applicability to biological problems, Raman spectroscopy is becoming a more common tool in biological research (4,5).

The introduction of laser light source has made possible the systematic study of the resonance Raman effect (6), in which Raman bands associated with vibrational modes that lead to excited-state distortions are enhanced, as the laser frequency approaches the electronic transition frequency(7). Resonance enhancement permits examination of the vibrational modes of the chromophores in a sample, unobscured by the vibrational modes of the molecular matrix. It provides a means of selecting out specific chemical groups by tuning the laser light to their electronic transition.

Porphyrins (or hemes) are attractive targets for resonance Raman spectroscopy, because of their intense absorption bands in the visible and near ultraviolet regions (see reviews such as 8-12). Indeed resonance Raman spectra were first reported for hemoglobin, a decade ago (13-15). In the resonance Raman spectra of hemoglobin excited in the visible electronic transitions of the heme, only the porphyrin macrocycle modes are enhanced and protein modes do not appear.

Carbon monoxide, a competitive inhibitor for oxygen-binding hemoproteins, binds to ferrous heme iron in very high affinity and is an useful probe for the environment around the distal site of the heme (via infrared and ^{13}C -NMR spectroscopies). However, the application of resonance Raman spectroscopy to carbonmonoxy form of these hemoproteins has been limited to pulse laser transient kinetic studies, because carbon monoxide dissociates from the heme iron easily upon illumination of laser light, generating deoxy species which interfere with the observation of signals from unphotolyzed complexes.

In this paper, a successful application of resonance Raman spectroscopy to the studies of various oxygen binding hemoproteins, such as hemoglobin, myoglobin, and cytochrome P-450_{sc}, using carbon monoxide as a probe for heme environment, are described. This paper consist of four parts. In part A, theoretical background for an understanding of Raman, particularly resonance Raman, effect is given. A brief survey of earlier experimental results concerning hemoproteins and their model complexes obtained by resonance Raman spectroscopy are, also, included in this part. In part B, a first succesful application of resonance Raman spectroscopy to study carbon monoxide bonding in HbCO and MbCO is presented. The results obtained were applicable to study the heme

environment of an unique hemoprotein, cytochrome P-450, in carbon monoxide-bound form. The results are described in parts C and D.

I. Theoretical Basis of Raman Effect

1. Physical Description

For vibrational Raman scattering the difference between the energy of the incident and scattered photons corresponds to the energy of a vibrational transition of the molecule. The energy and polarization differences between the Raman scattered and incident photons depend on the internal dynamic structure of the molecule. Thus, studies of the Raman spectra of molecules give informations on the vibrational modes, electronic structure and chemical environment of the molecule. The physical interpretation of Raman spectra requires an understanding of the interactions of the incident photon with the electronic and vibrational states of the molecule.

A simple physical picture of the Raman effect is visualized in Fig. A-1. An electromagnetic wave of frequency ν_0 is incident on a molecule. The oscillating electromagnetic field drives the electrons of the molecule at the incident frequency ν_0 with an amplitude which is a function of the molecular polarizability. Since the polarizability is a function of the nuclear coordinates of the molecule, nuclear vibrations modulate the polarizability with the frequency ν_v , the frequency of vibration of the nuclei. The oscillating electron cloud of the molecule is manifested as an oscillating dipole moment which becomes new source for emitting lights with frequency ν_0 (Rayleigh scattering), $\nu_0 + \nu_v$ (Anti-Stokes Raman scattering) and $\nu_0 - \nu_v$ (Stokes Raman scattering). The picture can be visualized more quantitatively by

examining the dipole moment induced in a molecule by an electromagnetic field (16).

$$\mu = \alpha E_0 \cos 2\pi\nu_0 t \quad (1)$$

where μ , the induced dipole moment, is proportional to the polarizability of the molecule, α , and to the amplitude of the electric field, E_0 , which oscillates with frequency ν_0 . The polarizability varies with the configuration of the nuclei which has a vibrational mode of frequency ν_v . For a molecule containing N atoms, there are $3N$ degrees of freedom available to the nuclei. Of these, $3N-6$ ($3N-5$ for a linear molecule) result in vibrations of the molecule. In general the vibrational motion is quite complicated. However, by using group theory it is possible to reduce this complicated vibrational motion to a set of independent normal modes of vibration. The polarizability may be expanded as a Taylor series based on the equilibrium internuclear configuration,

$$\alpha = \alpha_0 + \left(\frac{\partial \alpha_0}{\partial Q} \right)_0 Q + \dots \quad (2)$$

where Q is the normal coordinate of the vibration. For a diatomic molecule

$$Q_0 = A \cos 2\pi\nu_v t$$

where A is the amplitude of vibration. Defining $A \left(\frac{\partial \alpha_0}{\partial Q} \right)_0$ as α_1 and substitution in Eq. (1).

$$\mu = \alpha_0 E_0 \cos 2\pi\nu_0 t + \alpha_1 E_0 \cos 2\pi\nu_0 t \cos 2\pi\nu_V t \quad (3)$$

An oscillating dipole moment radiates light with intensity, I, (2,16).

$$I = \frac{16 \pi^2 \nu^4}{3c^2} \mu^2 \quad (4)$$

Substituting Eq. (3) into Eq. (4) and using a trigonometric identity yields:

$$I = \frac{16 \pi^2}{3c^3} \left(\nu_0^4 \alpha_0^2 E_0^2 \cos^2 2\pi \nu_0 t + \right. \\ \left. (\nu_0 + \nu_V)^4 \alpha_1^2 E_0^2 \cos^2 2\pi (\nu_0 + \nu_V) t + \right. \\ \left. (\nu_0 - \nu_V)^4 \alpha_1^2 E_0^2 \cos^2 2\pi (\nu_0 - \nu_V) t + \right. \\ \left. \text{cross terms} \right) \quad (5)$$

A number of features are evident from Eq. (5). The intensity, I, is proportional to the fourth power of the radiated frequency. Thus, for example, the scattering efficiency for 300 nm light is 16 times as high as for 600 nm light.

The first term in Eq. (5) represents elastic (i.e. Rayleigh) scattering, because the frequency radiated is ν_0 . The second and third terms are responsible for the Anti-Stokes and Stokes Raman scattering, because the frequency radiated is $\nu_0 + \nu_V$ and $\nu_0 - \nu_V$, respectively. The cross terms can be neglected since the power they propagate integrates to zero (16).

2. Isotopic Substitution

Isotopic substitution is a very useful aid in the analysis of particular vibrational modes. By making the assumption, which is generally valid, that the force constants (or bond strength) are unaffected by isotopic substitution, the shift in observed frequency can be attributed principally to mass effects. Then, by identifying a band(s) which show a shift(s) and by measuring the extent of the shift upon isotopic replacement it is often possible to gain insight into the contribution of the substituted atom in the normal mode appearing in the spectrum. Vibrations which involve large amplitude of the replaced atom should show frequency shifts appreciably, and the larger the isotopic mass difference is, the greater the frequency shift will be.

For a diatomic molecule, vibration frequency is given by the equation:

$$\nu = \frac{1}{2\pi} \left[k \left(\frac{m_A + m_B}{m_A m_B} \right) \right]^{\frac{1}{2}} = \frac{1}{2\pi} \left(\frac{k}{\mu} \right)^{\frac{1}{2}} \quad (6)$$

where m_A and m_B refer to the masses of a and b, respectively; k is the force constant; and μ is the reduced mass equal to $m_A m_B / (m_A + m_B)$ for the diatomic molecule. Let's assume the hydrogen atom in C-H is replaced with deuterium, giving C-D. The atomic weights are C, 12; H, 1; and D, 2. Thus the ratio of frequency is

$$\begin{aligned}\nu_{C-H} / \nu_{C-D} &= \sqrt{\mu_{C-D} / \mu_{C-H}} \\ &= \sqrt{\frac{C \cdot D}{C + D} \cdot \frac{C + H}{C \cdot H}} \\ &= 1.3628\end{aligned}$$

Since ν_{C-H} for alkane chain occurs near 2900 cm^{-1} , we can predict that ν_{C-D} will appear near 2100 cm^{-1} . This is in fact where the C-D stretch is observed. Usually, the treatment of a pair of neighboring atoms in a molecule as a diatomic oscillator is a gross oversimplification, but it works well in the case of the C-H stretch.

3. Quantum Mechanical Description

Although the classical description of Raman scattering is useful for a physical insight into the Raman effect, the magnitude of α_0 and α_1 and, more important, the interaction of the electronic and vibrational states of the molecule are not detailed. A quantum mechanical approach is necessary to describe the states of the molecule, the interaction between the vibrational and electronic states and the interaction between the photon and the molecule.

The interaction between the photon and the electronic and vibrational states of the molecule is manifested in the elements of the polarizability tensor. Using time-dependent perturbation theory of the

interaction of radiation and matter, the polarizability ($\alpha_{\rho\sigma}$, which denotes a $\rho\sigma$ component of polarizability tensor) can be shown to be (2):

$$(\alpha_{\rho\sigma})_{mn} = \sum_e \left[\frac{\langle n | R_\rho | e \rangle \langle e | R_\sigma | m \rangle}{E_e - E_m - E_0} + \frac{\langle m | R_\sigma | e \rangle \langle e | R_\rho | n \rangle}{E_e - E_n + E_0} \right] \quad (7)$$

where the summation is over all of the vibronic states $|e\rangle$ of the molecule, R_σ and R_ρ are the dipole moment operators along σ and ρ .

E_e , E_m and E_n are the energies of the states $|e\rangle$ (excited state), $|m\rangle$ (initial state) and $|n\rangle$ (final state) and E_0 is the energy of the incident photon. The state functions of the molecule may be separated into electronic and vibrational parts using the Born-Oppenheimer approximation (17).

$$\begin{aligned} \psi_g &= \theta_g(\xi, Q) \Phi_i^g(Q) = |g\rangle |i\rangle \\ \psi_e &= \theta_e(\xi, Q) \Phi_v^e(Q) = |e\rangle |v\rangle \end{aligned} \quad (8)$$

where $\theta_g(\xi, Q)$ is the electronic wave function for the state $|g\rangle$ and is a function of the electronic coordinates, ξ , and nuclear coordinates Q . $\Phi_i^g(Q) = |i\rangle$ is the i 'th vibrational state wave function of the ground electronic state and is a function of the nuclear coordinates. $|e\rangle$ is an excited electronic state and $|v\rangle$ is v 'th vibrational state wave function of the excited electronic state $|e\rangle$.

Eq. (7) may be modified to:

$$(\alpha_{pr})_{gi,jj} = \sum_{ev} \left[\frac{\langle j || (g | R_p | e) || v \rangle \langle v || (e | R_r | g) || i \rangle}{E_{ev} - E_{gi} - E_0} + \frac{\langle i || (g | R_r | e) || v \rangle \langle v || (e | R_p | g) || j \rangle}{E_{ev} - E_{gj} + E_0} \right] \quad (9)$$

where each of the matrix elements $(g | R_r | e)$ represent the electronic transition moment at a particular nuclear configuration Q , and $|j\rangle$ is a vibrational state function of the ground electronic state. Eq. (9) is an expression for the Raman tensor for the vibrational transition $i - j$. For incident light of energy E_0 the energy of the Raman scattered light is $E_0 - (E_{gj} - E_{gi})$.

However, the Born-Oppenheimer stationary electronic states of the system are perturbed by vibrations of the nuclei. The perturbation operator is (17):

$$h_a = \left(\frac{\partial \mathcal{H}}{\partial Q_a} \right)^0 \Delta Q_a \quad (10)$$

where \mathcal{H} is the electronic Hamiltonian, and ΔQ_a is the displacement of the normal mode, a . The superscript 0 indicates that the expression is evaluated at the equilibrium nuclear configuration. Using first order perturbation theory for small coordinate displacement on the Born-Oppenheimer excited state, $|e\rangle$ and ground state $|g\rangle$ (Herzberg-Teller expansion):

$$|e\rangle = |e^0\rangle + \sum_a \sum_{s \neq e} \frac{\langle s | h_a | e^0 \rangle \Delta Q_a}{E_e^0 - E_s^0} |s^0\rangle \quad (11a)$$

$$|g\rangle = |g^0\rangle + \sum_a \sum_{t \neq g} \frac{\langle t | h_a | g^0 \rangle \Delta Q_a}{E_g^0 - E_t^0} |t^0\rangle \quad (11b)$$

in which the summations are over all of the vibrational modes, a . The effect of the vibrational perturbation operator is to create a new basis set of wavefunctions which are linear combinations of the original Born-Oppenheimer states. The summation over electronic states is labeled by s in Eq. (11a) and labeled by t in Eq. (11b). The summation over s and t each span the entire basis set except for the diagonal components ($|s\rangle \neq |e\rangle$ and $|t\rangle \neq |g\rangle$). The superscript o indicates wave functions and energies evaluated at the equilibrium nuclear configuration in the ground electronic state (18).

Combining Eqs. (9) and (11) and assuming the wave functions are real yields to the first order in Q_a (19):

$$(\alpha_{pr})_{gi, gj} = A + B + C$$

$$A = \sum_{e \neq g} \sum_v \left[\frac{(g^o | R_o | e^o)(e^o | R_p | g^o)}{E_{ev} - E_{gi} - E_o} + \frac{(g^o | R_p | e^o)(e^o | R_o | g^o)}{E_{ev} - E_{gj} + E_o} \right] \langle u || v \rangle \langle v || j \rangle$$

$$B = \sum_{e \neq g}' \sum_v \sum_{s \neq e}' \sum_a \left[\left\{ \frac{(g^o | R_o | e^o)(e^o | R_a | s^o)(s^o | R_p | g^o)}{E_{ev} - E_{gi} - E_o} + \frac{(g^o | R_p | e^o)(e^o | R_a | s^o)(s^o | R_o | g^o)}{E_{ev} - E_{gj} + E_o} \right\} \frac{\langle u || v \rangle \langle v || Q_{a || j} \rangle}{E_e^o - E_s^o} \right. \\ \left. + \left\{ \frac{(g^o | R_o | s^o)(s^o | R_a | e^o)(e^o | R_p | g^o)}{E_{ev} - E_{gi} - E_o} + \frac{(g^o | R_p | s^o)(s^o | R_a | e^o)(e^o | R_o | g^o)}{E_{ev} - E_{gj} + E_o} \right\} \frac{\langle u || Q_{a || v} \rangle \langle v || j \rangle}{E_e^o - E_s^o} \right]$$

$$C = \sum_{e \neq g}' \sum_{t \neq g}' \sum_v \sum_a \left[\left\{ \frac{(g^o | R_a | t^o)(t^o | R_o | e^o)(e^o | R_p | g^o)}{E_{ev} - E_{gi} - E_o} + \frac{(g^o | R_a | t^o)(t^o | R_p | e^o)(e^o | R_o | g^o)}{E_{ev} - E_{gj} + E_o} \right\} \frac{\langle u || v \rangle \langle v || Q_{a || j} \rangle}{E_g^o - E_t^o} \right. \\ \left. + \left\{ \frac{(g^o | R_o | e^o)(e^o | R_p | t^o)(t^o | R_a | g^o)}{E_{ev} - E_{gi} - E_o} + \frac{(g^o | R_p | e^o)(e^o | R_o | t^o)(t^o | R_a | g^o)}{E_{ev} - E_{gj} + E_o} \right\} \frac{\langle u || Q_{a || v} \rangle \langle v || j \rangle}{E_g^o - E_t^o} \right]$$

(12)

where $|i\rangle$ indicates the initial vibrational state, $|j\rangle$ the final vibrational state and $|v\rangle$ labels the vibrational sublevels of the intermediate electronic state.

Equation (12) expresses one of the theoretical formulations for Raman polarizability. It describes the intensity of Raman scattering when the energy of the incident photon is far from an electronic transition of the molecule (i.e., far from resonance).

A number of important features are evident from Eq. (12). Term A is responsible for Rayleigh scattering because of the Franck-Condon overlap factors $\sum_v \langle i|v\rangle \langle v|j\rangle = \delta_{ij}$. Thus, there are no allowed vibrational transitions. (However, a further expansion of the A term may lead to Raman intensity). Terms B and C give rise to Raman scattering via the vibrational terms

$$\sum_v \langle i|v\rangle \langle v|Q_a|j\rangle = \langle i|Q_a|j\rangle = \delta_{i,j\pm 1}$$

Thus, the selection rule is $j = i \pm 1$.

The C term results from the mixing of the ground state with excited electronic states of the molecule. In general, the difference in energy between the ground state and any excited state is greater than the difference in energy between adjacent excited states. As a result, the ratio of Raman intensities of the C term to the B term is

$$\frac{I_C}{I_B} \approx \left(\frac{E_e^0 - E_s^0}{E_t^0 - E_g^0} \right)^2 \ll 1$$

Thus the C term is in general less important in Raman scattering than the B term (17).

4. Resonance Raman Theory

As the energy of the incident photons approach an electronic transition, the denominator in Eq. (12) becomes smaller and Eq. (12) predicts an increase of Raman and Rayleigh scattering. However, when the resonance condition exists, Eq. (12) suggests that the intensity will increase without limit. This is neither physically reasonable nor experimentally observed (20). This failure of Raman theory in the resonance case results from the inability of perturbation theory to deal with such a large perturbation (2).

This dilemma is resolved phenomenologically by the addition of a damping correction, $i\Gamma$, to the energy denomination in Eq. (12). The result is (21)

$$\begin{aligned}
 (\alpha_{\rho\sigma})_{gi,jj} &= A' + B' \\
 A' &= \sum_v \frac{(g^0|R_\rho|e^0)(e^0|R_\sigma|g^0)}{E_{ev} - E_{gi} - E_0 - i\Gamma} \langle i|v\rangle\langle v|j\rangle \\
 B' &= \sum_{e \neq g}' \sum_v \sum_{s \neq e}' \sum_a \left[\frac{(e^0|R_a|s^0)}{(E_e^0 - E_s^0)(E_{ev} - E_{gi} - E_0 - i\Gamma)} \right. \\
 &\quad \left. \left\{ (g^0|R_\sigma|e^0)(s^0|R_\rho|g^0)\langle i|v\rangle\langle v|Q_a|j\rangle + (g^0|R_\sigma|s^0)(e^0|R_\rho|g^0)\langle i|Q_a|v\rangle\langle v|j\rangle \right\} \right]
 \end{aligned}$$

(13)

The physical interpretation of the damping constant, $i\Gamma$ in the denominator is at present not well understood. However, it has been proposed to be associated with the lifetime of the resonant excited state (2,22) or linewidth of the excited vibronic state. In Eq. (13), factors containing $(E_{ev} - E_{gi} + E_0 - i\Gamma)^{-1}$ are discarded, since we are interested in the scattering tensor near resonance condition.

Several features of resonance Raman scattering of the fundamental are discernible upon examination of the A' and B' terms. The A' term has a numerator of Franck-Condon overlap term (i.e. $\langle i | v \rangle \langle v | j \rangle$), and, therefore, A'-term will contribute only to Rayleigh scattering, since $\sum_v \langle i | v \rangle \langle v | j \rangle = \delta_{ij}$, as described before.

This procedure leaves only the B' term in which coupling operators of the form $(e^0 | h_a | s^0)$ appear and leads to the suggestion that modes that are vibronically active in coupling excited electronic states will be enhanced as the exciting frequency approaches an allowed electronic transition (Fig. A-2).

Only the interactions between excited electronic states via vibrational coupling were considered in the Herzberg-Teller treatment. But if there is a displacement in the equilibrium internuclear distance for the excited state versus the ground state, this Herzberg-Teller expansion treatment could not be applicable no longer. Peticolas et al. (23) have shown that A-term in equation (12) could become responsible for Raman intensity. They rewrote the denomination of A-term as shown below.

$$\begin{aligned} E_{ev} - E_{gi} &= E_{ge} + \Omega \\ E_{ev} - E_{gj} &= E_{ge} + \Omega' \end{aligned}$$

where E_{ge} represents the energy difference for the electronic term and Ω, Ω' represent the energy difference for the vibrational term.

Thus A-term in equation (12) could be expanded as follows.

$$A = \sum'_{e \neq g} \sum_v \left[(g^0 | R_e | e^0) (e^0 | R_p | g^0) \left\{ \frac{1}{E_{ge} - E_0} - \frac{\Omega}{(E_{ge} - E_0)^2} + \dots \right\} \right. \\ \left. + (g^0 | R_p | e^0) (e^0 | R_e | g^0) \left\{ \frac{1}{E_{ge} + E_0} - \frac{\Omega'}{(E_{ge} + E_0)^2} + \dots \right\} \right] \\ \times \langle i || v \rangle \langle v || j \rangle \quad (14)$$

In usual Raman process ($i=0, j=1$) and non-resonant condition, we can obtain;

$$\Omega = v\hbar\omega^a \\ \Omega' = (v-1)\hbar\omega^a$$

here we approximate $\omega^a = \omega_g^a = \omega_e^a$.
approximation;

In harmonic oscillator

$$\sum_v \langle 0 || v \rangle \langle v || 1 \rangle = \langle 0 || 1 \rangle = 0$$

$$\sum_v v \langle 0 || v \rangle \langle v || 1 \rangle = -\sqrt{\frac{\mu \omega^a}{2\hbar}} |\Delta_a|$$

where μ refers to the reduced mass for the vibration and Δ_a refers to the displacement in the equilibrium internuclear distance for the excited (e) state versus the ground (g) state. Thus we obtain;

$$A = \sum_{e \neq g} \left[(g^0 | R_e | e^0) (e^0 | R_f | g^0) \frac{\hbar \omega^a}{(E_{ge} - E_0)^2} \sqrt{\frac{\mu \omega^a}{2 \hbar}} |\Delta_a| \right. \\ \left. + (g^0 | R_f | e^0) (e^0 | R_e | g^0) \frac{\hbar \omega^a}{(E_{ge} + E_0)^2} \sqrt{\frac{\mu \omega^a}{2 \hbar}} |\Delta_a| \right] \quad (15)$$

This result indicate that if the vibration is totally symmetric and there is a displacement in the equilibrium internuclear distance for the excited versus the ground state, A-term may also be responsible for Raman intensity.

In the exact resonant condition, this treatment can not hold no longer and other kind of treatment is necessary to obtain the Raman intensity via A-term.

Resonance Raman theory is presently in a developmental stage. A large number of workers are studying the theory and presenting various formulations (such as 23,24). The formulation used in this thesis contains the basic concept found in all of the other formulations of Raman theory. However other formulations include additional terms in the polarizability expression due to inclusion of the nuclear kinetic energy operator (non-adiabatic coupling) (24). Although the resulting expressions for Raman intensity may be quantitatively more correct, they make the equations much more complicated and make a interpretation of the Raman expressions more difficult. Therefore, the simplest and most concise formulation was chosen in this thesis.

II. Mechanism of Resonance Raman Enhancement of Metalloporphyrins

1. Porphyrin In-Plane Enhancement

The regular metalloporphyrin absorption spectra are dominated by a very strong band ($\epsilon \sim 1-6 \times 10^5 \text{ M}^{-1} \text{ cm}^{-1}$) near 400 nm, called the Soret band or B-band. Near 550 and 500 nm, there are two weaker bands ($\epsilon \sim 1-4 \times 10^4 \text{ M}^{-1} \text{ cm}^{-1}$), called α and β , or Q_0 and Q_1 , respectively.

The maximum symmetry of metalloporphyrins is D_{4h} , and the highest filled Simpson's (25,26) annulene orbital pair is split into a_{1u} and a_{2u} orbitals, which, however, remain close in energy. The lowest unfilled orbital pair, e_g , remains degenerate. The two promotions $a_{1u} \rightarrow e_g$ and $a_{2u} \rightarrow e_g$ both have E_u symmetry, and are subject to strong configuration interaction (27). The transition dipoles are added for the B-transition, and nearly canceled for the Q_0 -transition, accounting for its low, but nonzero intensity. Vibronic interactions between the B and Q_0 states generate Q_1 state borrowing absorption intensity from the B-band by B_{1g} , B_{2g} , or A_{2g} vibrations. Thus, Q_1 -band is separated 1200 cm^{-1} to higher energy from the Q_0 -band. This energy separation corresponds closely to the average frequency of porphyrin vibration modes.

(a) B-band Scattering

This four-orbital model (27) is able to explain even the main features of metalloporphyrin resonance Raman spectra (28-32). These are dominated by bands with frequencies in the range $1100-1650 \text{ cm}^{-1}$, corresponding to stretching of the porphyrin-ring π -bonds, as expected for enhancement via $\pi-\pi^*$ transitions.

Excitation near the intense B-band enhances totally symmetric modes, via A-term scattering (33). The strongest feature is a band near 1360 cm^{-1} , corresponding to the breathing mode of the C-N bonds (34). Even for this mode, the origin shift is small, as shown by analysis of the resonance CARS (coherent anti-Stokes Raman scattering) lineshapes (35), and as is also evident in the lack of any pronounced vibrational structure on the B absorption band (36). The large size of the porphyrin π -system keeps the excited-state distortion relatively small. The impressive enhancements that are seen with excitation in the B-band (37,38) are, therefore, due to the large electronic transition moment of B-band.

(b) Q-band scattering

With excitation in the Q_0 and Q_1 bands, A-term enhancement is much lower, because of the smaller electronic transition moment. The A-term scales with $(M_e^0)^2 = (g^0 | R_g | e^0)(e^0 | R_g | g^0)$, so that Q-band enhancement would be expected to be at least two orders of magnitude lower than B-band enhancement, if bandwidths and Franck-Condon factors were equal. The Q-band resonance Raman spectra are generally dominated by the non-totally-symmetric modes responsible for Q-B mixing and the generation of the Q_1 -absorption. The symmetry of these modes is given by the direct product of the electronic transition symmetries, $E_u \times E_u = A_{1g} + A_{2g} + B_{1g} + B_{2g}$. Because of the high symmetry of the molecule, A_{1g} modes are ineffective in mixing the transition moments (40). The remaining three symmetries are all represented among the modes observed in Q-band resonance Raman spectra. (B_{1g} and B_{2g} modes cannot be readily distinguished, since both give depolarized Raman bands, but they can be identified, via symmetry lowering, in the shape-line fluorescence (15)

or resonance Raman spectra (41) of free-base porphyrins, since $B_{1g} - A_g$ but $B_{2g} - B_{1g}$ when the D_{4h} symmetry is lowered to D_{2h} .)

Of particular interest are the A_{2g} modes, which give anomalously polarized resonance Raman bands (15). For randomly oriented molecules, the depolarization ratio, which is the intensity ratio of scattered light with polarization perpendicular and parallel to the incident polarization, is (7,15)

$$\rho = \frac{I_{\perp}}{I_{\parallel}} = \frac{3\gamma_s^2 + 5\gamma_{as}^2}{45\alpha^2 + 4\gamma_s^2}$$

where α^2 is the isotropic part of the Raman tensor, γ_s^2 is the symmetric anisotropy and γ_{as}^2 is the antisymmetric anisotropy.

In nonresonant scattering the Raman tensor is symmetric, leading to $\gamma_{as}^2 = 0$, and ρ cannot exceed 3/4. Non-totally-symmetric modes have zero diagonal tensor elements, and give polarized bands, $\rho = 3/4$. Totally symmetric modes have $\alpha^2 = 0$ and give polarized bands, $\rho = 3/4$. In resonance Raman scattering, however, the tensor need not be symmetric. If $\gamma_{as}^2 = 0$, a band may be anomalously polarized, $\rho = 3/4$.

All of the porphyrin modes come into resonance at the Q_0 maximum (0-0) (42) and then again at the Q_1 position expected for the vibration being monitored (0-1) (15). For B-term scattering equal enhancement is expected at resonance with the 0-0 and 0-1 transitions, since the numerators of the first two terms in Equation (12), $\langle 1|Q|0\rangle\langle 0|0\rangle$ and $\langle 1|1\rangle\langle 1|Q|0\rangle$, are equal in magnitude. They have the same sign for symmetric (B_{1g} and B_{2g}) and opposite sign for antisymmetric (A_{2g}) modes.

Since the frequency denominator of Equation (12) changes sign as the incident frequency passes through a resonance, the two terms interfere destructively for B_{1g} and B_{2g} modes but constructively for A_{2g} modes, at frequencies between the 0-0 and 0-1 transitions. For lower symmetries, modes of mixed polarization show a dispersion of the polarization ratio, which maximizes at $\nu_0 = (\nu_{00} + \nu_{10})/2$ (44), as has been observed for porphyrins (28-32). (Depolarization dispersion can also reflect splitting of the x and y components of the Q-band (45)). Off resonance, the terms cancel for antisymmetric vibrations at wavelengths outside the absorption band (42). This cancellation is the reason that anomalous polarization of vibrational bands is only seen under rigorous resonance conditions.

In actual Q_0 and Q_1 excitation profiles, the 0-0 and 0-1 maxima are not always of equal height. Higher 0-1 maxima have been attributed to non-adiabatic effects, whereby extra enhancement at higher vibrational level is predicted via nuclear-electron coupling with higher electronic states (46,47). Higher 0-0 maxima have been attributed to Jahn-Teller effect in the degenerate Q-state. If a mode is active in both interstate and intrastate (Jahn-Teller) coupling, then there can be interferences between the two mechanisms that affect the excitation profiles (48,49,50).

2. Out-of-Plane Enhancement

(a) Porphyrin Out-of-Plane Deformation

The out-of-plane modes of a planar metalloporphyrin involve bending of the in-plane bonds, and are all expected at low frequencies, < 1000

cm^{-1} . In D_{4h} symmetry, they span the representations A_{1u} , A_{2u} , B_{1u} , B_{2u} , and E_g .

Of these, only the E_g modes are Raman-active. There is no mechanism for E_g -enhancement via the in-plane electronic transitions alone. They can, however, be enhanced by vibronic mixing of in-plane (E_u) and out-of-plane (A_{2u}) electronic transitions: $E_u \times A_{2u} = E_g$. An example of this enhancement mechanism has recently been found (51) in the resonance Raman spectrum of $(\text{ImH})_2\text{Fe}^{2+}\text{PP}$ (ImH = imidazole, PP = protoporphyrin IX). When excited at 457.9 nm, this complex shows a band at 841 cm^{-1} which disappears upon deuteration of the methine carbon atoms of the porphyrin ring, and which is assignable to out-of-plane bending of the methine C-H bonds (52). From oriented-crystal spectroscopy, low-spin Fe^{2+} hemoproteins are known to have weak z-polarized (A_{2u}) absorptions near 457.9 nm, which are assigned (36) to porphyrin(a_{2u}) \rightarrow $\text{Fe}(d_{z^2}, a_{1g})$ charge-transfer (CT) transitions. The A_{2u} orbital concentrates electron density on the methine carbon atoms (53), C_m , and it is suggested (51) that the $E_g C_m\text{-H}$ mode is effective in mixing the out-of-plane CT transition with the nearby in-plane B-transition.

A band in the $((\text{ImH})_2\text{Fe}^{2+}\text{OEP})^+$ (OEP = octaethylporphyrin) resonance Raman spectrum, at 320 cm^{-1} , also disappears when ImH is replaced by CN^- . This band shifts down by 10 cm^{-1} when the methine carbon atoms are deuterated, and is assigned to out-of-plane deformation of the methine bridges. Its activation in parallel with the 255 and 359 cm^{-1} A_{2u} modes likewise suggests an A_{2u} assignment. It may be the same mode with that observed at 330 cm^{-1} in resonance Raman spectra of Mn^{3+}EP (EP = etioporphyrin) halide complexes by Asher and Sauer (55), and assigned

as out-of-plane because its intensity increased with increasing size of the halide ligands ($F^- < Cl^- < Br^- < I^-$), and, presumably, with the out-of-plane displacement of the Mn^{3+} ion. Also, its frequency shifted up slightly ($\sim 1\text{ cm}^{-1}$) on $^{37/35}Cl^-$ substitution, indicating coupling with the Mn-Cl stretching mode ($286 - 282\text{ cm}^{-1}$) (54). In FePP complexes as well, the 320 cm^{-1} band intensifies for five-coordinated out-of-plane structures (51).

Out-of-plane assignments have been suggested for $Mn^{3+}Mb$ resonance Raman bands at 170 and 280 cm^{-1} , which are activated upon azide binding to manganese-substituted heme (56). In $Fe^{3+}Mb$, resonance Raman bands in the 450 cm^{-1} region which shift down upon vinyl deuteration are assignable to pyrrole-folding modes (51). In hemoproteins, direct coupling of out-of-plane modes to the $\pi-\pi^*$ transitions can result from loss of the porphyrin mirror plane via asymmetric ligation, protein-induced distortion of the porphyrin ring (57,58), or asymmetric electrostatic fields in the heme-binding region (59).

(b) Axial-ligand Modes

i) $\pi-\pi^*$ Resonance

Metalloporphyrins can bind one or two ligands at the axial coordination sites of the central metal ion. Since the physical or chemical nature of heme group is modulated drastically by the axial ligands, it has been a matter of great interest to identify the metal-ligand stretching modes in the resonance Raman spectra. Although these modes are generally weak, it has proved possible to assign a number of them, using isotopic frequency shifts. It is important to clarify the enhancement mechanisms available to these modes, in order to

find optimal conditions for detecting them, or, more importantly, to reveal the exact electronic structure of heme.

It has been conventional wisdom that the in-plane porphyrin electronic transitions do not enhance M-L stretching modes, since the latter are out-of-plane vibrations. Unlike the porphyrin out-of-plane deformations, however, the M-L stretches are not restricted by symmetry from coupling to the in-plane electronic transitions. If a D_{4h} metalloporphyrin has two identical axial ligands, the $M-L_2$ symmetric stretch has A_{1g} symmetry (the asymmetric stretch, A_{2u} , is infrared but not Raman-active, unless the mirror plane is destroyed). If the ligands are not the same, or if there is only one axial ligand, the point group is lowered to C_{4v} , and the M-L stretch remains A_1 . Thus a M-L stretching mode can be enhanced by an in-plane transition, provided that the excitation alters the M-L bond length (in other words, not enhanced via B' term).

The feasibility of this enhancement mechanism is demonstrated by the excitation profile for the $Fe-O_2$ stretching mode of HbO_2 (oxyhemoglobin). The $Fe-O_2$ stretching frequency, which has been assigned to 567 cm^{-1} band by Brunner (60) with $^{18}O_2$ isotopic substitution technique was the first axial mode to be discovered. This mode is enhanced strongly in the B-band, and more weakly in the region of the Q-bands and this excitation profile roughly follows the absorption spectrum of HbO_2 and is in proportion to their transition moments. This observation was first made by Tsubaki et al. (61,62), and later confirmed by Walters and Spiro (63). The coupling of $\nu(Fe-O_2)$ to the in-plane $\pi-\pi^*$ transitiond can be understood on the basis of the electronic structure of oxy heme.

The high Fe-O₂ stretching frequency, around 570 cm⁻¹, bears on the long standing controversy (64-69) over the electronic structure of oxy heme. While this complex is formed from O₂ and Fe²⁺ porphyrin, many spectroscopic properties, including the high-frequency resonance Raman spectrum (70,71), are more consistent with low-spin Fe³⁺ than Fe²⁺, and the 0-0 stretching frequency observed by infrared spectroscopy (72-74), is in accord with an Fe³⁺-O₂⁻ formulation. The transfer of a d_π electron to O₂ appears to be essentially complete, but, of course, this transfer is compensated by σ-donation from O₂ to Fe; electronic-structure calculations (75) indicate that the net transfer of charge is small.

The enhancement of ν(Fe-O₂) stretching frequency was expected earlier (11) to be due to z-polarized transitions, which have been identified in the MbO₂ crystal spectrum (36,76). The z-polarized band at ~475 nm, close to the excitation wavelength initially used for the study of ν(Fe-O₂) (60), has been assigned to either O₂ - Fe charge transfer (77) or porphyrin π(a_{2u}) - Fe d_{z2}(a_{1g}) charge-transfer (78-80). Either transition should enhance ν(Fe-O₂), since either the bonding O₂ or the antibonding Fe(d_{z2}) orbitals are involved. The excitation profile, however, is flat in the region of this absorption, and the conclusion seems inescapable that charge transfer enhancement must be less than or comparable to the preresonance enhancement from the B-transition, presumably because the charge transfer transition moment, if any, is so small.

A similar π-π* enhancement mechanism can be expected for the stretching mode of other π-acceptor ligands. Indeed, the Fe-CO stretching frequency of HbCO and MbCO discovered via its CO isotopic

shifts by Tsubaki et al. (61,62) and the Fe-NO stretch of HbNO, discovered via its $^{15}/^{14}\text{NO}$ shift by Chottard and Mansuy (81), also show intensification in the B and Q_1 bands, and have flat profiles in between.

The π -acceptor character of O_2 ligand competes effectively with the porphyrin ring for back-bonding of the iron d_π electrons (71). The extent of back donation depends sensitively on the match of d_π and π^* orbital energies, and may be affected, for example, by alterations in the trans axial ligand (69) (Fig. A-3). For the diatomic ligands that bind to deoxyHb and deoxyMb, the Fe-XY stretching frequencies increase in the order $\text{CO} < \text{NO} < \text{O}_2$ (507, 551, 567 cm^{-1} , respectively). This is also the order of decreasing π^* -orbital energies (i.e. O_2 is the best π -acceptor among these), and the stretching frequencies reflect the expected trend of Fe d_π back donation to these π -acceptor ligands. The same trend is seen in the π -sensitive porphyrin skeletal frequencies (i.e. 1360 cm^{-1} band), which reflect the competition between porphyrin and axial-ligand π^* orbitals for the d_π electrons (71,82,83). When the trans axial ligand of NO-heme is lost, $\nu(\text{Fe-NO})$ increases by the amount expected on the basis of the decreased Fe-NO distance observed in TPP crystal structures (84,85), which is associated with the NO trans effect.

Recently the $\nu(\text{Fe(III)-CN}^-)$ vibration in carp cyanomet Hb was identified at 455 cm^{-1} via $^{12}\text{C}/^{15}\text{N}$ isotope shift by Tsubaki and Yu (unpublished results cited in ref. 61) and at 452 cm^{-1} in human cyanomet Hb by Rousseau and coworkers (86,87). Further, Yu et al. (88) found $\delta(\text{Fe(III)-C-N})$ bending vibration at 412 cm^{-1} . However, there is no enhancement of bound C-N stretching mode expected at 2130 cm^{-1} .

A similar π - π^* enhancement mechanism must be applicable for this case. The lone pair electrons of both CN^- and CO ligands coordinate to the $d_{z^2}(\text{Fe})$ orbital to form a σ -bond. However, in cyanomet complex, there may be a weaker π -bonding between $d_{\pi}(\text{Fe})$ and $\pi^*(\text{CN}^-)$, than that in carbonmonooxy complex due to diminished π -back bonding in Fe^{3+} heme; leading to the weaker Raman enhancement of $\nu(\text{Fe(III)-CN}^-)$ stretching vibration.

Because the heme iron atom is bound to an imidazole group in most hemoproteins, the Fe-ImH stretching frequency is of particular importance, but it has also proved to be elusive. Because the effective mass of the rigid imidazole ring is high, Fe-ImH modes are expected to fall in the $200\text{--}300\text{ cm}^{-1}$ range, where low-frequency porphyrin modes interfere. Metal-imidazole modes are generally found in this region (89).

As will be described later, for the bis-pyridine complex $(\text{py})_2\text{Fe}^{2+}\text{MP}$, the symmetric py-Fe-py stretch (py = pyridine) was located at 179 cm^{-1} via the 5 cm^{-1} downshift upon ligand perdeuteration. A normal-coordinate analysis showed this mode to be a breathing motion of essentially rigid py rings (90). Indeed, the frequency was well approximated with a linear triatom calculation, using the same Fe-py force constant, in which the py "atom" was given the full mass of the ring. The mass of the ImH ring is only slightly less than that of py, and the symmetric ImH-Fe-ImH mode has now been located at a slightly higher frequency, 200 cm^{-1} , for $(\text{ImH})_2\text{Fe}^{2+}\text{PP}$ via ImH ^{15}N (91) and $-d_3$ (92) isotope shifts.

Surprisingly, it is found at the same frequency for $((\text{ImH})_2\text{Fe}^{3+}\text{PP})^+$ (91,92), although the increase in oxidation state would have been

expected to increase the bond strength, and therefore the stretching frequency. Apparently the extra electron in $(\text{ImH})_2\text{Fe}^{2+}\text{PP}$ is completely delocalized to the porphyrin ring, as reflected in the lowest porphyrin skeletal frequencies (83), leaving the Fe-ImH bond strength unaltered. The ImH-Fe-ImH asymmetric stretch of $((\text{ImH})_2\text{Fe}^{3+}\text{OEP})^+$ has been identified at 377 cm^{-1} in the i.r. spectrum, via its ^{54}Fe shift (93). The large frequency difference between the in- and out-of-phase stretches, which depends largely on the ligand-metal mass ratio, is a further evidence of the high effective mass of the ImH ligand. A triatomic calculation with the full ImH mass gives a reasonable Fe-ImH force constant, $K = 1.63\text{ mdyne/\AA}$ (91,92).

For the Fe^{2+} complex, this mode, although weak, shows observable enhancement upon direct B-band excitation. ImH is not an effective π -acceptor, but stretching of the Fe-ImH bond should nevertheless lower the $d\pi$ -orbital energies, via polarization, and therefore modulate the strong Fe^{2+} π -back donation to the porphyrin e_g -orbitals (71,82,83). In the case of Fe^{3+} , however, the mode is not seen with B-excitation, but only with 457.9 nm in aqueous solution, at the edge of the (aggregation-induced) split B-band (91,92). The enhancement mechanism is uncertain; it may involve vibronic coupling. But the lack of direct π - π^* enhancement is consistent with the diminished π -backbonding in Fe^{3+} hemes.

For deoxy Hb (94,95) and deoxy Mb (96) and their model adduct, five-coordinated high-spin Fe^{2+} porphyrins prepared with the sterically hindered imidazole, 2-MeImH (97), the Fe-ImH frequency has been located around 220 cm^{-1} via its shift on ligand perdeuteration (94) or on ^{54}Fe substitution (95,96,98). This mode can be enhanced quite strongly upon

excitation near the B-band. Therefore, it is very likely that the similar enhancement mechanism expected for symmetric ImH-Fe-ImH stretch in $(\text{ImH})_2\text{Fe}^{2+}\text{PP}$ complex. However Spiro proposed another mechanism for $\pi-\pi^*$ coupling. In this five-coordinated heme, the Fe atom is out of the porphyrin plane by $\simeq 0.05$ nm (99,100), and when the Fe-ImH bond is stretched, the Fe atom moves toward the plane, thereby altering the interaction of the Fe orbitals with the porphyrin π and π^* orbitals.

Kitagawa et al. (101) have suggested that vibrational coupling with low frequency in-plane porphyrin modes might account for axial-mode enhancements. Vibrational coupling is expected to be weak, however, since the internal coordinates are orthogonal, or nearly so. If the metal atom is in the plane, then there is no kinematic coupling depends on axial-in-plane interaction constants, which are expected to be small. Therefore, it seems probable that the direct coupling of the axial stretches to the in-plane electronic transition is a more important factor in the enhancement.

A diatomic calculation, using the full 2-MeImH mass, gave a force constant of 0.96 m dyn/\AA (94). This is substantially smaller than that obtained for $((\text{ImH})_2\text{Fe}^{3+}\text{PP})^+$, as expected, since the Fe^{2+} ion is high-spin and the Fe-N(2-MeImH) bond is lengthened (99,100). The reason that the Fe-ImH mode nevertheless appears at a higher frequency for a diatom Fe-L, namely $(1/m_{\text{Fe}} + 1/m_{\text{L}})^{-1}$, is less than the reduced mass for the symmetric mode of a linear triatom, L-Fe-L, which is just m_{L} (89).

It would be very useful to be able to monitor the internal modes of bound imidazole, in view of the ubiquitous occurrence of imidazole in hemoproteins, but such modes have not been reported, despite the

extensive resonance Raman spectroscopy of hemoproteins and imidazole complexes. Both ImH - Fe and Fe - ImH charge-transfer transition should occur somewhere in the u.v.-visible region, but it is difficult to predict their locations, and the intensities may be quite low (see also Ligand-M Charge -Transfer).

ii) Charge-Transfer Resonance

Porphyrin - M Charge-Transfer Because transition-metal ions have partially filled d-orbitals, a variety of charge-transfer transitions are possible for their complexes with porphyrins. Figure A-3 is a qualitative orbital energy diagram, which includes a set of d-orbitals and the four porphyrin frontier orbitals that dominate in the visible and near-u.v. spectrum. The relative ordering of these orbitals has been examined (27) for a wide range of complexes, using extended Huckel calculations and the available spectroscopic data. The center of gravity of the d-orbitals drops with increasing effective nuclear charge on the metal, from left to right across the periodic table, and from lower to higher oxidation states.

The splitting of the d-orbitals depends on the ligand field of the porphyrin and axial ligands. The strong in-plane porphyrin fields drives the $d_{x^2-y^2}$ orbital up, usually above the porphyrin e_g^* orbitals (Fig. A-3). The position of the d_z^2 orbital is highly variable, depending on the axial ligands. Strong-field ligands, such as NO or CN^- , drive it up to or beyond $d_{x^2-y^2}$, while for weak field or absent axial ligands it falls toward the d_{π} (d_{xz} and d_{yz}) and d_{xy} orbitals. The position of the d_{π} orbitals, relative to the nonbonding d_{xy} , is influenced by π -bonding. They are stabilized by π -acceptor ligands such as NO and O_2 .

and by the porphyrin ring, and destabilized by π -donor ligands such as OH^- and halides.

Charge transfer can take place from the filled porphyrin orbitals, a_{2u} and a_{1u} , to d-orbital vacancies, or from occupied d-orbitals to the vacant porphyrin orbitals, e_g^* . The latter process is, however, parity-forbidden. This restriction can be removed by mixing in metal p-orbital character, for complexes lacking inversion symmetry, but it is unlikely that $d - e_g^*$ transitions can contribute significantly to resonance Raman enhancement. The $a_{2u} \rightarrow d_z^2$ transition is allowed ($a_{1u} \rightarrow d_z^2$ and $a_{1u}, a_{2u} \rightarrow d_{x^2-y^2}$ are not), but the orbital overlap is poor. The transition is weak, but it can be identified in polarized-crystal spectra via its z-polarization, and several $a_{2u} - d_z^2$ assignments have been suggested (36).

The $a_{2u}, a_{1u} \rightarrow d_{xy}$ transitions are forbidden, but $a_{2u}, a_{1u} \rightarrow d\pi$ transitions are allowed, and are polarized in the plane. These have been assigned near 600 nm for high-spin Fe^{3+} and around 1200 to 1500 nm for low-spin Fe^{3+} (27,36). The large reduction in transition energy between high- and low-spin Fe^{3+} is attributable to interelectronic-repulsion effects (27). The $a_{2u}, a_{1u} \rightarrow d\pi$ transitions have not been identified in the spectra of high-spin Fe^{2+} porphyrins (36). For low-spin Fe^{2+} , they are necessarily absent, since the d orbitals are completely filled.

As noted above, absorption bands near 600 nm have been attributed to $a_{2u}, a_{1u} \rightarrow d\pi$ transitions of high-spin Fe^{3+} hemes. They are comparable in intensity to the Q-bands, with which they are no doubt strongly mixed. Asher et al. (102) reported specific enhancement of Fe-axial-ligand modes between 400 and 500 cm^{-1} for methemoglobin (Hb^{3+})

complexes of fluoride, hydroxide, and azide. The Fe-OH assignment, at 497 cm^{-1} in Hb^{3+}OH and 490 cm^{-1} in Mb^{3+}OH (103), was confirmed by its $^{18}\text{OH}^-$ shift (102,104). Two bands, 471 and 443 cm^{-1} , have been assigned to Fe-F stretching in Hb^{3+}F^- , based on their excitation profiles (102); the lower frequency was suggested to be due to H-bonding to a water molecule having partial occupancy of a site in the heme pocket (102). Both frequencies are appreciably lower in Mb: 461 and 422 cm^{-1} . The higher-frequency band has been shown (104) to have a 2 cm^{-1} ^{54}Fe isotope shift, confirming the Fe-F assignment.

Later Tsubaki et al. (105) confirmed by $^{15}\text{N}_3$ substitution that the 411 cm^{-1} band in Mb^{3+}N_3 (413 cm^{-1} in Hb^{3+}N_3 (102)) was indeed due to Fe- N_3 stretching, but they also showed, via its temperature dependence, that this band was associated with the low-spin rather than the high-spin component of Mb^{3+}N_3 . Therefore its enhancement at 647.1 nm could not be due to the $a_{2u}, a_{1u} \rightarrow d\pi$ charge transfer transitions, which are at much lower energy for low-spin Fe^{3+} hemes. It was attributed instead to a $\text{N}_3^- - \text{Fe}^{3+}(\text{low-spin})$ charge transfer transition.

A similar assignment has to be considered for the Fe-OH band of Hb^{3+}OH and Mb^{3+}OH , which also contain spin mixtures, but Asher and Schuster (103) showed that the Fe-OH excitation profile of Mb^{3+}OH tracked those of the high-spin porphyrin skeletal modes, at 1545 and 1608 cm^{-1} , while the low-spin mode at 1644 cm^{-1} peaked at higher energy, 580 nm , where the low-spin Q-band is expected. Thus enhancement via the high spin $a_{2u}, a_{1u} - d\pi$ transitions seems likely. Hb^{3+}F and Mb^{3+}F contain purely high-spin hemes, and the enhancement via the strong 600 nm band (103) must be attributed to the $a_{2u}, a_{1u} - d\pi$ transition ($\text{F}^- - \text{Fe}^{3+}$ charge transfer being most unlikely at this low an energy); the

Q_0 -band has been assigned (33,106) at 528 nm. Tsubaki et al. (105) argue, however, that Fe-ligand modes are unlikely to be strongly involved in the $a_{2u}, a_{1u} \rightarrow d_{\pi}$ excited states and point to the lack of an identifiable Fe-ligand stretch in the resonance Raman spectrum of high-spin acid ferricytochrome c, when excited in its 620 nm absorption band (107).

The Fe-F frequency seen for 5-coordinated heme fluoride is much higher, 606 cm^{-1} , because the absence of a trans axial ligand allows the Fe^{3+} ion to move out of the heme plane and form a strong bond to F^- (102). The 5-coordinated N_3^- frequency, 421 cm^{-1} , is only slightly higher than that seen for $\text{Hb}^{3+}\text{N}_3^-$, reflecting the compensating effects of the absence of a trans ligand, and the high \rightarrow low-spin transition. The recently assigned (108) $\text{Fe}^{3+}\text{-S(Cys)}$ stretch, 351 cm^{-1} , of substrate-bound cytochrome P-450_{cam} is at nearly the same frequency as the Fe-Cl stretch in $(\text{Cl}^-)\text{Fe}^{3+}\text{OEP}$ (109), 360 cm^{-1} , confirming five-coordination of the heme in this form of the protein (108).

Ligand - M Charge-Transfer Charge-transfer transitions are also possible to or from the axial ligands of metalloporphyrins. The situation is shown diagrammatically on the right side of Figure A-3. Transitions are possible from filled π or σ orbitals on the ligands to vacancies in any of the d-orbitals (L - M charge-transfer), or from (partially) filled d-orbitals to π^* -orbitals on the ligands (M - L charge-transfer). All of these transitions are allowed (strictly speaking, only one of the linear combinations of each pair of σ , π , or π^* orbitals on a symmetric ML_2 unit can take part in an allowed transition), but their intensities will vary with the extent of orbital

overlap. Highest intensities are expected for $L(\sigma) - M(d_z^2)$, $L(\pi) - M(d_{xy})$, and $M(d_{xy}) - L(\pi^*)$ transitions. The energies of these transitions are not easy to anticipate, since the d-orbital energies are influenced by their interactions with the porphyrin and with the axial ligands in a concerted manner. From the properties of simple complexes, it is expected that for Fe^{3+} , L - M charge-transfer transitions will occur in the visible region for oxidizable ligands such as Br^- , RS^- and N_3^- , while visible region M - L charge-transfer transition can occur from low-spin Fe^{2+} to ligands with low-lying π^* -orbitals. For many ML combinations, the transitions shown in Figure A-3 lie in the near or far u.v.

Because metalloporphyrin absorption spectra are dominated by the intense, broad $\pi - \pi^*$ transitions, it is difficult to locate L - M or M - L charge-transfer absorptions, and the few cases where they are believed to provide resonance Raman enhancements were found serendipitously. Thus early studies of bis-pyridine(py) Fe^{2+} porphyrins ("hemochromes") showed strong enhancement of internal modes of the bound pyridine ligands (83). These modes, as well as py-Fe-py symmetric stretch located at 179 cm^{-1} , were identified via their frequency shifts upon perdeuteration of py (90). Their excitation profiles were distinct from those of the porphyrin modes (90), and coincided with a bump on the absorption spectrum at 490 nm, which had been suggested (110) to arise from an $Fe^{2+} - py$ charge-transfer transition. This assignment was supported by an intensity analysis (90) of the py modes of $(py)_2Fe^{2+}MP$, and of its $py-d_5$ analog, which showed the excited-state geometry to be consistent with population of the first py π^* -orbital. Consistent with this assignment, an

analysis of the relative intensities indicated a pattern of bond-length changes in the excited state similar to that expected for occupation of the lowest pyridine π^* -orbital (90).

Yu and Tsubaki (56) observed resonance Raman bands at 2039 and 650 cm^{-1} for the azide complex of Mn^{3+} -substituted Mb, whose strong $^{15}\text{N}_3^-$ shifts implicated them as internal azide modes. They were both depolarized, implying that the modes are not totally symmetric with respect to the local (linear) N_3^- geometry (the complex as a whole has only mirror symmetry, since the MnN_3 unit is undoubtedly bent, as in other azides). They were assigned as the antisymmetric N_3^- stretch and the in-plane N-N-N bend. As with other Mn^{3+} porphyrins, $\text{Mn}^{3+}\text{Mb}(\text{N}_3^-)$ shows strong absorptions at 380 and 470 nm, due to mixed a_{2u} , a_{1u} - $d\pi$, e_g^* transitions (see above), but the internal azide modes were found to be enhanced between these bands, implying enhancement via an additional charge-transfer transition involving the azide; the enhancement mechanism was attributed to vibronic mixing between this extra charge-transfer transition and the intense in-plane transitions. Yu and Tsubaki (56) suggested that the extra charge-transfer transition was $\text{N}_3^-(\pi) - \text{porphyrin}(\pi^*)$ rather than $\text{N}_3^-(\pi) - \text{Mn}(d_{z^2})$ or $\text{N}_3^-(n) - \text{Mn}(d_{z^2})$ in character, since no band attributable to $\text{Mn}-\text{N}_3^-$ stretching was observed. In view of the probable proximity of porphyrin e_g^* and $\text{Mn}^{3+} d\pi$ -orbitals, $\text{N}_3^-(\pi) - \text{Mn}(d\pi)$ character is also likely. Lack of $\text{Mn}-\text{N}_3^-$ enhancement via such a transition would not be surprising on the precedent of the transferrin resonance Raman spectrum (111), which shows no strong Fe^{3+} -ligand modes upon excitation into a phenolate - $\text{Fe}^{3+}(d\pi)$ charge-transfer band, although phenolate-ring modes are strongly enhanced; the excitation was suggested (111) not alter the Fe-O bond

length appreciably because of the nonbonding character of the initial (phenolate π) and final ($\text{Fe}^{3+} d_{\pi}$) orbitals.

The $\text{Fe}^{3+}-\text{N}_3^-$ mode is seen in the azide complex of Fe^{3+} myoglobin, as mentioned above, and was shown by Tsubaki et al. (105) to be due to the low-spin form. It is enhanced in the vicinity of 600 nm (105), and since no porphyrin - Fe^{3+} charge-transfer transition is expected at this wavelength, a $\text{N}_3^- - \text{Fe}^{3+}$ transition may be responsible. But another $\text{N}_3^- - \text{Fe}^{3+}$ charge-transfer transition seems definitely to be located near 406.7 nm, the position of the B-band, since at this wavelength the resonance Raman spectrum revealed the antisymmetric N_3^- stretch at 2024 cm^{-1} (low-spin form) and a depolarized, $^{15}\text{N}_3^-$ -sensitive band, assigned to the out-of-plane N-N-N bend (105). (it had previously been thought to be the $\text{Fe}-\text{N}_3$ stretch (104)). Again vibronic mixing of the charge-transfer and B-bands was invoked to explain the depolarized enhancement. Tsubaki et al. assigned the 400 nm charge-transfer transition to $\text{N}_3^-(\pi) - \text{Fe}^{3+}(d_z^2)$ and the 600 nm charge-transfer transition to $\text{N}_3^-(n) - \text{Fe}^{3+}(d_z^2)$, on the grounds that enhancements of internal azide modes are expected for $\text{N}_3^-(\pi)$ but not $\text{N}_3^-(n)$ excitations, and none are seen with 600 nm excitation. This assignment places an azide n-orbital $\sim 8000 \text{ cm}^{-1}$ above the π -orbital; this level ordering could presumably result from the sp^2 hybridization of the terminal N atom, associated with a bent $\text{Fe}-\text{N}_3$ unit, which would leave a relatively high-energy lone pair n-orbital.

Tsubaki and Yu (112) found that excitation of Co-substituted MbO_2 and HbO_2 at 406.7 nm produces enhancement of both $\text{Co}-\text{O}_2$ and $\text{O}-\text{O}$ stretching modes, as already described briefly. Two $\nu(\text{O}-\text{O})$ frequencies are observed, suggesting different CoO_2 conformations. One

of them interacts with a coincident porphyrin mode, producing a pair of bands. at 1103 and 1137 cm^{-1} ; $^{18}\text{O}_2$ substitution decouples the interaction, shifting $\nu(\text{O-O})$ to 1069 cm^{-1} , and leaving the porphyrin band at 1123 cm^{-1} with increased intensity. In view of the enhancement of both $\nu(\text{Co-O}_2)$ and $\nu(\text{O-O})$, resonance with a $\text{O}_2(\pi^*) - \text{Co}(d_z^2)$ charge-transfer transition near 400 nm was suggested. A similar transition was earlier assigned by Nakamoto et al. (113) to 500 nm bands of the binuclear O_2 adducts $(\text{LCo}(\text{salen}))\text{O}_2$ (L = pyridine, pyridine-N-oxide, and dimethylformamide; salen = N,N'-ethylenebis(salicylideneimine)) on the basis of resonance Raman enhancements of $\nu(\text{Co-O}_2)$ and $\nu(\text{O-O})$ in these complexes. Because the higher $\text{O}_2 \pi^*$ -orbital is empty in Fe^{2+} porphyrin adducts, the analogous transition is absent for MbO_2 or HbO_2 ; Tsubaki and Yu did, however, find evidence for a similar $\nu(\text{O-O})$ -porphyrin mode interaction in the intensification of the MbO_2 1125 cm^{-1} band upon $^{18}\text{O}_2$ substitution (112).

References

1. Krishnan, R.S. (1971) "The Raman Effect" vol. I (A. Anderson ed.) Dekker. Inc., New York.
2. Konigstein, J.A. (1972) "Introduction to the Theory of the Raman Effect" Reidal Publishing Co., Dordrecht, Holland.
3. Sushchinskii, M.M. (1972) "Raman Spectra of Molecules and Crystals" Israel Program for Scientific Translations, New York.
4. Tu, A.T. (1982) "Raman Spectroscopy in Biology" John Wiley & Sons, Inc., New York.
5. Carey, P.R. (1982) "Biochemical Applications of Raman and Resonance Raman Spectroscopies" Academic Press, New York.
6. Kiefer, W. (1977) in "Advances in Infrared and Raman Spectroscopy" vol. 3, (R.J.H. Clark and R.E. Hester eds.) Heyden, London, pp1
7. Spiro, T.G., and Stein, P. (1977) Ann. Rev. Phys. Chem. 28, 501.
8. Spiro, T.G. (1975) Biochim. Biophys. Acta 263, 830.
9. Felton, R.H., and Yu, N.-T. (1978) in "The Porphyrins" vol. 3, Part A (Dolphin, D. ed) Academic Press, New York, p. 347.
10. Kitagawa, T., Ozaki, Y., and Kyogoku, Y. (1978) in "Advances in Biophysics" 11, 153.
11. Asher, S.A. (1981) in "Methods in Enzymology" vol. 76 (A. Eraldo, L.B. Bernardi, E. Chiancone eds.) Academic Press. p. 371.
12. Spiro, T.G. (1982) in "Iron Porphyrins" Part II (A.B.P. Lever and H.B. Gray eds.) Addison-Wesley Publishing Co., Massachusetts, p. 89.
13. Strekas, T.C., and Spiro, T.G. (1972) Biochim. Biophys. Acta 263, 830.
14. Brunner, H., Mayer, A., and Sussner, H. (1972) J. Mol. Biol. 70, 153.
15. Spiro, T.G., and Strekas, T.C. (1972) Proc. Natl. Acad. Sci. USA 69, 2622.

16. Chantry, G.W. (1971) "The Raman Effect" vol. I (A. Anderson ed.) M. Dekker, Inc., New York.
17. Albrecht, A.C. (1961) J. Chem. Phys. 34, 1476.
18. Albrecht, A.C. (1960) J. Chem. Phys. 33, 156.
19. Tang, J., and Albrecht, A.C. (1970) in "Raman Spectroscopy" vol II (H.A.Szymanski ed.) Plenum Press, New York.
20. Behringer, J. (1967) in "Raman Spectroscopy" vol. I (H.A.Szymanski) Plenum Press, New York.
21. Albrecht, A.C., and Hutley, M.C. (1971) J. Chem. Phys. 55, 4438.
22. Adar, F., Gouterman, M., and Aronwitz, S. (1976) J. Chem Phys.
23. Peticolas, W.L., Nafie, L., Stein, P., and Fanconi, B. (1970) J. Chem. Phys. 52, 1576.
24. Mingardi, M., and Siebrand, W. (1974) J. Chem. Phys. 62, 1074.
25. Simpson, W.T. (1948) J. Chem. Phys. 16, 1124.
26. Simpson, W.T. (1949) J. Chem. Phys. 17, 1218.
27. Gouterman, M. (1979) in "The Porphyrins" vol. III, Part A (D. Dolphin ed.), Academic Press, New York, p. 1.
28. Verma, A.L., and Bernstein, H.J. (1974) J. Raman Spectrosc. 2, 163.
29. Verma, A.L., and Bernstein, H.J. (1974) J. Chem. Phys. 61, 2560.
30. Mendelsohn, R., Sunder, S., Verma, A.L., and Bernstein, H.J. (1975) J. Chem. Phys. 62, 37.
31. Verma, A.L., Mendelsohn, R., and Bernstein, H.J. (1974) J. Chem. Phys. 61, 383.
32. Verma, A.L., Asselin, M., Sunder, S., and Bernstein, H.J. (1975) J. Raman Spectrosc. 4, 295.
33. Strekas, T.C., Packer, A., and Spiro, T.G. (1973) J. Raman Spectrosc. 1, 197.

34. Kitagawa,T., Abe,M., Kyogoku,K., Ogoshi,H., Sugimoto,H., and Yoshida,Z. (1977) Chem. Phys. Lett. 48, 55.
35. Dutta,P.K., Dallinger,R., and Spiro,T.G. (1980) J. Chem. Phys. 73, 3580.
36. Makinen,M.W., and Churg,A.K. (1982) in "Physical Bioinorganic Chemistry" (A.B.P. Lever and H.B. Gray, eds.) Addison-Wesley, Mass.
37. Champion,P.M., Gunsalus,J.C., and Wagner,G.C. (1978) J. Am. Chem. Soc. 100, 3473.
38. Remba,R.D., Champion,P.M., Fitchen,D.B., Chiang,R., and Hager,L.P. (1979) Biochemistry 18, 2280.
39. Champion,P.M., and Albrecht,A.C. (1979) J. Chem. Phys. 71, 1110.
40. Perrin,M.H., Gouterman,M., and Perrin,C.L. (1969) J. Chem. Phys. 50, 4137.
41. Kitagawa,T., Ogoshi,H., Watanabe,E., and Yoshida,Z. (1975) J. Phys. Chem. 79, 2629.
42. Strekas,T.C., and Spiro,T.G. (1973) J. Raman Spectrosc. 1, 387.
43. Carey,P.R., and Salares,B.R. (1980) in "Advances in Infrared and Raman Spectroscopy" vol. 7 (R.J.H. Clark and R.E. Hester eds.) Heyden, London, p.1.
44. Mortensen,O.S. (1975) Chem. Phys. Lett. 30, 406.
45. Collins,D.W., Champion,P.M., and Fitchen,D.B. (1976) Chem. Phys. Lett. 40, 416.
46. Shelnutt,J.A., O'Shea,D.C., Yu,N.-T., Cheung,L.D., and Felton,R.H. (1976) J. Chem. Phys. 64, 1156.
47. Friedman,J.M., and Hochstrasser,R.M. (1973) Chem. Phys. 1, 457.
48. Shelnutt,J.A. (1980) J. Chem. Phys. 72, 3948.
49. Champion,P.M., and Albrecht,A.C. (1981) J. Chem. Phys. 75, 3211.

50. Shelnutt, J.A., O'Shea, D.C., Yu, N.-T., Cheung, L.D., and Felton, R.H. (1976) *J. Chem. Phys.* 64, 1156.
51. Choi, S., and Spiro, T.G. (cited in ref. 12)
52. Ogoshi, H., Masai, N., Yoshida, Z., Takemoto, T. and Nakamoto, K. (1971) *Bull. Chem. Soc. Japan* 44, 49.
53. Longuet-Higgins, H.C., Rector, C.W., and Platt, J.R. (1950) *J. Chem. Phys.* 18, 1174.
54. Asher, S., and Sauer, K. (1976) *J. Chem. Phys.* 64, 4115.
55. Collins, D.M., Countryman, R., and Hoard, J.L. (1972) *J. Am. Chem. Soc.* 94, 2066.
56. Yu, N.-T., and Tsubaki, M. (1980) *Biochemistry* 19, 4647.
57. Takano, T. (1977) *J. Mol. Biol.* 110, 537.
58. Takano, T. (1977) *J. Mol. Biol.* 110, 569.
59. Warshel, A., and Weiss, R.M. (1981) *J. Am. Chem. Soc.* 103, 446.
60. Brunner, H. (1974) *Naturwiss.* 61, 129.
61. Tsubaki, M., Srivastava, R.B., and Yu, N.-T. (1982) *Biochemistry* 21, 1132.
62. Armstrong, R.S., Irvin, M.J., and Wright, P. (1982) *J. Am. Chem. Soc.* 104, 626.
63. Walters, M.A., and Spiro, T.G. (1982) *Biochemistry* 21, 6989.
64. Weiss, J. (1964) *Nature* 203, 83.
65. Pauling, L. (1964) *Nature* 203, 182.
66. Wayland, B.B., Minkiewicz, J.V., and Abd-Elmageed, M.E. (1974) *J. Am. Chem. Soc.* 96, 2795.
67. Wayland, B.B., and Abd-Elmageed, M.E. (1974) *J. Am. Chem. Soc.* 96, 9809.
68. Reed, C.A., and Chung, S.K. (1977) *Proc. Natl. Acad. Sci. USA* 74,

1780.

69. Drago, R.S., and Corden, B.B. (1980) *Accts. Chem. Res.* 13, 353.
70. Yamamoto, T., Palmer, G., Gill, D., Salmeen, I.T., and Rimai, L. (1973) *J. Biol. Chem.* 248, 5211.
71. Spiro, T.G., and Strekas, T.C. (1974) *J. Am. Chem. Soc.* 96, 338.
72. Barlow, C.H., Maxwell, J.C., Wallace, W.J. and Caughey, W.S. (1973) *Biochem. Biophys. Res. Commun.* 55, 91.
73. Maxwell, J.C., Volpe, J.A., Barlow, C.H., and Caughey, W.S. (1974) *Biochem. Biophys. Res. Commun.* 58, 166.
74. Collman, J.P., Brauman, J.I., Halbert, B.R., and Suslick, K.S. (1976) *Proc. Natl. Acad. Sci. USA* 73, 3333.
75. Case, D.A., Huynh, B.H., and Karplus, M. (1979) *J. Am. Chem. Soc.* 101, 4433.
76. Makinen, M.W., and Eaton, W.A. (1973) *Ann. N. Y. Acad. Sci.* 206, 210.
77. Eaton, W.A., Hanson, L.K., Stephens, P.J., Sutherland, J.C., and Dunn, J.B.R. (1978) *J. Am. Chem. Soc.* 100, 4991.
78. Churg, A.K., and Makinen, M.W. (1978) *J. Chem. Phys.* 68, 1913.
79. Churg, A.K., and Makinen, M.W. (1978) *J. Chem. Phys.* 69, 2668.
80. Makinen, M.W., Churg, A.K., and Glick, H.A. (1978) *Proc. Natl. Acad. Sci. USA* 75, 2291.
81. Chottard, G., and Mansuy, D. (1977) *Biochem. Biophys. Res. Commun.* 77, 1333.
82. Kitagawa, T., Iizuka, T., Saito, M., and Kyogoku, Y. (1975) *Chem. Lett.* 849.
83. Spiro, T.G., and Burke, J.M. (1976) *J. Am. Chem. Soc.* 98, 5482.
84. Scheidt, W.R., and Piciulo, P.L. (1976) *J. Am. Chem. Soc.* 98, 1913.
85. Scheidt, W.R., and Frisse, M.E. (1975) *J. Am. Chem. Soc.* 97, 17.

86. Rousseau,D.L., and Ondrias,M.R. (1983) Annu. Rev. Biophys. Bioeng. 12, 357.
87. Henry,E.R. (1980) Ph.D. Dissertation (Princeton Univ., Princeton, NJ)
88. Yu,N.-T., Benko,B., Kerr,E.A., and Gersonde,K. (1984) Proc. Natl. Acad. Sci. USA 81, 5106.
89. Nakamoto,K. (1978) "Infrared and Raman Spectra of Inorganic and Coordination Compounds" 3rd ed., Wiley-Interscience, New York, p. 212.
90. Wright,P.G., Stein,P., Burke,J.M., and Spiro,T.G. (1979) J. Am. Chem. Soc. 101, 3531.
91. Desbois,A., and Lutz,M. (1981) Biochim. Biophys. Acta 671, 257.
92. Mitchell,M., Choi,S., and Spiro,T.G. (cited in ref. 12)
93. Ogoshi,H., Watanabe,E., Yoshida,Z., Kincaid,J., and Nakamoto,K. (1973) J. Am. Chem. Soc. 95, 2845.
94. Kincaid,J., Stein,P., and Spiro,T.G. (1979) Proc. Natl. Acad. Sci. USA 76, 549. 4156.
95. Nagai,K., Kitagawa,T., and Morimoto,H. (1980) J. Mol. Biol. 136, 271.
96. Kitagawa,T., Nagai,K., and Tsubaki,M. (1979) FEBS Lett. 104, 376.
97. Collman,J.P., and Reed,C.A. (1973) J. Am. Chem. Soc. 95, 2048.
98. Hori,H., and Kitagawa,T. (1980) J. Am. Chem. Soc. 102, 3608.
99. Hoard,J.L., and Scheidt,W.R. (1973) Proc. Natl. Acad. Sci. USA 70, 3919.
100. Hoard,J.L., and Scheidt,W.R. (1974) Proc. Natl. Acad. Sci. USA 71, 1578.
101. Kitagawa,T., Abe,M., Kyogoku,Y., Ogoshi,H., Watanabe,G., and

- Yoshida,Z. (1976) J. Phys. Chem. 80, 1181.
102. Asher,S.A., Vickery,L.E., Schuster,T.M., and Sauer,K. (1977) Biochemistry 16, 5849.
103. Asher,S.A., and Schuster,T.M. (1979) Biochemistry 18, 5377.
104. Desbois,A., Lutz,M., and Banerjee,R. (1979) Biochemistry 18, 1510.
105. Tsubaki,M., Srivastava,R.B., and Yu,N.-T. (1981) Biochemistry 20, 946.
106. Eaton,W.A., and Hochstrasser,R.M. (1968) J. Chem. Phys. 49, 985.
107. Lanir,A., Yu,N.-T., and Felton,R.H. (1979) Biochemistry 18, 1656.
108. Champion,P.M., Stallard,B.R., Wagner,G.C., and Gunsalus,I.C. (1982) J. Am. Chem. Soc. 104, 5469.
109. Colthup,N.B., Daly,L.H., and Weiberley,F.E. (1975) in "Infrared and Raman Spectroscopy" 2nd ed., Academic Press, New York p.275.
110. Kobayashi,H., and Yanagawa,Y. (1972) Bull. Chem. Soc. Japan 45, 450.
111. Gaber,B.P., Miskowski,V., and Spiro,T.G. (1974) J. Am. Chem. Soc. 96, 6868.
112. Tsubaki,M., and Yu,N.-T. (1981) Proc. Natl. Acad. Sci. USA 78, 3581.
113. Nakamoto,K., Suzuki,M., Ishiguro,T., Kozuka,M., Nishida,Y., and Kida,S. (1980) Inorg. Chem. 19, 2822.

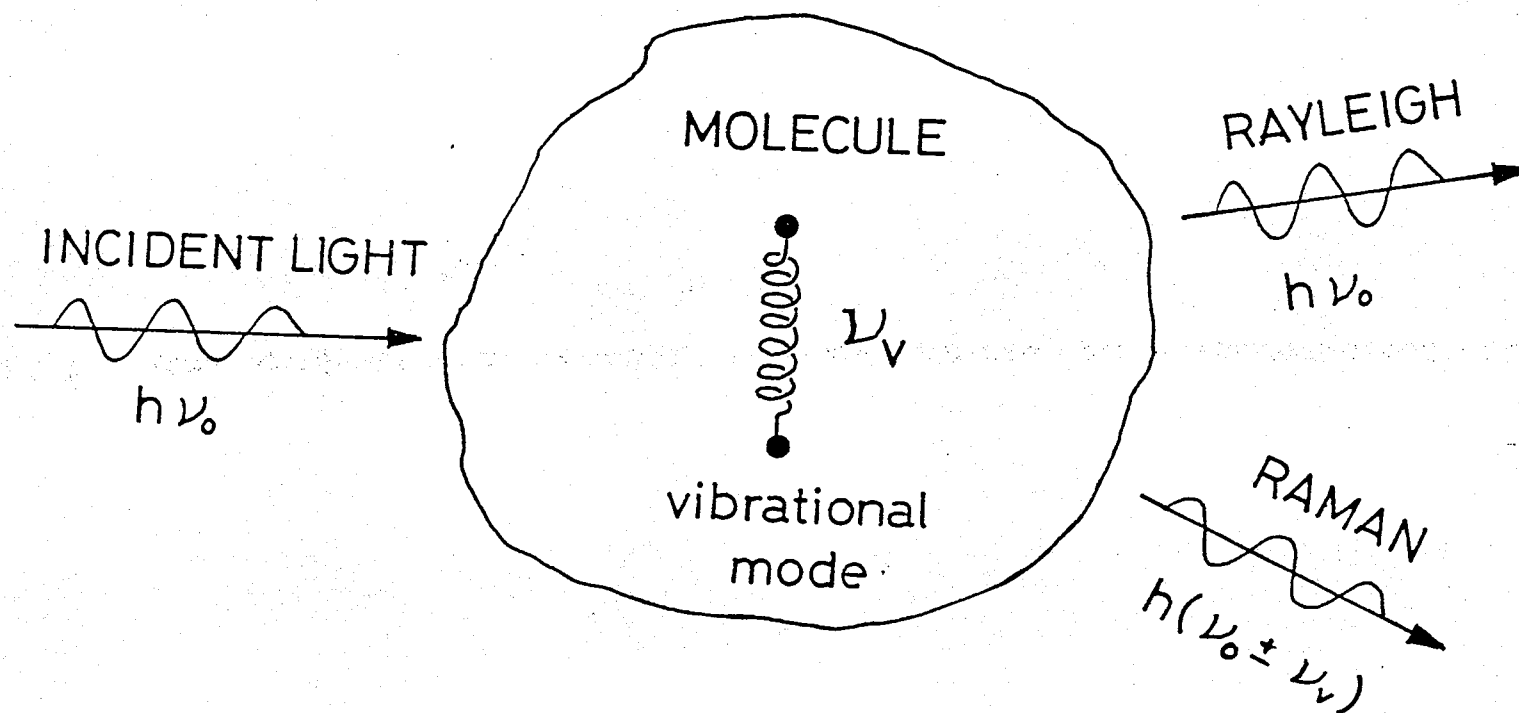


Figure A-1. Physical picture of Rayleigh and Raman light scattering.

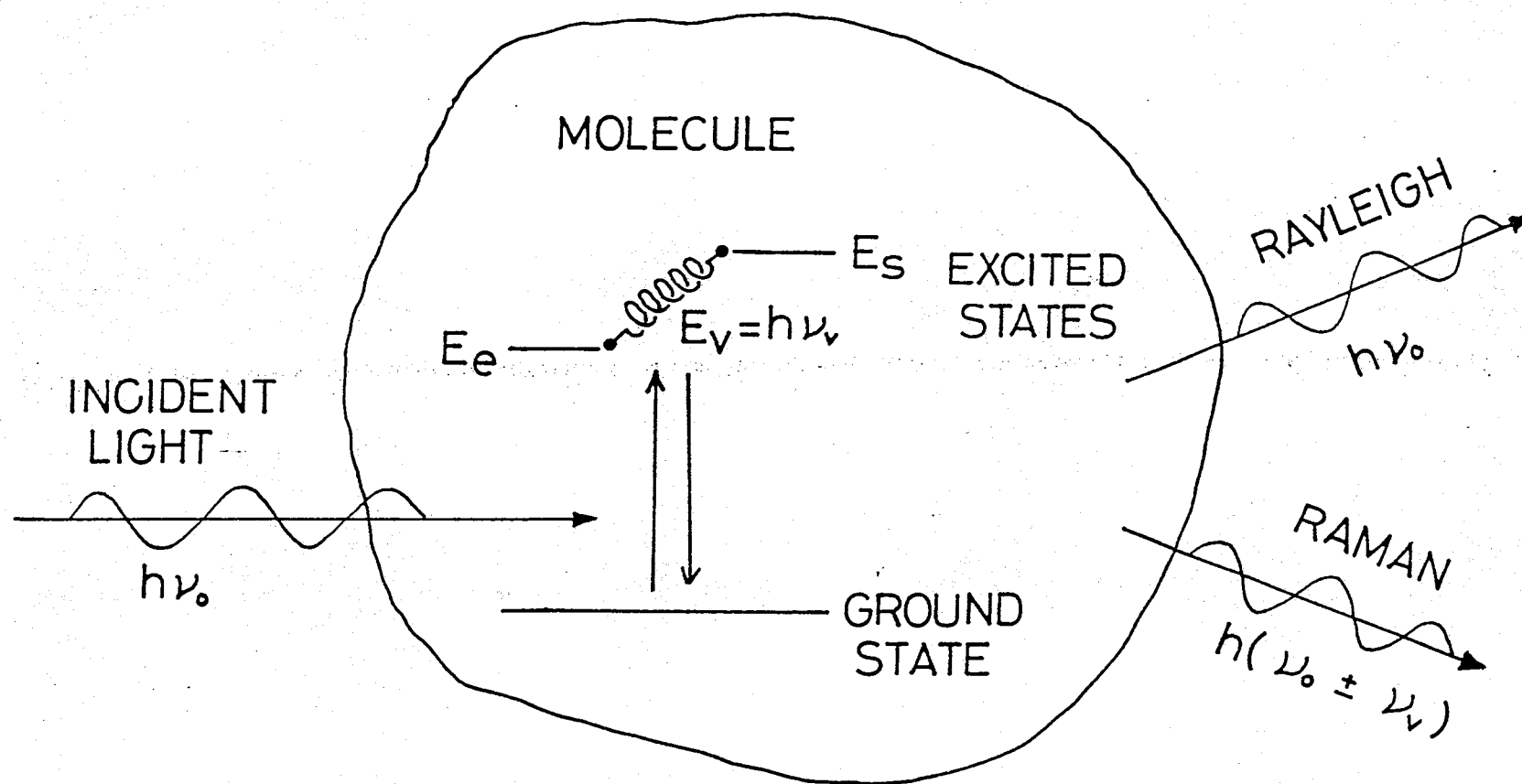
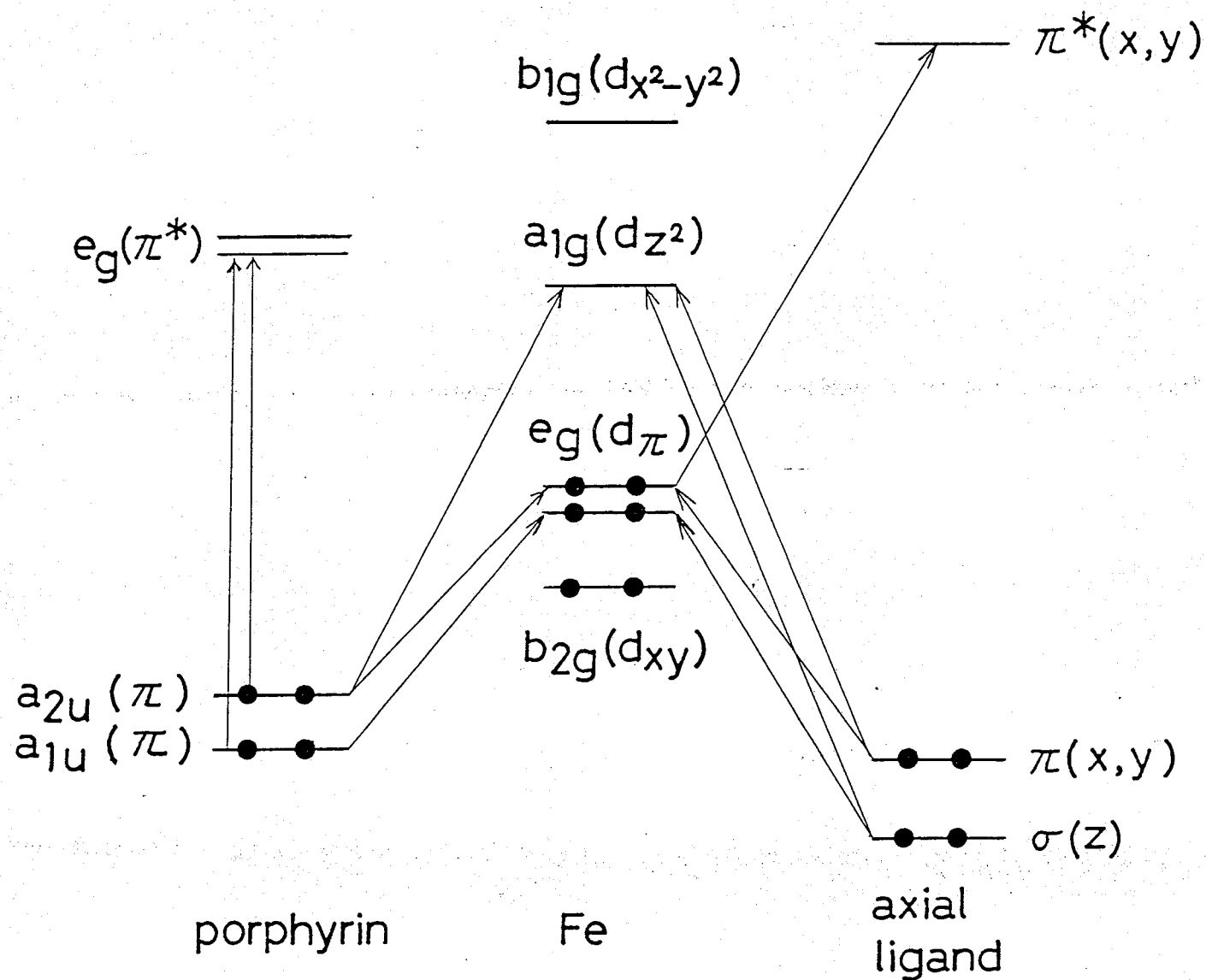


Figure A-2. Physical picture of the vibrational mixing between electronic states.

Figure A-3. Schematic diagram of the frontier orbitals of a low-spin Fe^{2+} porphyrin with axial ligands. The arrows represent allowed transitions.



Part B. Resonance Raman Investigation of Carbon Monoxide Bonding in HbCO and MbCO

0. Introduction

Carbon monoxide, a competitive inhibitor for oxygen-binding hemoproteins, is a useful probe for heme environment around the distal site. Unlike dioxygen, it is incapable of oxidizing the heme. The bound C-O stretching vibration, $\nu(\text{C-O})$, can be readily detected by infrared (IR) spectroscopy. Carbon monoxide bound to hemoglobin A (HbA) shows a sharp single absorption band at 1951 cm^{-1} (1), whereas in human hemoglobin variants, Hb Zurich ($\alpha 63\text{ E7 His} \rightarrow \text{Arg}$) exhibits its bound $\nu(\text{C-O})$ at 1958 cm^{-1} (β) and 1951 cm^{-1} (α), and carbonmonoxy HbM Saskatoon ($\beta 63\text{ E7 His} \rightarrow \text{Tyr}$) absorbs at 1970 cm^{-1} (β) and 1951 cm^{-1} (α) (2,3). Thus, the substitution of distal His E7 by other amino acid residues alters the $\nu(\text{C-O})$ frequency in the mutant subunits but not in the normal subunits. More interesting is the observation of multiple $\nu(\text{C-O})$ frequencies (1933 , 1944 , and 1967 cm^{-1}) in the IR spectrum of the monomeric CO complex of sperm whale myoglobin, which was interpreted as indicating three different heme-carbonyl conformers in the same heme cavity (4), although only one conformer has been reported in crystals by neutron diffraction studies (5).

Unlike infrared spectroscopy, detection of axial ligand vibrations by resonance Raman scattering of hemoproteins in dilute aqueous solution is not restricted to the narrow "window" region because water is a weak Raman scatterer (6). In fact, several iron-ligand stretching vibrations such as $\text{Fe}^{2+}\text{-O}_2$, $\text{Fe}^{2+}\text{-NO}$, $\text{Fe}^{3+}\text{-OH}$, $\text{Fe}^{3+}\text{-N}_3$, and $\text{Fe}^{3+}\text{-CN}$ have been identified by resonance Raman spectroscopy with the ligand isotope

substitution technique (7-10). Moreover, internal ligand vibrations can also be resonance enhanced by tuning the excitation wavelength into a responsible charge-transfer band (10-12).

Thus, resonance Raman spectroscopy appears to be a powerful technique to study the direct interaction between the heme and its axial ligands. However, its application to HbCO or MbCO has been limited to pulse laser transient kinetic studies (13-18), although a preliminary work using continuous wave laser excitation was reported by Rimai et al (19). Identification of $\nu(\text{Fe-CO})$ has been difficult because carbon monoxide dissociates from heme easily upon illumination of laser light, generating deoxy species which interfere with the observation of signals from unphotolyzed complexes.

In this part, the feasibility of obtaining high-quality resonance Raman spectra of HbCO and MbCO which contain negligible contribution from photolyzed deoxy species will be demonstrated. With the excitation wavelength at 406.7 nm, two Raman lines at 507 (512) and 578 (577) cm^{-1} in HbCO (MbCO) are sensitive to CO isotope substitution. On the basis of a linear Fe-C-O configuration (tilted away from the heme normal by 13°) as revealed by the X-ray crystallographic studies of human HbACO (at 2.7 Å resolution) (20), the pattern of observed isotope shifts and normal coordinate calculations permit us to establish that the most intense line at 507 (512) cm^{-1} (in the 100-650 cm^{-1} region) is the $\nu(\text{Fe-CO})$ stretching, and the weaker one at 578 (577) cm^{-1} is a $\delta(\text{Fe-C-O})$ bending mode. Further the resonance enhancement of the bound $\nu(\text{C-O})$ vibration at 1951 (1944) cm^{-1} in HbCO (MbCO) was observed in agreement with those observed by infrared spectroscopy. In

addition, a significant broadening of the λ (Fe-CO) line in carp HbCO upon quaternary structure change from R to T could be found..

I. Experimental

1. Preparation of Proteins

Sperm whale myoglobin (Sigma) was purified in the carbon monoxy form as described previously (10). Human hemoglobin A (HbA) was prepared in oxy form by the usual procedure from whole blood (21) and, then, was converted to the carbon monoxy form. Carp Hb was kindly donated by Dr. R.W.Noble and was prepared from washed red blood cell by lysis (22). Because considerable amounts of oxidized carp Hb were formed during transportation, complete reduction of carp Hb was performed by using sodium dithionite under a carbon monoxide atmosphere followed by anaerobic gel filtration (Sephadex G-25f, Whatman) to form carp HbCO. Separation of each carp Hb fraction was performed by the method of Tan et al. (22) with slight modification. Carp Hb hemolysate in the carbon monoxy form was charged onto a DEAE-cellulose (DE-52, Whatman) column, 2 x 20 cm, equilibrated with 2 mM sodium borate buffer, pH 9.0. The fractions were eluted by a linear gradient of borate concentration at pH 9.0 at 4°C, the starting buffer being 1 L of 2 mM sodium borate and the final buffer being 1 L of 20 mM sodium borate buffer. The flow rate was 30 mL/h, and all the buffers used for fractionation had been bubbled by carbon monoxide gas to avoid the oxidation of heme. Hb Kansas was a kind gift from Dr. K.Nagai. All the hemoglobin samples used were gel filtered against 1 mM Na_2HPO_4 and deionized by passage through a Dintzis column (23).

2. Preparation of Carbon Monoxide Derivatives

Hb (or Mb) solution was diluted with an appropriate buffer and transferred into a cylindrical quartz Raman cell with rubber septum. The solution was deoxygenated by repeated evacuation and flushing of pure nitrogen and, then, carbon monoxide gas was introduced to ensure that all hemes were saturated with CO. This procedure is necessary because residual dioxygen in the solution could replace the carbon monoxide upon laser illumination. The quantum yield for photodissociation of carbon monoxide derivatives is much higher than those of oxygenated hemoproteins. Extreme care was taken to avoid the formation of oxidized heme in solution especially at low pH, which may affect the Raman spectrum significantly because of the closer proximity of the Soret maxima of oxidized derivatives to the excitation wavelength. The extent of oxidation can be estimated from Raman spectra in both higher frequency (1200-1700 cm^{-1}) and lower frequency (100-700 cm^{-1}) regions. Although the spectra were compared with and without sodium dithionite under an atmosphere of carbon monoxide gas, no difference was observed between them.

Carbon monoxide was obtained from the following manufacturers: $^{12}\text{C}^{16}\text{O}$ from Matheson (CP grade), $^{13}\text{C}^{16}\text{O}$ from Bio-Rad (93.1 atom % ^{13}C), and $^{12}\text{C}^{18}\text{O}$ and $^{13}\text{C}^{18}\text{O}$ from Prochem (99.0 atom % ^{18}O , 91.7 atom % ^{13}C , and 98.5 atom % ^{18}O , respectively).

3. Measurement of Raman Spectra

The Raman cell (diameter 1.95 cm) was kept in a rotating (2000 rpm) cell holder for laser irradiation to avoid local heating and to reduce the photodissociation, and a 90° scattering geometry was used to obtain Raman spectra at room temperature. Under the spinning condition, the

time required for the sample to pass through a 20-micrometer laser beam is $\sim 10^{-5}$ s. The 406.7 nm emission of a krypton ion laser (Spectra-Physics Model 171-01) was employed for excitation, and the laser power was maintained at 10 mW at sample point unless otherwise stated. The scattered light was analyzed by using a multichannel Raman system which consists of a dry ice-cooled silicon-intensified target (SIT) detector, a detector controller, a microprocessor-based OMA 2 console (PAR 1215), and a Spex 1402 0.85-m Czerny-Turner double monochromator. This Raman system has been described in detail previously (24). All the wavenumbers reported here are accurate to ± 1 cm^{-1} for sharp lines and ± 2 cm^{-1} for broad lines.

II. Results

1. High-Frequency Region Spectra

In Figure B-1 are presented two sets of Raman spectra in the 1250-1750 cm^{-1} region: the first set (curves 1 and 2) for HbACO and the second set (curves 3 and 4) for MbCO. Curves 1 and 3 were obtained with a lower laser power (6 mW) than curves 2 and 4 (15 mW). With increasing laser power, intensity increases at 1357 (1357), 1471 (1472), and 1566 (1565) cm^{-1} in the spectra of HbACO (MbCO) whereas the 1586 cm^{-1} line shows an intensity reduction. These Raman intensity changes are due to the formation of deoxy HbA (deoxy Mb) caused by partial photodissociation of bound CO. The deoxy HbA spectrum (Figure B-2, upper panel) excited at the same wavelength support this interpretation; the 1587- cm^{-1} line disappears, and the 1358- and 1473- cm^{-1} lines are dominant in the spectrum. Since the quantum yields for photodissociation of MbCO (0.97) and HbACO (0.46) are high, significant

amounts of deoxy derivatives are expected to be formed upon laser irradiation (25-27). However, closer proximity of the excitation wavelength (406.7 nm) to the Soret band maxima of the carbon monoxy derivatives than to those of the deoxy derivatives gives rise to much stronger Raman scattering intensity in the region below 700-cm^{-1} for carbon monoxy derivatives. With the assumption that the Soret band maxima are very close to the 0-0 origin, the theories of resonance Raman scattering intensity (28) predict somewhat enhanced intensity for deoxy HbA Raman modes in the $1300\text{-}1700\text{-cm}^{-1}$ region because these modes are expected to have their 0-1 excitation profile maxima at 406.7 nm.

Resonance Raman spectra of HbACO (Figure B-1, curve 1) and oxy-HbA (Figure B-2, lower panel) in the $1250\text{-}1750\text{-cm}^{-1}$ region exhibit both similarities and differences. The most noticeable differences occur at $1498 - 1506$, $1633 - 1640$, and $1372 - 1377\text{ cm}^{-1}$.

2. Detection of Bound C-O Stretch

The bound CO internal stretching vibration of HbACO was detected as a single line as shown in Figure B-3. Its frequency shifts from 1951 ($^{12}\text{C}^{16}\text{O}$) to 1908 ($^{13}\text{C}^{16}\text{O}$), 1908 ($^{12}\text{C}^{18}\text{O}$), and 1861-cm^{-1} ($^{13}\text{C}^{18}\text{O}$). The first three frequencies are in good agreement with the results obtained by infrared spectroscopy (1,2,29). The corresponding spectra for sperm whale MbCO are shown in Figure B-4, where the main $\nu(\text{C-O})$ stretch appears at 1944 cm^{-1} with a shoulder near 1933-cm^{-1} in the spectrum of Mb $^{12}\text{C}^{16}\text{O}$. Upon isotope substitution, the main $\nu(\text{C-O})$ stretch shifts to 1896-cm^{-1} (both $^{13}\text{C}^{16}\text{O}$ and $^{12}\text{C}^{18}\text{O}$) and 1850-cm^{-1} ($^{13}\text{C}^{18}\text{O}$), all of them with a shoulder at the lower frequency side.

3. Detection of Fe-CO Stretch and Fe-C-O Bending Frequencies

Lower frequency region spectra of deoxy-HbA and -Mb excited at 406.7 nm are extremely weak and featureless except for lines around 220 cm^{-1} which have been assigned as an Fe-N_E(His F8) stretching vibration in the deoxy state (30). The Raman scattering cross section of the deoxy species is far smaller than that of the carbon monoxy derivatives. Indeed, lower frequency region ($100\text{--}700\text{ cm}^{-1}$) spectra of HbACO and MbCO are almost independent of excitation laser power (10–40 mW). The lower frequency region spectrum of HbA¹²C¹⁶O is dominated by the appearance of a sharp and polarized ($\rho = 0.055$) line at 507 cm^{-1} (Figure B-5), which was noticed by Rimai et al. (1975) with near-Soret excitation (441.6 nm) although they interpreted it as a porphyrin ring mode corresponding to the 485 cm^{-1} line in HbA₂O₂. However, carbon monoxide isotope substitution experiments revealed clearly that this line exhibits a monotonous frequency shift toward lower energy with the mass of carbon monoxide increasing from ¹²C¹⁶O to ¹³C¹⁸O (Figure B-5). In addition, another isotope-sensitive line with much weaker intensity at 578 cm^{-1} for HbA¹²C¹⁶O could be noticed, which shifts to 563 cm^{-1} upon substitution by ¹³C¹⁶O, to 576 cm^{-1} by ¹²C¹⁸O, and to 560 cm^{-1} by ¹³C¹⁸O.

In the spectra of MbCO (Figure B-6), the two isotope-sensitive lines appear at 512 and 577 cm^{-1} . The one at 512 cm^{-1} shows a monotonous frequency shift toward lower energy, whereas the one at 577 cm^{-1} shows "zigzag" frequency shifts in the order ¹²C¹⁶O - ¹³C¹⁶O - ¹²C¹⁸O - ¹³C¹⁸O.

For the Fe-CO stretching vibration, the carbon and oxygen atoms can be treated as a dynamic unit because the C-O stretching force constant

is much larger than the Fe-C stretching force constant. Thus, one would expect that the Fe-CO stretching frequency is simply dependent on the sum of the masses of both carbon and oxygen. Indeed, this appears to be the case for the line at 507- (HbA^{12,16}C¹⁶O) or 512-cm⁻¹ (Mb^{12,16}C¹⁶O). On the other hand, for an Fe-C-O bending mode, the amplitude of vibration of the bound carbon is far greater than that of the terminal oxygen, since the moments of oscillation of these two atoms around the much heavier iron atom must approximately cancel. Therefore, one would predict that the effects of isotope substitution for terminal oxygen upon $\delta(\text{Fe-C-O})$ frequency can be relatively small if compared to those for bound carbon. Accordingly, the Raman line at 578-cm⁻¹ for HbA^{12,16}C¹⁶O and at 577-cm⁻¹ for Mb^{12,16}C¹⁶O are assignable to an Fe-C-O bending mode.

To confirm these assignments, a normal coordinate analysis based on the simplified model; imidazole-Fe-C-O was calculated. The porphyrin ring was neglected in this model because the porphyrin plane is assumed to be perpendicular to the plane containing the fifth and sixth ligands of iron, i.e., imidazole and carbon monoxide. It is further assumed that the out-of-plane porphyrin ring mode is not significantly coupled with ligand-related vibrations. Imidazole was treated as a single dynamical unit with a mass of 68 amu. The structural parameters used in this model are as follows: $r(\text{Fe-Im}) = 2.00 \text{ \AA}$, $r(\text{Fe-C}) = 1.80 \text{ \AA}$, $r(\text{C-O}) = 1.30 \text{ \AA}$, $\phi(\text{Im-Fe-C}) = 167.0^\circ$, and $\phi(\text{Fe-C-O}) = 180.0^\circ$. These numbers are based on the results of X-ray and neutron crystallographic studies on HbACO and MbCO (20,5). The Urey-Bradley force field was used for the potential function, and the force constants used were transferred from similar systems with a slight adjustment for best fit.

These force constants (in mdyn/Å) are $K(\text{Fe-Im}) = 1.33$, $K(\text{Fe-C}) = 2.85$, $K(\text{C-O}) = 15.80$, $H(\text{Im-Fe-C}) = 0.57$, $H(\text{Fe-C-O})_{\text{in plane}} = 0.50$, and $H(\text{Fe-C-O})_{\text{out of plane}} = 0.50$. Stretching-stretching interaction force constants between two adjacent bonds are $F((\text{Im-Fe})-(\text{Fe-C})) = 0.10$ mdyn/Å and $F((\text{Fe-C})-(\text{C-O})) = 1.20$ mdyn/Å. The deformation-deformation interaction between two angles was neglected in the calculations. The normal mode analysis was performed according to Wilson's GF-matrix method (31). There are total of six normal vibrations in this model, and each normal vibration was defined in terms of the following internal coordinate: $R_1 = \nu(\text{Im-Fe})$, $R_2 = \nu(\text{Fe-C})$, $R_3 = \nu(\text{C-O})$, $R_4 = \delta(\text{Im-Fe-C})$, $R_5 = \delta_{\text{in plane}}(\text{Fe-C-O})$, and $R_6 = \delta_{\text{out of plane}}(\text{Fe-C-O})$. Listed in Table B-I are the observed and calculated frequencies. The pattern of isotope shifts for $^{13}\text{C}^{16}\text{O}$, $^{12}\text{C}^{18}\text{O}$, and $^{13}\text{C}^{18}\text{O}$ agrees well between observed and calculated values.

There may be a question of whether the carbon atom indeed binds directly to iron (1). Normal coordinate analysis, based on the model Im-Fe-O-C, has been performed with its results also listed in Table B-I. The structural parameters are the same except for the exchange of carbon and oxygen. To fit the experimentally observed frequencies, following force constants were used (in mdyn/Å): $K(\text{Fe-Im}) = 1.33$, $K(\text{Fe-O}) = 2.60$, $K(\text{O-C}) = 15.80$, $H(\text{Im-Fe-O}) = 0.57$, $H(\text{Fe-O-C})_{\text{in plane}} = 1.1$, $H(\text{Fe-C-O})_{\text{out of plane}} = 1.1$, $F((\text{Im-Fe})-(\text{Fe-O})) = 0.1$, and $F((\text{Fe-O})-(\text{O-C})) = 1.2$. It is readily seen that the isotope shifts for ν_2 (Table B-I) based on this model do not agree with the observed ones. This may be taken as independent evidence that carbon rather than oxygen binds directly to iron in HbACO and MbCO.

Careful examination of lower frequency region spectra reveals additional important information. (1) The line width of the $\nu(\text{Fe-CO})$ mode in MbCO is considerably greater than that of HbACO, indicating multiple $\nu(\text{Fe-CO})$ stretching frequencies, consistent with the multiple $\nu(\text{C-O})$ stretching frequencies observed by IR spectroscopy and in the present Raman study. Multiple $\nu(\text{C-O})$ frequencies have been ascribed to three heme-carbonyl conformers due to different local environments of the iron-carbonyl group (4). (2) The porphyrin ring mode at 586 cm^{-1} in Mb^{12,16}C¹⁶O and Mb^{12,18}C¹⁸O exhibits an anomalous intensity increase (see Figure B-6) which is presumably caused by being too close to the $\delta(\text{Fe-C-O})$ bending vibration at 576 cm^{-1} (weak resonance interaction, resulting in intensity borrowing).

4. Quaternary Structure Change

The effect of quaternary structure change on the strength of the Fe-ligand bond is of particular importance in understanding the nature of cooperative oxygen binding to hemoglobin. In the absence of bonding geometry change, the Fe-ligand stretching frequency is a measure of the Fe-ligand bond strength. Here, the influence of the quaternary structure change on $\nu(\text{Fe-CO})$ in HbCO was examined, which may be considered as an ideal model for oxyhemoglobin. Human oxy HbA and HbACO are known to be in the R structure even in the presence of inositol hexaphosphate (IHP) (32). In Figure B-7, the resonance Raman spectra ($100\text{--}700\text{ cm}^{-1}$) of HbACO at pH 8.3 (upper spectrum), 6.0 (middle spectrum), and 6.0 with IHP (lower spectrum) were presented. These three spectra are essentially identical, i.e., no noticeable changes (within $\pm 1\text{ cm}^{-1}$) in $\nu(\text{Fe-CO})$ and $\delta(\text{Fe-C-O})$. Examination of the

$\nu(\text{C-O})$ mode at 1951 cm^{-1} under the same conditions also revealed no detectable changes, as expected. Somewhat unexpected was the observation that addition of IHP also produced no detectable effect on the HbCO Kansas spectrum (Figure B-8), although Kincaid et al. (33) reported a small decrease (0.7 cm^{-1}) in the IR $\nu(\text{C-O})$ frequency. Hb Kansas is an interesting human Hb variant whose quaternary structure can be switched in its ligated forms from the R to the T state by IHP (34-37). Under present experimental conditions (heme concentration $100\text{ }\mu\text{M}$), some dimer formation (as much as 50 %) may be expected (38).

However, the absence of asymmetric line broadening at 507 cm^{-1} led us to conclude that the $\nu(\text{Fe-CO})$ vibration (hence the Fe-C bond strength) is the same in both R and T forms. Thus, no significant change in either Fe-C or C-O bond energy is induced by switching the quaternary structure from the R to the T form in HbCO Kansas. The absence of bond tension between the iron atom and the proximal histidine is also suggested (see Discussion).

Carp Hb is another interesting hemoglobin which is a mixture of three components; its quaternary structure in the ligated state can also be converted to the T structure upon addition of IHP at lower pH, even in relatively low protein concentration, and the addition of IHP stabilizes the ligated molecule completely in the T structure (22,39-41). In Figure B-9 are shown the spectra ($100\text{--}700\text{ cm}^{-1}$) of carp HbCO at pH 8.3 and 6.0 with IHP. Without IHP, the $\nu(\text{Fe-CO})$ mode at 508 cm^{-1} exhibited a very slight broadening when the pH was changed from 8.3 to 6.0. However, the addition of IHP (2.4 mM) at pH 6.0 induced a more pronounced broadening on the lower energy side of the $\nu(\text{Fe-CO})$ mode (see Figure B-9, upper panel). The results suggest the presence of a

new conformer (or conformers). To make sure that this broadening was not caused by partial oxidation of the heme, resonance Raman spectra of carp aquomet Hb with IHP at pH 6.0 were measured for comparison (Figure B-9, lower panel). In addition, three components of carp Hb (denotes as fractions A, B, and C following the notation of Tan et al.(22)) were separated and examined for their resonance Raman spectra. It is concluded that the broadening of the $\nu(\text{Fe-CO})$ stretching from R to the T state is common to all three components. Figure B-10 shows only results from fractions A and B.

III. Discussion

1. Porphyrin Ring Vibrations

Soret and Q (α and β) absorption bands are due to $\pi-\pi^*$ transitions in the porphyrin from the a_{1u} and a_{2u} to the e_g^* orbitals (42,42), and the $a_{1u}-e_g^*$ and $a_{2u}-e_g^*$ transitions have similar transition dipoles so that their intrinsic intensities before mixing are also similar. Since the two transition moments belong to the same representation of the symmetry group (E_u), these two states can be mixed by configuration interaction. Of the two new excited states, the higher energy state generates the Soret band while the lower energy state gives rise to the Q (α and β) bands. Based on symmetry, e_g^* can interact with the d_π (d_{xz} and d_{yz}) orbitals through back-donation, and as a result, charge is transferred from the metal orbital to the porphyrin π^* orbitals.

Although the gross electronic structure of heme is similar in HbCO and oxy Hb, the frequencies and relative intensities of the

corresponding lines are somewhat different, as first noticed by Rimai et al. (19). Several porphyrin ring modes (1372, 1471, 1498, and 1633 cm^{-1}) in the spectrum of HbACO exhibit lower frequencies than those corresponding modes (1377, 1473, 1506, and 1640 cm^{-1}) in the oxy Hb spectrum. This may be explained by the extent of the $d_{\pi}(\text{Fe}) - \pi^*(\text{porphyrin})$ interaction; the frequencies are raised when the axial ligands are replaced by better π acceptors, which compete with the porphyrin π^* orbitals for the $d_{\pi}(\text{Fe})$ electrons.

Since the lowest empty orbital of CO is relatively higher than $\pi^*(\text{O}_2)$ orbitals in energy, the interaction between $d_{\pi}(\text{Fe})$ and $\pi^*(\text{CO})$ is weaker than that between $d_{\pi}(\text{Fe})$ and $\pi^*(\text{O}_2)$, causing stronger interaction between $d_{\pi}(\text{Fe})$ and $\pi^*(\text{porphyrin})$. Thus, the resulting higher electron population in π^* porphyrin orbitals leads to lower frequencies of porphyrin ring modes in HbCO.

2. Fe-CO Stretching Vibration

Through the $d_{\pi}(\text{Fe}) - \pi^*(\text{porphyrin})$ orbital interaction, the electronic excitation at the porphyrin ring by the illumination of laser light at the Soret or Q (α and β) bands can affect the $d_{\pi}(\text{Fe}) - \pi^*(\text{ligand})$ interaction indirectly, leading to the photodissociation of the sixth ligand. The external ligands such as NO, CO, O_2 , or alkyl isocyanides are bound to heme iron(II) through the $d_{\pi}(\text{Fe}) - \pi^*(\text{ligand})$ interaction in addition to the $d_z^2(\text{Fe}) - \pi^*(\text{ligand})$ interaction (44,45), whereas ligands such as CN, N_3 , and imidazole ligate to the heme iron(III) almost entirely by the $d_z^2(\text{Fe}) - \text{lone-pair}(\text{ligand})$ interaction. Thus, "ferric like" reduced hexacoordinated Hbs (such as oxy Hb, HbCO, and HbNO) are known to be photodissociable more or less,

while low-spin oxidized derivatives are photoinsensitive. The difference in photodissociability among oxy Hb, HbCO, HbNO, Hb-(alkyl isocyanide) is presumably due to the relative degree of contribution of the $d_{\pi}(\text{Fe}) - \pi^*(\text{ligand})$ interaction in the Fe-ligand bond. As mentioned in the preceding section, the absolute strength of the $d_{\pi}(\text{Fe}) - \pi^*(\text{CO})$ interaction itself is smaller than that of the $d_{\pi}(\text{Fe}) - \pi^*(\text{O}_2)$ interaction, but the $d_{z^2}(\text{Fe}) - \text{lone-pair}(\text{ligand})$ interaction, which is a primary interaction in the Fe-O₂ bond, is so weak in the Fe-CO bond because of bonding geometry that the contribution of the $d_{\pi}(\text{Fe}) - \pi^*(\text{CO})$ interaction in the Fe-CO bond is much larger than that of $d_{\pi}(\text{Fe}) - \pi^*(\text{O}_2)$ in the Fe-O₂ bond. Indeed, this may be the reason why HbCO is the most photodissociable among the ferric-like reduced hexacoordinated Hbs.

Since O₂ is both a better π acceptor and σ donor than CO, one would expect a stronger Fe-O bond. This is consistent with the observation that the $\nu(\text{Fe-O}_2)$ stretching frequency (570-cm^{-1}) is higher than the $\nu(\text{Fe-CO})$ stretching frequency ($507\text{-}512\text{-cm}^{-1}$). (Comparison of force constants for Fe-C and Fe-O bonds in hemoglobin is difficult because of the uncertainty in CO bonding geometry. However, in the Fe(II) "picket fence" system, the force constants are estimated as 2.61 mdyn/\AA for the Fe-O bond and 2.51 mdyn/\AA for the Fe-C bond.) This may seem paradoxical since the affinity for CO is much higher than that for O₂. The difficulty is removed when one considers the charge reorganization among several bonds (i.e., C-O bond, Fe-proximal histidine, and porphyrin skeleton) upon ligand binding. Since the overall free-energy change associated with ligand binding, which determines the binding affinity, is not localized at the iron-ligand bond, the iron-ligand bond

strength alone may not be a good indication of binding affinity. In fact, Kerr et al. (46) found that the $\nu(\text{Fe-CO})$ for low-affinity $\text{Fe}^{2+}(\text{TpivPP})(1,2\text{-Me}_2\text{Im})$ is higher than that for the high-affinity $\text{Fe}^{2+}(\text{TpivPP})(1\text{-MeIm})$, whereas the $\nu(\text{Fe-O}_2)$ is lower for the low-affinity heme.

Preliminary studies of excitation profiles of the Fe-ligand stretching modes such as $\nu(\text{Fe-O}_2)$, $\nu(\text{Fe-CO})$, and $\nu(\text{Fe-NO})$ revealed that these modes can be enhanced everywhere from the Soret to the Q band, and their Raman intensities follow the profiles of visible absorption spectra. This phenomenon can be easily understood if one considers the importance of the $d_{\pi}(\text{Fe})-\pi^*(\text{ligand})$ interaction which is indirectly influenced by the electronic configuration change in the porphyrin ring through the $d_{\pi}(\text{Fe})-\pi^*(\text{porphyrin})$ interaction. Laser excitation into the $\pi-\pi^*$ porphyrin transition may lead to the elongation (or dissociation) of the Fe-CO bond in the excited state, which should be effective in shifting the origin of the potential energy curve along this coordinate. Thus, through the Franck-Condon scattering mechanism, one could observe the resonance enhancement of the Fe-CO stretching vibration (28). In this regard, the strong Raman intensity of the Fe-CO stretching mode might be a good indicator for the extent of the relative contribution of the $d_{\pi}(\text{Fe})-\pi^*(\text{CO})$ interaction in the Fe-CO bond.

3. Fe-C-O Bending Vibration

The $\delta(\text{Fe-C-O})$ bending vibration at 577 cm^{-1} detected in our present study of HbCO and MbCO adds an interesting dimension to the CO binding studies. Both intensity and frequency are expected to be sensitive to

the CO bonding geometry, i.e., linear perpendicular, linear tilted, or bent with varying Fe-C-O angles. At present, there are still some questions about the detailed Fe-CO geometry in carbon monoxy hemoproteins (47-50,20). Resonance Raman techniques may become a powerful tool to probe the exact nature of the bending or tilting of the coordinated CO ligand.

Another interesting aspect of the δ (Fe-C-O) bend is its position relative to the ν (Fe-CO) stretch. In MbCO and HbCO, the δ (Fe-C-O) bend appears at 577-cm^{-1} , which is higher than the ν (Fe-CO) stretch at 510-cm^{-1} . However, in a nonheme Fe-CO system, it is known that the δ (Fe-C-O) frequency is lower than the ν (Fe-CO) frequency (51).

4. Carp HbCO and Quaternary Structure Change

At neutral pH, carp Hb exhibits the usual cooperative ligand binding, characteristic of the T - R quaternary structure transition. At lower pH (6.0), in the presence of organic phosphate such as IHP, both liganded and unliganded derivatives adopt the T structure according to equilibrium and kinetic studies (22,39-41). Thus, this Hb provides a good opportunity for examining the effects of quaternary structure change on heme-associated vibrations, particularly the iron-ligand stretching mode by resonance Raman spectroscopy.

The iron-ligand stretching frequency provides the most valuable and direct information about the nature of the heme-ligand interaction. This frequency is expected to respond to any changes in electron donation to the iron. Of particular interest is the sensitivity of this vibration to bond tension between the iron atom and the proximal histidine. Kerr et al. (46) studied the effect of proximal tension on

the $\nu(\text{Fe-CO})$ frequency in the CO complexes of Fe(II) "picket fence" porphyrin, $\text{Fe}^{2+}(\text{TpivPP})$. When the proximal base is changed from 1-methylimidazole (unhindered) to 1,2-dimethylimidazole (sterically hindered), the $\nu(\text{Fe-CO})$ increases from 489 to 496-cm^{-1} (in benzene). In the case of oxy complexes, they found a reverse effect; i.e., the proximal tension is to decrease the $\nu(\text{Fe-O}_2)$ from 571 to 565 cm^{-1} (also in benzene). This confirms the earlier report by Walters et al. (52) that there is a 4-cm^{-1} difference in $\nu(\text{Fe-O}_2)$ between $\text{Fe}^{2+}(\text{TpivPP})(1\text{-MeIm})(\text{O}_2)$ and $\text{Fe}^{2+}(\text{TpivPP})(1,2\text{-Me}_2\text{Im})(\text{O}_2)$ (in CH_2Cl_2). In contrast, Hori and Kitagawa (53) found the insensitivity of $\nu(\text{Fe-O}_2)$ to such a proximal tension in the same heme system.

Carbon monoxide is an excellent resonance Raman visible ligand for studying the effects of quaternary structure change because the $\nu(\text{Fe-CO})$ stretching mode is very strong in the resonance Raman spectra. The observed asymmetric broadening on the lower energy side of the $\nu(\text{Fe-CO})$ mode in the T state of carp HbCO (see Figure B-9) is a very interesting phenomenon. What can be the cause of this broadening? We could definitely rule out the possibilities of partial oxidation, contribution of deoxy species, and the formation of intermediate of photoproducts. The spectral features are independent of laser power (5-30 mW), the addition of excess sodium dithionite, and the rotating speed of our Raman cell (500-2000 rpm). It appears that in the T-state carp HbCO, there is a small fraction of minor conformer (or conformers) with weaker Fe-CO bond or a somewhat different CO distortion in equilibrium with the major conformer which has the same Fe-CO bond as in the R-state. If the broadening were caused by the proximal base tension, one would expect it to appear on the higher energy side instead

of the lower energy side as is actually observed. This implies that there is no appreciable Fe-N_ε(Hi F8) bond tension in the T-state carp HbCO. At present, no complete data are available on the factors affecting the $\nu(\text{Fe-CO})$ frequency. However, recent studies on "strapped" hemes with steric hindrance on the distal side (54) revealed that the $\nu(\text{Fe-CO})$ frequency is lower with less CO distortion (55).

Additional evidence for the absence of localized bond tension in the T-state Hb is provided by the work of Nagai et al. (30,56), who observed that the $\nu(\text{Fe-O}_2)$ frequency is the same between the R-state (oxy HbA) and the T-state (oxy Hb Kansas and oxy HbM Milwaukee in the presence of IHP at low pH). Comparison of $\nu(\text{Fe-O}_2)$ in the R and T states of carp Hb is difficult because carp oxy Hb is readily oxidized in the presence of IHP at lower pH (57). Present studies on the T-state HbCO Kansas (Figure B-8) also indicate the absence of localized bond tension between the heme iron and proximal histidine.

Finally, the insensitivity of the iron-ligand vibration to quaternary structure change was also found in carp cyanomet-Hb. The $\text{Fe}^{3+}\text{-CN}$ stretching vibration, identified at 455-cm^{-1} by the isotope substitution, did not exhibit any noticeable change upon R - T conversion. However, we do not know at present if the $\nu(\text{Fe-CN})$ frequency is sensitive to the proximal base tension.

References

1. Alben, J.O., and Caughey, W.S. (1968) *Biochemistry* 7, 175.
2. Caughey, W.S., Alben, J.O., McCoy, S., Boyer, S.H., Charache, S., and Hathaway, P. (1969) *Biochemistry* 8, 59.
3. Tucker, P.W., Phillips, S.E.V., Perutz, M.F., Houtchens, R.A., and Caughey, W.S. (1978) *Proc. Natl. Acad. Sci. USA* 76, 1076.
4. Makinen, M.W., Houtchens, R.A., and Caughey, W.S. (1979) *Proc. Natl. Acad. Sci. USA* 76, 6042.
5. Norvell, J.C., Nunes, A.C., and Schoenborn, B.P. (1975) *Science* 190, 568.
6. Yu, N.-T. (1977) *CRC Crit. Rev. Biochem.* 4, 229.
7. Brunner, H. (1974) *Naturewissenschaften* 61, 129.
8. Chottard, G., and Mansuy, D. (1977) *Biochem. Biophys. Res. Commun.* 77, 5849.
9. Asher, A.S., Vickery, L.E., Schuster, T.M., and Sauer, K. (1977) *Biochemistry* 16, 5849.
10. Tsubaki, M., Srivastava, R.B., and Yu, N.-T. (1981) *Biochemistry* 20, 946.
11. Wright, P.G., Stein, P., Burke, J.M., and Spiro, T.G. (1979) *J. Am. Chem. Soc.* 101, 3531.
12. Yu, N.-T., and Tsubaki, M. (1980) *Biochemistry* 19, 4647.
13. Woodruff, W.H., and Farquharson, S. (1978) *Science* 201, 833.
14. Dallinger, R.F., Nestor, J.R., and Spiro, T.G. (1978) *J. Am. Chem. Soc.* 100, 6252.
15. Lyons, K.B., Friedman, J.M., and Flenry, P.A. (1978) *Nature* 275, 566.
16. Coppey, M., Tourbez, H., Valat, P. and Alpert, B. (1980) *Nature* 284, 568.

17. Friedman, J.M., and Lyons, K.B. (1980) *Nature* 284, 570.
18. Turner, J., Spiro, T.G., Nagumo, M., Nicol, M.F., and El-Sayed, M.A. (1980) *J. Am. Chem. Soc.* 102, 3238.
19. Rimai, L., Salmeen, I., and Petering, D.H. (1975) *Biochemistry* 14, 378.
20. Baldwin, J.M. (1980) *J. Mol. Biol.* 136, 103.
21. Kilmartin, J.V., Hewitt, J.A., and Wooton, J.F. (1975) *J. Mol. Biol.* 93, 203.
22. Tan, A.L., De Young, A., and Noble, R.W. (1972) *J. Biol. Chem.* 247, 2493.
23. Nozaki, Y., and Tanford, C. (1967) *Methods in Enzymology* 11, 733.
24. Yu, N.-T., and Srivastava, R.B. (1980) *J. Raman Spectrosc.* 9, 166.
25. Stanford, M.A., Swartz, J.C., Phillips, T.E., and Hoffman, B.M. (1980) *J. Am. Chem. Soc.* 102, 4492.
26. Noble, J.C., Brunori, M., Wyman, J., and Antonini, E. (1967) *Biochemistry* 6, 1216.
27. Sawicki, C.A., and Gibson, Q.H. (1979) *J. Biol. Chem.* 254, 4058.
28. Felton, R.H., and Yu, N.-T. (1978) in "The Porphyrins" (D. Dolphin, ed.) vol. III, Chapter VIII, Academic Press, New York.
29. Satterlee, J.D., Teintze, M., and Richards, J.H. (1978) *Biochemistry* 17, 1457.
30. Nagai, K., Kitagawa, T., and Morimoto, H. (1980) *J. Mol. Biol.* 136, 271.
31. Wilson, E.B., Jr., Decius, J.C., and Cross, P.C. (1955) "Molecular Vibrations" McGraw-Hill, New York.
32. Perutz, M.F., Kilmartin, J.V., Nagai, K., Szabo, A., and Simon, S.R. (1976) *Biochemistry* 15, 378.
33. Kincaid, J.R., Spiro, T.G., Valentine, J.S., Saperstein, D.D., and

- Rein, A.J. (1979) *Inorg. Chim. Acta* 33, L181.
34. Ogawa, S., Mayer, A., and Shulman, R.G. (1972) *Biochem. Biophys. Res. Commun.* 49, 1485.
35. Gibson, Q.H., Riggs, A., and Inamura, T. (1973) *J. Biol. Chem.* 248, 5876.
36. Anderson, L. (1975) *J. Mol. Biol.* 94, 33.
37. Kilmartin, J.V., Anderson, N.L., and Ogawa, S. (1978) *J. Mol. Biol.* 123, 71.
38. Atha, D.H., Johnson, M.L., and Riggs, A.F. (1979) *J. Biol. Chem.* 254, 12390.
39. Tan, A.L., Noble, R.W., and Gibson, Q.H. (1973) *J. Biol. Chem.* 248, 2880.
40. Tan, A.L., and Noble, R.W. (1973) *J. Biol. Chem.* 248, 7412.
41. Pennelly, R.R., Tan-Wilson, A.L., and Noble, R.W. (1975) *J. Biol. Chem.* 250, 7239.
42. Gouterman, M. (1961) *J. Mol. Spectrosc.* 6, 138.
43. Zerner, M., Gouterman, M., and Kobayashi, H. (1966) *Theor. Chim. Acta* 6, 363.
44. Kitagawa, T., Kyogoku, Y., Iizuka, T., and Saito, M.I. (1976) *J. Am. Chem. Soc.* 98, 5169.
45. Tsubaki, M., and Yu, N.-T. (1981) *Proc. Natl. Acad. Sci. USA* 78, 3581.
46. Kerr, E.A., Mackin, H.C., and Yu, N.-T. (1983) *Biochemistry* 22, 4373.
47. Huber, R., Epp, O., and Formanek, H. (1970) *J. Mol. Biol.* 52, 349.
48. Heidner, E.J., Ladner, R.C., and Perutz, M.F. (1976) *J. Mol. Biol.* 104, 707.
49. Steigemann, W., and Weber, E. (1979) *J. Mol. Biol.* 127, 309.
50. Padlan, E.A., and Love, W.E. (1975) *J. Biol. Chem.* 249, 4067.

51. Kroeker, R.M., Hansma, P.K., and Kaska, W.C. (1980) J. Chem. Phys. 72, 4845.
52. Walters, M.A., Spiro, T.G., Suslick, K.S., and Collman, J.P. (1980) J. Am. Chem. Soc. 102, 6857.
53. Hori, H., and Kitagawa, T. (1980) J. Am. Chem. Soc. 102, 3608.
54. Ward, B., Wang, C.B., and Chang, C.K. (1981) J. Am. Chem. Soc. 103, 5236.
55. Yu, N.-T., Kerr, E.A., Ward, B., and Chang, C.K. (1983) Biochemistry 22, 4534.
56. Nagai, K., Enoki, Y., and Kitagawa, T. (1980) Biochim. Biophys. Acta 624, 304.
57. Mayo, K.H., and Chien, J.C.W. (1979) Biochim. Biophys. Acta 581, 44.

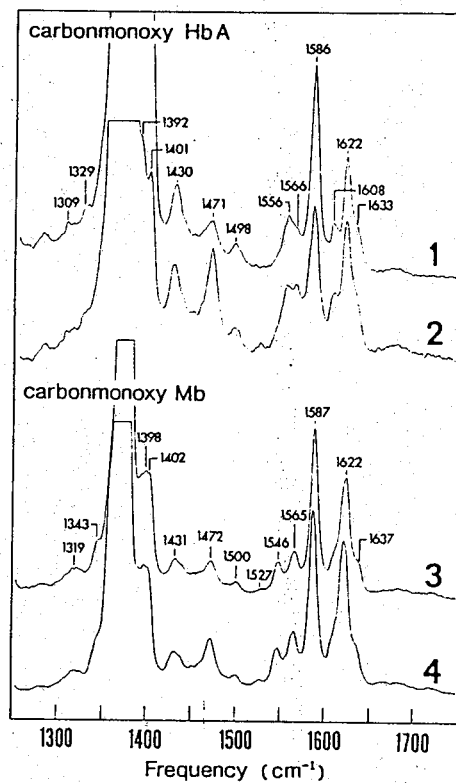


Figure B-1. Higher frequency region (1250–1750 cm^{-1}) spectra of (carbon monoxy)HbA (upper portion) and (carbon monoxy)Mb (lower portion). Conditions were the following: excitation wavelength, 406.7 nm; laser power, 5, 20, 7.5, and 12.5 mW at the sample in descending order (curves 1 \rightarrow 4); slit width, 100 μm ; slit height, 0.2 cm; delay, 10 000 (303 s). Sample conditions were $\sim 60 \mu\text{M}$ (carbon monoxy)HbA or -Mb (heme basis) in 0.05 M Tris-HCl, pH 8.4, buffer.

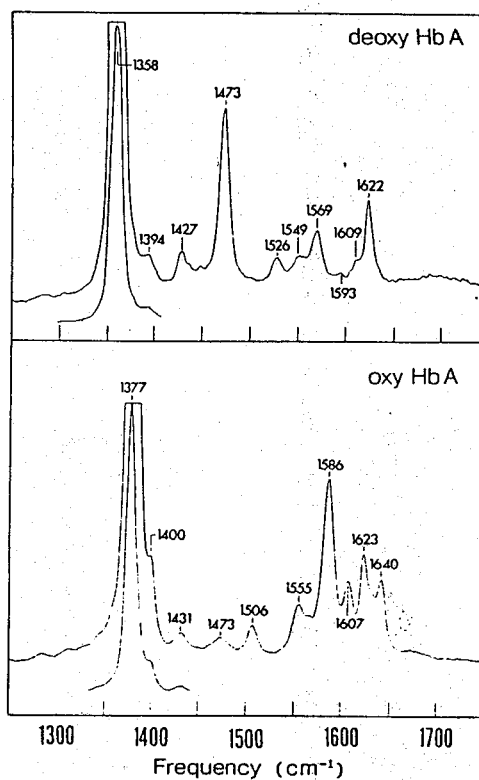


Figure B-2. Higher frequency region (1250–1750 cm^{-1}) spectra of deoxy-HbA (upper panel) and oxy-HbA (lower panel). Conditions are the same as in Figure 1, except for the excitation laser powers which are 15 mW for deoxy-HbA and 18 mW for oxy-HbA.

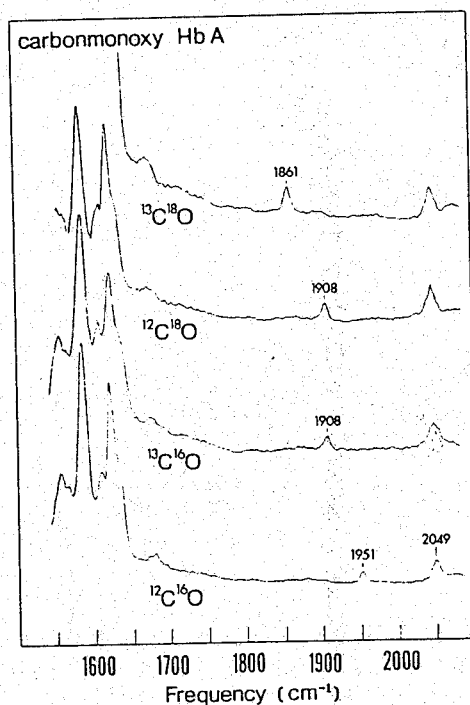


Figure B-3. Carbon monoxide isotope effects on higher frequency region (1500–2100 cm^{-1}) spectra of (carbon monoxy)HbA. The spectra are arranged in the order of masses of carbon monoxide isotopes. Conditions are the same as in Figure 1 except for the excitation laser power, which is 10 mW.

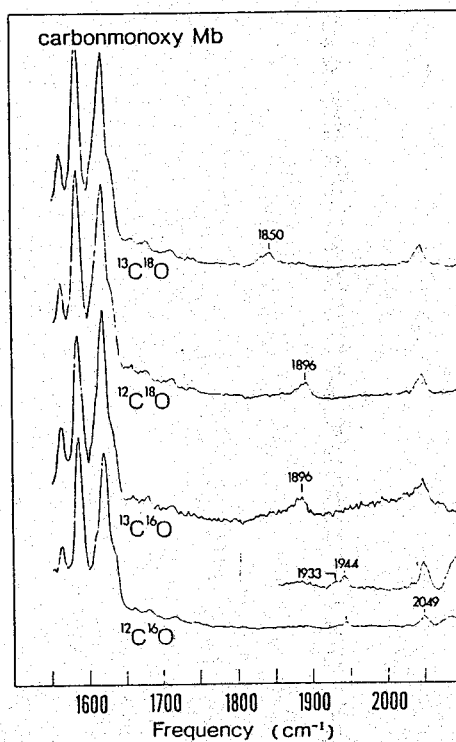


Figure B-4. Carbon monoxide isotope effects on higher frequency region (1500–2100 cm^{-1}) spectra of (carbon monoxy)Mb. The spectra are arranged in the order of masses of carbon monoxide isotopes. Conditions are the same as in Figure 1 except for the excitation laser power, which is 10 mW.

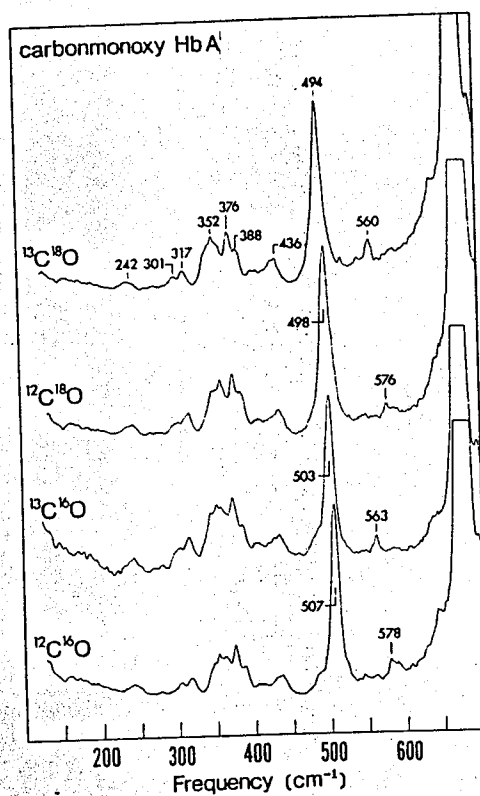


Figure B-5. Carbon monoxide isotope effects on lower frequency region (100–700 cm⁻¹) spectra of (carbon monoxy)HbA. The spectra are arranged in the order of masses of carbon monoxide. Other conditions are the same as in Figure 1.

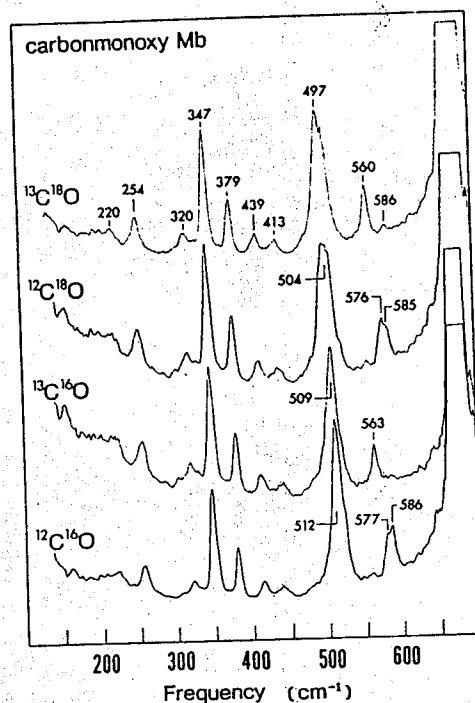


Figure B-6. Carbon monoxide isotope effects on lower frequency region (100–700 cm⁻¹) spectra of (carbon monoxy)Mb. The spectra are arranged in the order of masses of carbon monoxide isotopes. Other conditions are the same as in Figure 1.

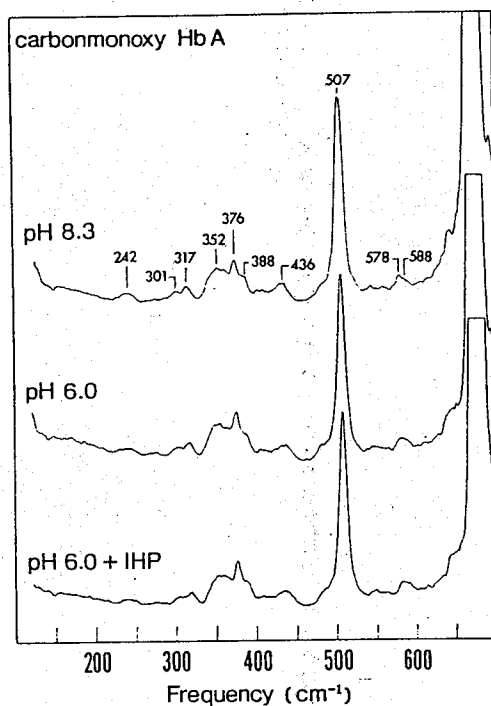


Figure B-7. pH and IHP effects on the lower frequency region (100–700 cm^{-1}) spectra of (carbon monoxy)HbA. Conditions were $\sim 60 \mu\text{M}$ (carbon monoxy)HbA (heme basis) in 0.05 M Tris-HCl, pH 8.4, buffer (upper spectrum), 0.05 M citrate-phosphate, pH 6.0, buffer (middle spectrum), and 0.05 M citrate-phosphate, pH 6.0, buffer in the presence of IHP (10 mM) (lower spectrum). Other conditions are the same as in Figure 1.

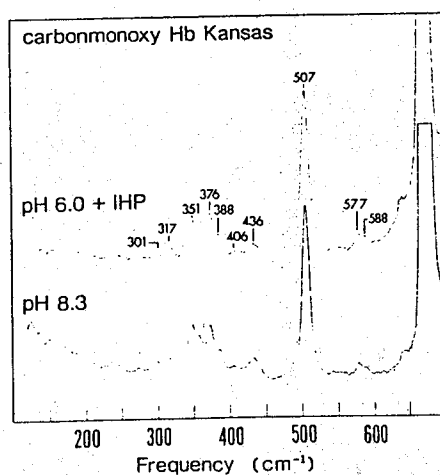


Figure B-8. pH and IHP effects on the lower frequency region (100–700 cm^{-1}) spectra of (carbon monoxy)Hb Kansas. Conditions were $\sim 100 \mu\text{M}$ (carbon monoxy)Hb Kansas (heme basis) in 0.05 M citrate-phosphate, pH 6.0, buffer in the presence of IHP (10 mM) (upper spectrum) and 0.05 M Tris-HCl, pH 8.4, buffer (lower spectrum). Other conditions are the same as in Figure 1.

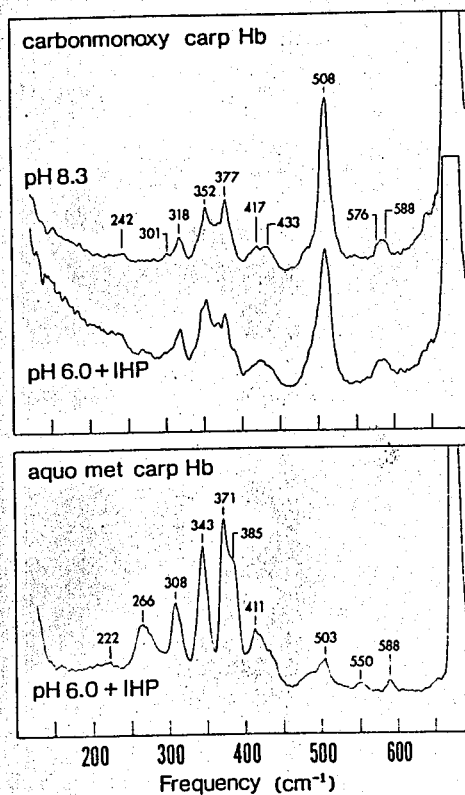


Figure B-9. pH and IHP effects on the lower frequency region ($100\text{--}700\text{ cm}^{-1}$) spectra of carp (carbon monoxide)Hb (upper panel). Conditions were $\sim 60\text{ }\mu\text{M}$ carp (carbon monoxide)Hb (heme basis) in 0.05 M Tris-HCl, pH 8.4, buffer (upper spectrum) and 0.05 M citrate-phosphate, pH 6.0, buffer in the presence of IHP (2.4 mM) (lower spectrum). Other conditions are the same as in Figure 1. Lower frequency region ($100\text{--}700\text{ cm}^{-1}$) spectra of carp aquomet-Hb in 0.05 M citrate-phosphate, pH 6.0, buffer in the presence of IHP (2.5 mM). Other conditions are the same as in Figure 1 (lower panel).

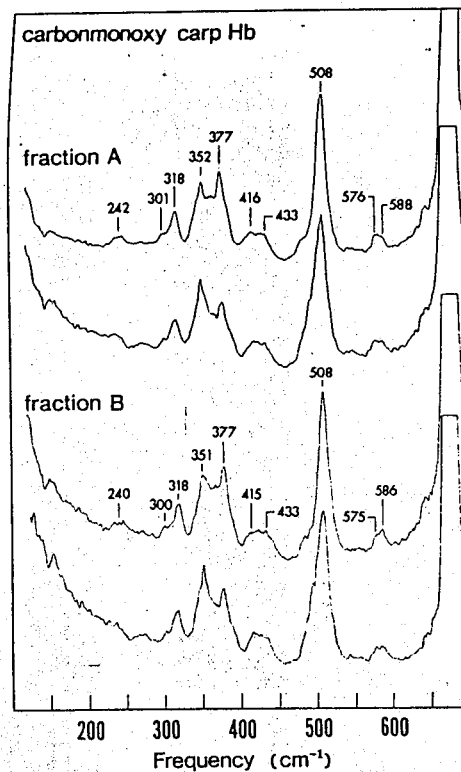
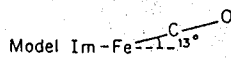
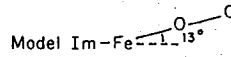


Figure B-10. pH and IHP effects on lower frequency region ($100\text{--}700\text{ cm}^{-1}$) spectra of carp (carbon monoxide)Hb fraction A (upper portion) and fraction B (lower portion). Conditions were $60\text{ }\mu\text{M}$ carp (carbon monoxide)Hb (heme basis) in 0.05 M Tris-HCl, pH 8.4, buffer (upper spectra of each portion) and in 0.05 M citrate-phosphate, pH 6.0, buffer in the presence of IHP (2.5 mM) (lower spectra of each portion). Other conditions are the same as in Figure 1.

Table B-I. Comparison of Observed and Calculated Frequencies in HbCO

no.	$^{12}\text{C}^{16}\text{O}$	$^{13}\text{C}^{16}\text{O}$ (shift)	$^{12}\text{C}^{18}\text{O}$ (shift)	$^{13}\text{C}^{18}\text{O}$ (shift)	assignment ^a
(A) Observed Frequencies (cm^{-1})					
ν_1	1951	1908 (43)	1908 (43)	1861 (90)	$\nu(\text{C-O})$
ν_2	578	563 (15)	576 (2)	560 (18)	$\delta(\text{Fe-C-O})$
ν_3	507	503 (4)	498 (9)	494 (13)	$\nu(\text{Fe-C})$
(B) Calculated Frequencies (cm^{-1}), Based on the					
<div style="text-align: center;">  <p>Model Im-Fe-C-O 13°</p> </div>					
ν_1	1948	1904 (44)	1905 (43)	1858 (90)	
ν_2	579	561 (18)	574 (5)	556 (23)	
ν_3	507	502 (5)	496 (11)	491 (16)	
(C) Calculated Frequencies (cm^{-1}), Based on the					
<div style="text-align: center;">  <p>Model Im-Fe-O-C 13°</p> </div>					
ν_1	1947	1904 (43)	1899 (48)	1856 (91)	
ν_2	576	570 (6)	554 (22)	548 (28)	
ν_3	506	501 (5)	495 (11)	490 (16)	
^a $\nu(\text{A-B})$, stretching of bond A-B; $\delta(\text{A-B-C})$, bending of bond angle A-B-C.					

Part C. Resonance Raman Detection of a $\nu(\text{Fe-CO})$ Stretching Frequency in
Cytochrome P-450_{scc}¹

0. Introduction

Resonance Raman spectroscopy is a powerful technique for probing the oxygen binding site of hemoproteins (1,2) as mentioned in Part A. Although the use of carbon monoxide, a competitive inhibitor for oxygen-binding hemoproteins, in resonance Raman spectroscopy had been limited to pulse laser transient kinetic studies due to its photodissociability, recently it has become available as the ligand for continuous-wave (CW) laser-excited resonance Raman study. Tsubaki et al.(3) first demonstrated the feasibility of obtaining high-quality resonance Raman spectra of HbCO (and MbCO), which contain negligible contribution from photolyzed species. With the excitation wavelength at Soret band, three Raman lines, which are sensitive to CO isotope substitution, could be observed simultaneously at 507(512), 578(577), and 1951(1944) cm^{-1} ; and each line is assignable to the $\nu(\text{Fe-CO})$ stretching, the $\delta(\text{Fe-C-O})$ bending, and the bound $\nu(\text{C-O})$ stretching

Footnotes

¹ Abbreviations: cytochrome P-450_{scc}, mitochondrial cytochrome P-450 which catalyzes the cholesterol side chain cleavage reaction to form pregnenolone; cytochrome P-450_{cam}, the camphor-hydroxylating cytochrome P-450 isolated from Pseudomonas putida.

frequencies, respectively. (These observations were described in detail in Part B.) Thus, CO is an ideal ligand of choice for resonance Raman study of oxygen-binding site in hemoproteins.

Cytochrome P-450 is an unique family in the class of iron protoporphyrin IX-containing hemoproteins, because its ferrous-carbonyl complex has a Soret band maximum around 450 nm, which is approximately 30 nm longer than that observable for the other members of this class (4,5). This anomaly had been ascribed to the cysteinyl heme axial ligand trans to CO (6-9). Actually this Fe-S bond was detected by resonance Raman spectroscopy using isotopically labeled (^{54}Fe and ^{34}S) samples of the oxidized cytochrome P-450_{cam}-substrate complex (10). Moreover this $\nu(\text{Fe-S})$ stretching mode observed at 351-cm^{-1} disappears upon depletion of the substrate, indicating that the substrate binding produces a significant change in the Fe-S interaction (10).

The present study was conducted to probe, by resonance Raman spectroscopy, the dioxygen binding site of cytochrome P-450_{scc} using CO as the observable ligand. Cytochrome P-450_{scc} exists in mitochondrial inner membrane of adrenal cortex and catalyzes the cholesterol side chain cleavage reaction to form pregnenolone ("scc" stands for side chain cleavage).

I. Experimental

1. Preparation of Cytochrome P-450_{scc}

Cytochrome P-450_{scc} was isolated and purified from bovine adrenocortical mitochondria according to the method as described in part D. The purified preparation was homogenous upon SDS-polyacrylamide

gel electrophoresis (11) and its monomeric molecular weight value was estimated to be 50,000. The heme content was 20.0 nmoles/mg protein. Amino acid composition of this preparation was essentially the same as Ogishima et al. (12). The NH_2 -terminal sequence was determined by automated Edman degradation on a gas-phase protein sequencer (Applied Biosystems, Model 470A) and the sequence coincided with that of Ogishima et al. (12) up to 15 cycles. The enzymatic activity of the side-chain cleavage of cholesterol was determined by the method of Ando and Horie (13). The specific activity was 10.0 nmoles/min/nmol of cytochrome P-450_{scc}. The concentration of cytochrome P-450_{scc} was calculated from the CO difference spectra of the reduced enzyme, using the extinction coefficient of $91.0 \text{ mM}^{-1} \text{ cm}^{-1}$ between 448 and 490 nm (5). All spectral measurements were performed in 200 mM potassium phosphate buffer (pH 7.4), 20% (v/v) glycerol, 0.1% Emulgen 913, 0.25% sodium cholate and 0.1 mM EDTA.

2. Preparation of Carbon monoxide Form of Cytochrome P-450_{scc}

Reduction of cytochrome P-450_{scc} was performed in a cylindrical Raman cell, after bubbling with CO gas for a while, by adding some grains of solid dithionite, and the cell was kept in an anaerobic condition during the measurements. For isotope experiments, 0.25 ml of enzyme solution was, first, transferred to a 1.0 ml air-tight syringe, and , then, 0.5 ml of isotopically labeled CO gas was introduced. Then, a 10 μl volume of aqueous sodium dithionite (approximately a 5-fold molar excess of reducing agent to enzyme) was added, and the sample was mixed gently for a while to ensure complete formation of ferrous-carbonyl complex. The sample was, then, transferred directly to the Raman cell. Optical

absorption spectra of the reduced CO complex were measured on a Shimadzu UV-240 spectrophotometer equipped with an automatic wavelength calibrator (± 0.3 nm) before and after recording the resonance Raman spectra.

3. Measurement of Resonance Raman Spectra

Excitation wavelengths employed for resonance Raman measurements were 441.6 nm from a He-Cd laser (Kimmon Electric, Model CD 4801R) and 457.9 nm from an Ar laser (NEC, Model GLG 3300); the spectra were recorded on a JASCO R-800D Raman spectrophotometer. Calibration of the Raman spectrophotometer was carried out with indene or fenchone as standard.

Temperature of the sample was maintained at around -18.5°C by a specifically designed cell holder. Photodissociation of CO from native enzyme upon laser illumination was negligible even without spinning of the Raman cell. The low photodissociability of CO from cytochrome P-450 has already been reported (14-16). The subzero temperature is essential for measurements of the ferrous-carbonyl complex of cytochrome P-450_{scc}; at room temperature, the native ferrous-carbonyl complex form is easily converted to its denatured form, cytochrome P-420, during the laser illumination (16).

CO was purchased from Seitetsu Kagaku, Tokyo ($^{12}\text{C}^{16}\text{O}$) and from Shoko Tsusho, Tokyo ($^{12}\text{C}^{18}\text{O}$, 99% enriched). All other chemicals and reagents used were of the highest quality commercially available and were used without further purification.

III. Results

1. Detection of Fe-CO Stretch

In Figure C-1 we present the lower-frequency region (200-600-cm⁻¹) Raman spectra of CO-complexed cytochrome P-450_{scc} obtained with 441.6 nm excitation. There are at least six Raman bands at 237, 284, 316, 350, 380 and 477 cm⁻¹ in this region. A Raman band around 420 cm⁻¹ is due to glycerol in the solvent, and there is another glycerol Raman band at 486 cm⁻¹ with comparable intensity to the 420 cm⁻¹ feature beneath the strong Raman band at 477 cm⁻¹. When the spectrum of ¹²C¹⁶O complex is compared directly with the spectrum of ¹²C¹⁸O complex, only the Raman band at 477 cm⁻¹ shows a 7-cm⁻¹ downshift, indicating that this band is assignable to the $\nu(\text{Fe-CO})$ stretching frequency. This 7-cm⁻¹ downshift upon isotopic substitution is very close to that of the $\nu(\text{Fe-CO})$ stretching frequency in HbCO (a 9-cm⁻¹ downshift from 507 to 498-cm⁻¹ upon the same isotopic substitution) (3). This band is most intense in the lower-frequency region, and similar spectra were obtained when excited at 457.9 nm. This situation is very close to those of HbCO and MbCO upon Soret excitation (3). There may be some weak Raman bands of porphyrin ring (such as pyrrole folding modes) in the 400-500 cm⁻¹ region; but the strong 477 cm⁻¹ band and two glycerol Raman bands at 420 and 484 cm⁻¹ prevented their observation.

More detailed studies on lower-frequency region spectra of cytochrome P-450_{scc} will be presented Part D. High-frequency region (1200-1700 cm⁻¹) spectra of cytochrome P-450_{scc} have already been reported by Shimizu et al.(17), and, therefore, not included in this part.

2. Detection of Bound C-O Stretch

The bound CO internal stretching vibration was detected as shown in Figure C-2. Its frequency shifts from 1953 ($^{12}\text{C}^{16}\text{O}$) to 1907 cm^{-1} ($^{12}\text{C}^{18}\text{O}$) upon isotope substitution. The observed frequency is in good agreement with those of O'Keefe et al. (18) obtained for cytochrome P-450_{cam} with substrate (1940 cm^{-1}), cytochrome P-450 from rabbit liver pretreated with phenobarbital (1948 cm^{-1}) and cytochrome P-448 from rabbit liver pretreated with 3-methylcholanthrene (1954- cm^{-1}) by infrared spectroscopy. Again the situation is quite similar to that of HbCO; the bound CO internal stretching in HbCO can be resonance enhanced upon Soret excitation. Moreover, its frequency shift is practically the same as in this case; i.e., from 1951 ($^{12}\text{C}^{18}\text{O}$) to 1908- cm^{-1} ($^{12}\text{C}^{18}\text{O}$) (3).

These similarities imply the resonance enhancement of the $\delta(\text{Fe-C-O})$ bending vibration in 500-600- cm^{-1} region. However, we could not detect any such band in this region.

III. Discussion

1. Fe-C-O Bonding Geometry

The stretching frequencies, either $\nu(\text{Fe-CO})$ or $\nu(\text{C-O})$, may be influenced by numerous factors. However, the stretching vibrations of the Fe-C-O system are not expected to couple significantly to the in-plane porphyrin ring vibrations. Thus, to a reasonable approximation, the Fe-C-O system may be treated as an isolated three-body oscillator model, although there are distinct interactions with trans Fe-S linkage, as will be discussed later. The Fe-C-O

bending force constants are generally much smaller than the stretching force constants for Fe-C and C-O and, thus, may be neglected. The expression for the two stretching vibrations (ν_1 for Fe-CO; ν_2 for C-O) may be given by (10):

$$\lambda_{1,2} = \frac{1}{2} (k_1/\mu_1 + k_2/\mu_2) \pm \frac{1}{2} \left[(k_1/\mu_1 + k_2/\mu_2)^2 - 4k_1k_2 \left(\frac{1}{M} + \sin^2\theta/m_c^2 \right) \right]^{\frac{1}{2}} \quad (1)$$

where $\lambda_1 = 4\pi^2(c\nu_1)^2$, $\lambda_2 = 4\pi^2(c\nu_2)^2$;

c is the speed of light; μ_1 , k_1 and μ_2 , k_2 are the reduced masses and force constants of Fe-C and C-O systems, respectively; m_c is the carbon mass and M^2 is given by:

$$M^2 = (m_{Fe} m_c m_o) / (m_{Fe} + m_c + m_o) \quad (2)$$

and θ is Fe-C-O bond angle.

The plus sign in Equation (1) corresponds to the C-O stretching vibration and the minus sign corresponds to the Fe-CO stretching vibration.

At this point, we do not know a value of the Fe-C-O bond angle, θ , in the ferrous-carbonyl complex of cytochrome P-450_{scc}. However, in this case, CO is expected to bind to the heme iron in a linear and perpendicular fashion for the following reasons.

(a) X-ray crystallographic study of a model for the ferrous carbonyl state of cytochrome P-450 ($SC_2H_5Fe^{2+}TTP(CO)$); where TTP denotes the dianion of tetra-p-tolylporphyrin) indicates a linear and perpendicular fashion in CO binding to the heme iron (19).

(b) In general, the active site of cytochrome P-450 (proto heme IX) is considered to be located in a large, relatively open, hydrophobic cleft or depression in the surface of the apoprotein (20).

(c) Even C-22 substituted steroid derivatives, such as 22-amin-23,24-bisnor-5-cholen-3 β -ol (22-ABC) which is more than 10 Å in length, can directly bind to the heme iron of cytochrome P-450_{scc} in very high affinity (21).

(d) It is known that the bent configuration of the Fe-CO linkage is favourable for the photodissociation (15). Thus, the low photodissociability of CO from ferrous-carbonyl complex of cytochrome P-450_{scc} may suggest the linear bonding of CO.

(e) It is known that the distortion of the Fe-C-O linkage enhances the intensity of the Fe-C-O bending mode relative to that of the Fe-CO stretching mode (22). Therefore, the absence of the Fe-C-O bending mode in the spectra may be an indirect evidence of the linear bonding of carbon monoxide.

Thus, it is reasonable to assume the Fe-C-O bond angle, θ , to be 180° in Equation(1). Then we can obtain the following equations:

$$16\pi^4 c^4 \nu_1^2 \nu_2^2 = k_1 k_2 / M^2 \quad (3)$$

$$4\pi^2 c^2 (\nu_1^2 + \nu_2^2) = k_1 / \mu_1 + k_2 / \mu_2 \quad (4)$$

From these two equations we can estimate each stretching force constant, k_1 and k_2 , using the observed data. In the case of $^{12}\text{C}^{16}\text{O}$, for example, k_1 and k_2 are calculated to be 2.67 and 14.43 mdyne/Å, respectively. To compare these values with other usual

ferrous-carbonyl complexes (i.e., with imidazole as fifth ligand) with no steric interactions, we chose the ferrous-carbonyl complex of Heme 5 with N-methyl imidazole as a fifth ligand trans to CO. In this model complex, CO is known to bind to the heme iron in a linear and perpendicular fashion as expected in cytochrome P-450_{scc} CO-complex (22). In the case of $^{12}\text{C}^{16}\text{O}$ as the ligand, it was found that $\nu(\text{Fe-CO}) = 495 \text{ cm}^{-1}$ and $\nu(\text{C-O}) = 1954 \text{ cm}^{-1}$ (22), which correspond to 2.88 and 14.41 mdyne/Å for the values of k_1 and k_2 , respectively. It is very interesting to note that the Fe-CO stretching force constant is reduced by approximately 7.3% in the cytochrome P-450_{scc} system, whereas the bound C-O stretching force constant is practically the same. The cause of the reduction in the Fe-CO stretching force constant must be ascribed, therefore, to the heme axial ligand trans to CO.

2. Effect of Cysteiny1 Axial Ligand on the Fe-CO Stretch

The implication of a cysteiny1 heme axial ligand in cytochrome P-450 system was first supported by the similarity of the electron paramagnetic resonance spectra of native cytochrome P-450 and metmyoglobin complexed with exogenous thiol containing ligands (6). Much spectroscopic evidence of Fe-S⁻ coordination has accumulated (7-9). The unique physicochemical and enzymatic properties common to various molecular species of cytochrome P-450 can be attributed to common primary structure. The most important, and hence probably most conserved, region is the active center that contains the heme-binding residue. It was reported that only one region is markedly conserved throughout the six species of cytochrome P-450, whose complete primary structures have been determined (23,24). Furthermore, a cysteine

residue near the center of this region is common to all the cytochrome P-450 sequences. Thus, this cysteine residue is most likely the heme-binding amino acid residue.

Another direct evidence for the Fe-S⁻ bond in cytochrome P-450 system was provided by resonance Raman spectroscopy using isotopically labeled (⁵⁴Fe and ³⁴S) samples of the oxidized cytochrome P-450_{cam}-substrate complex (10). A Raman band at 351 cm⁻¹ was assigned to the $\nu(\text{Fe-S})$ stretching force mode.

Thus, it is most likely that the thiolate ligation trans to CO causes the weakening of Fe-CO bond strength compared to those of HbCO or MbCO.

To visualize the effect of cysteinyl heme axial ligation on the $\nu(\text{Fe-CO})$ stretching and bound $\nu(\text{C-O})$ stretching frequencies, we plotted the $\nu(\text{Fe-CO})$ stretching frequencies vs. the $\nu(\text{C-O})$ stretching frequencies for several ferrous-porphyrin CO-complex with nitrogen atom as the fifth ligand as shown in Figure C-3. We found well-behaved linear relationship:

$$\nu(\text{C-O}) = K(\nu(\text{Fe-CO}) - A) (\text{cm}^{-1}) \quad (5)$$

where $K = -1.38326$ and $A = 1914.56$. This relationship was first suggested by Yu et al (22). As the distal steric hindrance increases, the $\nu(\text{Fe-CO})$ frequency increases with a concomitant decreasing of the bound $\nu(\text{C-O})$ frequency. Thus, various ferrous-porphyrin-CO complex, having a nitrogen atom as a fifth ligand with different Fe-CO distortion, can be located along the line in Figure C-3. At this point we must emphasize that the linear and perpendicular configuration of CO binding in cytochrome P-450_{scc} contributes partly to the reduction in

$\nu(\text{Fe-CO})$ frequency compared to those of HbCO and MbCO (507 and 512 cm^{-1} , respectively), which showed a distorted Fe-C-O linkage with respect to the porphyrin ring in X-ray diffraction studies. This distortion causes the increase in $\nu(\text{Fe-CO})$ frequency by 12-17 cm^{-1} compared to that of the ferrous-carbonyl complex of Heme 5, which is expected to have a comparable Fe-C-O configuration with cytochrome P-450_{scc}.

When the data point for the cytochrome P-450_{scc}-CO complex was plotted in the same manner, we found that this complex cannot be classified into ferrous-porphyrin-CO complexes with a nitrogen atom as the fifth ligand, as shown in Figure C-3, which shows a substantial divergence towards the left side of the line. This indicates that the bonding configuration of Fe-C-O alone cannot explain the unusual decrease in $\nu(\text{Fe-CO})$ stretching frequency of cytochrome P-450_{scc} and that there is a distinct difference in Fe-CO bonding nature between cytochrome P-450_{scc} and other usual heme complexes.

CO is bound to ferrous heme iron through $d\pi(\text{Fe}) - \pi^*(\text{CO})$ interaction in addition to $d_z^2(\text{Fe}) - \pi^*(\text{CO})$ interaction (3), and both interactions determine the strength of the Fe-CO bond. On the other hand, a cysteinyl thiolate anion (S^-) has two lone pairs available for bonding (for example, $3p_y$ and $3p_z$), and can bind to the heme iron through $3p_y - d\pi$ interaction (π -bonding) in addition to $3p_z - d_z^2$ interaction (σ -bonding). The $3p_z^2 - d_z^2$ interaction is common to usual heme complex with a nitrogen atom as fifth ligand. Thus, additional interaction in Fe- S^- linkage causes the weakening of $d\pi(\text{Fe}) - \pi^*(\text{CO})$ interaction as a result of the competition for $d\pi(\text{Fe})$ electron, leading to weaker bond strength of the Fe-CO bond. In other words, the strong Fe- S^- bond causes the weaker Fe-CO bond.

A similar conclusion, that weaker the proximal Fe-ligand bond, the stronger the Fe-CO bond, was deduced from the studies on Fe^{2+} (mesotetra($\alpha,\alpha,\alpha,\alpha$ -o-pivalamidophenyl)porphyrin)-tetrahydrofuran-CO complex, in which tetrahydrofuran has the weakest field and weakest ligand and leads to a stronger thanusual bonding of CO to the heme iron (25). The $\nu(\text{Fe-CO})$ frequency appeared at 527-cm^{-1} . Unfortunately, no data are available for the bound $\nu(\text{C-O})$ frequency of this complex. However, in a similar complex, Fe^{2+} -deuteroporphyrin-tetrahydrofuran-CO, the bound $\nu(\text{C-O})$ frequency is reported at 1955 cm^{-1} by infrared spectroscopy (26). Assuming that $\nu(\text{Fe-CO})$ frequency and $\nu(\text{C-O})$ frequency are the same in both complexes, we may plot this point in Figure C-3 and find a considerable divergence towards the right side of the line, in a direction just opposite to that observed for the cytochrome P-450_{scc}-CO complex. This is consistent with our conclusion.

References

1. Tsubaki, M. and Yu, N.-T. (1981) Proc. Natl. Acad. Sci. USA 78, 3581.
2. Tsubaki, M. and Yu, N.-T. (1982) Biochemistry 21, 1140.
3. Tsubaki, M., Srivastava, R.B. and Yu, N.-T. (1982) Biochemistry 21, 1132.
4. Klingenberg, M. (1958) Arch. Biochem. Biophys. 75, 376.
5. Omura, T. and Sato, R. (1964) J. Biol. Chem. 239, 2370.
6. Murakami, K. and Mason, H.S. (1967) J. Biol. Chem. 242, 1102.
7. Wagner, G.C., Gunsalus, I.C., Wang, M.Y. and Hoffman, B.M. (1981) J. Biol. Chem. 256, 6266.
8. LoBrutto, R., Scholes, C.P., Wagner, G.C., Gunsalus, I.C. and Debrunner, P.G. (1980) J. Am. Chem. Soc. 102, 1167.
9. Hahn, J.E., Hodgson, K.O., Andersson, L.A. and Dawson, J.H. (1982) J. Biol. Chem. 257, 10934.
10. Champion, P.M., Stallard, B.R., Wagner, G.C. and Gunsalus, I.C. (1982) J. Am. Chem. Soc. 104, 5469.
11. Laemmli, U.K. (1970) Nature 227, 680.
12. Ogishima, T., Okada, Y., Kominami, S., Takemori, S. and Omura, T. (1983) J. Biochem. (Tokyo) 94, 1711.
13. Ando, N. and Horie, S. (1972) J. Biochem. (Tokyo) 72, 583.
14. Champion, P.M., Gunsalus, I.C. and Wagner, G.C. (1978) J. Am. Chem. Soc. 100, 3743.
15. Shimada, H., Iizuka, T., Ueno, R. and Ishimura, Y. (1979) FEBS Lett. 98, 290.
16. Ozaki, Y., Kitagawa, T., Kyogoku, Y., Imai, Y., Hashimoto-Yutsudo, C. and Sato, R. (1978) Biochemistry 17, 5826.
17. Shimizu, T., Kitagawa, T., Mitani, F., Iizuka, T. and Ishimura, Y. (1981)

- Biochim. Biophys. Acta 670, 236.
18. O'Keefe, D.H., Ebel, R.E., Peterson, J.A., Maxwell, J.C. and Caughey, W.S. (1978) Biochemistry 17, 5845.
 19. Caron, C., Mitschler, A., Riviere, G., Ricard, L., Schappacher, M. and Weiss, R. (1979) J. Am. Chem. Soc. 101, 7401.
 20. Coon, M.J. and White, R.E. (1980) in "Metal Ion Activation of Oxygen", (Spiro, T.G. ed) p.73., John Wiley & Sons, New York.
 21. Sheets, J.J. and Vickery, L.E. (1982) Proc. Natl. Acad. Sci. USA 79, 5773.
 22. Yu, N.-T., Kerr, E.A., Ward, B. and Chang, C.K. (1983) Biochemistry 22, 4534.
 23. Kawajiri, K., Gotoh, O., Sogawa, K., Tagashira, Y., Muramatsu, M. and Fujii-Kuriyama, Y. (1984) Proc. Natl. Acad. Sci. USA 81, 1649.
 24. Morohashi, K., Fujii-Kuriyama, Y., Okada, Y., Hirose, T., Inayama, S. and Omura, T. (1984) Proc. Natl. Acad. Sci. USA 81, 4647.
 25. Kerr, E.A., Mackin, H.C. and Yu, N.-T. (1983) Biochemistry 22, 4373.
 26. Scheidt, W.R., Haller, K.J., Fones, M., Mashiko, T. and Reed, C.A. (1981) Biochemistry 20, 3653.
 27. Armstrong, R.S., Irwin, M.J. and Wright, P.E. (1982) J. Am. Chem. Soc. 104, 626.
 28. Fuchsman, W.H. and Appleby, C.A. (1979) Biochemistry 18, 1309.
 29. Yu, N.-T., Benko, B., Kerr, E.A. and Gersonde, K. (1984) in "Proceedings of the IXth International Conference on Raman Spectroscopy" p.758, Organizing Committee for the IXth International Conference on Raman Spectroscopy, c/o The Chemical Society of Japan, Tokyo, Japan.
 30. Collman, J.P., Brauman, J.I., Halbert, T.R. and Suslick, K.S. (1976) Proc. Natl. Acad. Sci. USA 73, 3333.

31. Jones, E.D., Budge, J.R., Ellis, P.E., Jr., Linard, J.E.,
Summerville, D.A. and Basolo, F. (1979) J. Organometallic Chem. 181,
151.
32. Anzenbacher, P., Fidler, V., Schenkman, J.B., Kirkup, R.E. and Spiro,
T.G. (1984) in "Proceedings of the IXth International Conference on
Raman Spectroscopy" p.474., Organizing Committee for the IXth
International Conference on Raman Spectroscopy, c/o The Chemical
Society of Japan, Tokyo, Japan.
33. Makino, R., Iizuka, T., Ishimura, Y., Uno, T., Nishimura, Y. and
Tsuboi, M. (1984) *ibid* p.492.

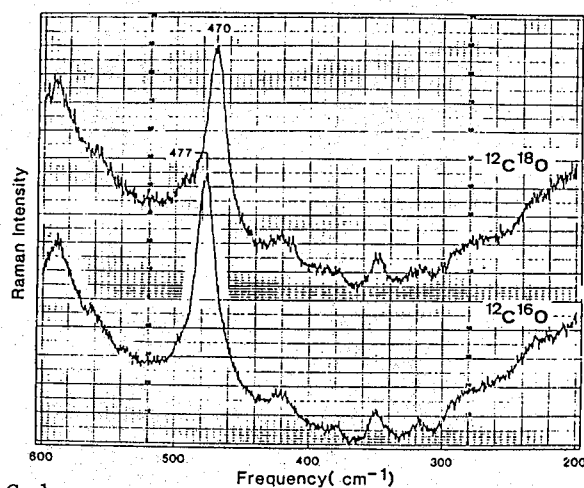


Figure C-1. CO isotope effect on resonance Raman spectra of the ferrous-carbonyl complex of cytochrome $P-450_{\text{sec}}$ in the lower-frequency region ($200-600 \text{ cm}^{-1}$). Excitation wavelength, 441, 6 nm; laser power, 18 mW at sample point; entrance slit width and height, $250 \mu\text{m}$ and 12 mm, respectively; protein concentration, $30 \mu\text{M}$ on heme basis.

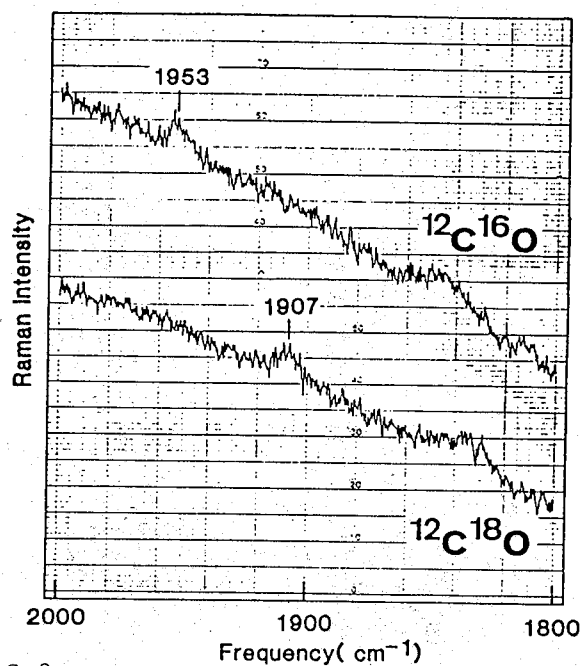


Figure C-2. CO isotope effect on resonance Raman spectra of the ferrous-carbonyl complex of cytochrome $P-450_{\text{sec}}$ in $1800-2000 \text{ cm}^{-1}$ region. Conditions are the same as for Fig. 1.

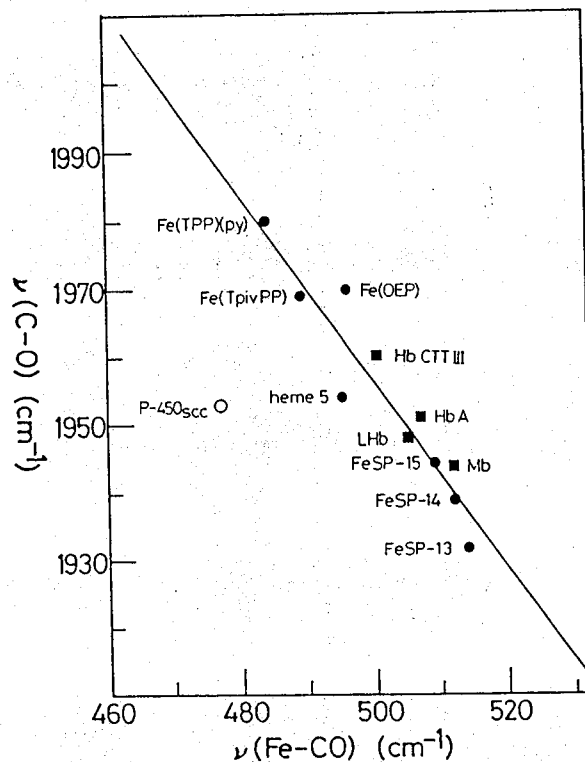


Figure C-3. $\nu(\text{Fe-CO})$ frequency vs. bound $\nu(\text{C-O})$ frequency plots for various ferrous-heme-carbonyl complexes. ■, data points for native heme proteins: sperm whale myoglobin (Mb), human hemoglobin A (Hb A), leg hemoglobin (LHb), and hemoglobin from insect larvae of *Chironomus thummi thummi* (Hb CTT III); data taken from Refs. 3, 27, 28 and 29. ●, various heme model complexes; data are taken from Refs. 22, 25, 26, 30 and 31. ○, data point for cytochrome P-450_{scc}.

Part D. Effects of Cholesterol and Adrenodoxin on the Heme Moiety of

Cytochrome P-450_{scc}: A Resonance Raman Study

Footnotes

¹ Abbreviations used are: cytochrome P-450_{scc}, cytochrome P-450 in mitochondria of adrenal cortex which functions in cholesterol side-chain cleavage reaction; cytochrome P-450_{cam}, cytochrome P-450 obtained from Pseudomonas putida grown on D-camphor as the sole carbon source; cytochrome P-450_{11 β} , cytochrome P-450 in mitochondria of adrenal cortex which functions in steroid 11 β -hydroxylation; cytochrome P-450_{LM2}, the major phenobarbital-inducible cytochrome P-450 in rabbit liver microsomes.

² The concentration of cholesterol is the maximum assuming cholesterol is fully solved. However, low solubility in aqueous solution and the non-specific binding to protein other than the substrate binding site may reduce its actual concentration.

³ The designation of porphyrin ring modes are based on Kitagawa et al.(35) and Abe et al.(36).

0. Introduction

Side chain cleavage of cholesterol to pregnenolone is the rate-limiting step in steroid hormone biosynthesis (1). This process is catalyzed by mitochondrial cytochrome P-450_{scc}¹, together with its NADPH-specific electron transport system (adrenodoxin reductase plus adrenodoxin)(2). It is known that, although heme iron of cholesterol-free cytochrome P-450_{scc} is fully low spin state, cholesterol-binding to the substrate binding site of cytochrome P-450_{scc} causes the spin state conversion from low to high (2).

Adrenodoxin, an iron-sulfur protein, forms 1:1 complexes with both NADPH-adrenodoxin reductase and cytochrome P-450_{scc}. While the binding of adrenodoxin and cholesterol to cytochrome P-450_{scc} exhibits strong positive cooperativity, adrenodoxin nevertheless binds to cholesterol-free cytochrome (3). During electron transfer, the complexes appear to function sequentially by "adrenodoxin shuttle mechanism" (2,3) rather than via a ternary complex of all three proteins (4): i.e. adrenodoxin first forms its complex with and accepts an electron from adrenodoxin reductase, then dissociates, and finally forms a 1:1 complex with and transfers an electron to cytochrome P-450_{scc}. Total of six electrons are necessary for the oxidative side chain cleavage of cholesterol by this system.

Resonance Raman scattering from hemoproteins can provide some important informations on the structure of the heme moiety (5-8). Recent studies on cytochrome P-450_{scc}-CO-complex, we observed, for the first time, the resonance enhancement of Fe-CO stretching frequency and bound C-O stretching frequency at 477 and 1953 cm⁻¹, respectively (9,10). This unusually low Fe-CO stretching frequency, compared to

those of carbonmonoxy hemoglobin and myoglobin (507 and 512 cm^{-1} , respectively)(11), was interpreted as a direct indication of a weaker Fe-CO bond strength caused by a cysteinyl thiolate ligand trans to CO and a linear and perpendicular coordination of CO to the heme.

In this study, we report the resonance Raman spectra cytochrome P-450_{scc} in oxidized and CO-reduced states, and discuss the effects of cholesterol (substrate) and adrenodoxin-binding on the heme moiety of both states.

I. Experimental

1. Purification of Cytochrome P-450_{scc}

Cytochrome P-450_{scc} was purified as follows. Bovine adrenal glands were obtained from local slaughterhouse. Their connective tissues and fat tissues were removed with scissors as possible as we can, then the glands were separated carefully into adrenocortexes and medullas. The capsules of the cortexes were scraped off with razor. The mitochondrial fraction was obtained from the adrenocortexes by the method of Hiwatashi et al. (12).

Adrenocortical mitochondria depleted of adrenodoxin and NADPH-adrenodoxin reductase with sonication were suspended in 100 mM potassium phosphate buffer (pH 7.4) containing 20%(v/v) glycerol and 1 mM EDTA. Sodium cholate was added to the suspension (about 12-16 mg protein/ml) at the ratio of protein:sodium cholate of 2:1 (w/w). The solution was stirred for 45 min at 4°C and, then, spun at 78,740 x g (30,000 rpm) for 90 min on a Beckman L-8 ultracentrifuge. The supernatant was incubated at room temperature for 30 min, then, mixed with a slurry of DEAE-cellulose previously equilibrated with 10 mM

potassium phosphate buffer (pH 7.8) containing 20%(v/v) glycerol, 0.1%(v/v) Emulgen 913, 0.25%(w/v) sodium cholate and 0.1 mM EDTA (buffer A). The slurry was poured into a glass column. After the packing, the column was washed extensively with buffer A (about 2000 ml) over night. When a clear reddish band was formed in the bottom of the column, the column was treated with a 2000 ml-linear gradient of NaCl concentration (0-0.3 M) in buffer A. The eluate was collected with 17 ml fractions automatically. Cytochrome P-450_{scc}-rich fractions were eluted during this treatment as a sharp peak, and were combined and directly applied to a column of hydroxyl apatite gel previously equilibrated with buffer A. The cytochrome was adsorped at the top of the column as a clear red band. The column was washed succeedingly with 500 ml each of 10, 20, and 40 mM of potassium phosphate buffer (pH 7.8) containing the same ingredients with buffer A. The cytochrome P-450_{scc} was, then, eluted with 80 mM potassium phosphate buffer (pH 7.4) containing 20% glycerol, 0.1% Emulgen 913, 0.25% sodium cholate, and 0.1 mM EDTA. The eluate was dialyzed extensively against 10 mM potassium phosphate buffer (pH 6.5) containing 20% glycerol, 0.1% Emulgen 913, and 0.1 mM EDTA (buffer B) at 4° C. The dialyzate was applied to a column of CM-Sepharose CL-6B previously equilibrated with buffer B. The cytochrome was adsorped in the column as a dark red band; and the column was washed with buffer B, then with 10 mM potassium phosphate buffer (pH 7.4) containing 20% glycerol, 0.1% Emulgen 913, and 0.1 mM EDTA. The cytochrome was desorped by a 600 ml-linear gradient of NaCl concentration (0-0.3 M) in 10 mM potassium phosphate buffer (pH 7.4) containing 20% glycerol, 0.1% Emulgen 913, and 0.1 mM EDTA. The eluate was collected with 10 ml fractions automatically, and cytochrome P-450_{scc}-rich

fractions were analyzed with SDS-polyacrylamide gel electrophoresis and fractions with a single protein-staining band were combined.

SDS-polyacrylamide gel electrophoresis was performed as Laemmli (13) and the molecular weight of cytochrome P-450_{scc} was estimated to be 53,000 daltons.

2. Depletion of Emulgen 913 from the Purified Cytochrome P-450_{scc}

Emulgen 913 in purified sample was removed by an adrenodoxin-Sepharose 4B column chromatography (14,15). Cytochrome P-450_{scc} was dialyzed extensively against 300 volumes of 10 mM potassium phosphate buffer (pH 7.4) containing 20% glycerol and 0.1 mM EDTA at 4° C with several changes. The dialyzate was loaded onto a column of adrenodoxin-Sepharose 4B previously equilibrated with the same buffer; the cytochrome was adsorbed at the top of the column as a reddish band. The column was washed with the equilibrating buffer (10 column volumes) followed by the same buffer containing 85 mM NaCl until the absorption at 280 nm of the eluate decreased lower than 0.025. The adsorbed cytochrome was eluted with the equilibrating buffer containing 0.20% sodium cholate and 300 mM NaCl. The eluate was collected and peak fractions were combined, dialyzed against 10 mM potassium phosphate buffer containing 20% glycerol and 0.1 mM EDTA. The resulting sample was in a pure low spin form and practically free from Emulgen 913 judged by the absorption spectra in the ultraviolet region.

3. Measurements of Optical Absorption Spectra

Optical absorption spectra of cytochrome P-450_{scc} were measured on a Shimadzu UV-240 spectrophotometer equipped with an automatic wavelength

calibrator (± 0.3 nm). The temperature of the sample was maintained by a circulation of water from thermo-bath to water-jacketed cell holder.

4. Measurements of Resonance Raman Spectra

Excitation wavelengths used for resonance Raman measurements were 441.6 nm from a He-Cd laser (Kimmon Electric, Model CD 4801R) and 457.9 and 488.0 nm from an Ar laser (NEC, Model GLG 3300); and the spectra were recorded on a JASCO R-800D Raman spectrophotometer. Calibration of the Raman spectrophotometer was carried out with indene or fenchone as standard. Sample solution in a cylindrical Raman cell was spun at 1000 rpm to minimize local heating, photodecomposition and photodissociation. All spectral measurements were performed in 10 mM potassium phosphate buffer (pH 7.4) containing 20% (v/v) glycerol, 100 mM NaCl and 0.1 mM EDTA at the protein concentration of 47.5 μ M, otherwise indicated.

II. RESULTS

1. Oxidized Form

Before the depletion of Emulgen 913, the sample was pure low spin form judged by visible absorption spectrum. In this stage, cytochrome P-450_{scc} could not be converted to high spin form even a saturated amount of cholesterol was added. This is due to the inhibitory effect of Emulgen 913 against substrate binding (16). Thus, it was necessary to remove Emulgen 913 from the purified sample to study the effect of cholesterol-binding on the heme moiety. We employed an adrenodoxin-Sepharose 4B column to remove Emulgen 913; this technique has been successfully used for the final purification step of

mitochondrial cytochromes P-450, such as cytochrome P-450_{11 β} and P-450_{scc}. The recovered enzyme from the adrenodoxin-Sepharose 4B column was pure low spin form, having absorption maxima at 567, 534, 417 and 360 nm identical to those of cytochrome P-450_{scc} in the presence of Emulgen 913 (0.1%) (Figure D-1, one dotted chain line). The absence of Emulgen 913 in the sample was clearly indicated by the weak absorption intensity at 278 nm, which was lower than Soret absorption at 417 nm and the ratio of A_{278}/A_{417} was comparable to, or even lower than, the cytochrome P-450_{scc} sample purified in other laboratory (17).

Upon addition of cholesterol² (28.6 μ M, and protein concentration 12.6 μ M), the Emulgen-depleted cytochrome P-450_{scc} could be converted to high spin form (approx. 50% high spin at 25° C) (Figure D-2a). To make 100% high spin form at this concentration, the temperature had to be lowered less than 10° C (Figure D-1, solid line). This strong temperature dependency of spin state was already reported (18).

The effect of adrenodoxin on the absorption spectra of cholesterol-bound cytochrome P-450_{scc} can be clearly seen in Figure D-2b. To maximize cholesterol-binding to cytochrome P-450_{scc} at room temperature we used relatively high ionic strength (100 mM NaCl) in buffer throughout because high ionic strength causes a decrease of apparent K_d for cholesterol (19). But it is also known that the strength of interaction between adrenodoxin and cytochrome P-450_{scc} is reduced considerably at high ionic strength because their interaction is electrostatic (19). Nevertheless only a 2.26 μ M of adrenodoxin caused a significant increase of high spin content as shown in Figures D-2a and b (cytochrome P-450_{scc} concentration 12.6 μ M); this indicates that adrenodoxin has high affinity for cholesterol-bound cytochrome P-450_{scc}.

even in this condition (100 mM NaCl) and forms a tight cholesterol-cytochrome P-450_{scc}-adrenodoxin complex to stabilize cytochrome P-450_{scc} heme completely in high spin state (3).

The resonance Raman spectra of cytochrome P-450_{scc} for higher frequency region (1300-1700 cm⁻¹) in various states as described above (but with a different protein concentration, i.e. 47.5 μM) are presented in Figure D-3. Excitation wavelength used was 441.6 nm from a He-Cd laser. As expected, in cholesterol-free state, the ν_{10} line³ appeared at 1638 cm⁻¹ in the Raman spectrum, i.e., at the normal frequency of the ferric low spin state. Other spin state markers, ν_3 and ν_{19} lines, can be seen at 1503 and 1584 cm⁻¹, respectively, characteristic for the ferric low spin state (Figure D-3, upper spectrum). When cholesterol was added (cholesterol concentration, 278.1 μM), the cytochrome P-450_{scc} heme spin state was converted almost in high spin (approx. 70% high spin at 10° C) judged by visible absorption spectra. In this condition the resonance Raman spectrum of the cytochrome exhibited the mixture of low and high spin states (Figure D-3, middle spectrum). When 36.3 μM of adrenodoxin was added additionally, the spectrum was completely devoid of low spin signals (Figure D-3, lower spectrum). The ν_{10} line shifted to 1620 cm⁻¹ and ν_{19} line disappeared. The ν_3 line shifted to around 1485 cm⁻¹ and was overlapped with a strong glycerol band at 1470 cm⁻¹. The ν_{11} line appeared at 1567 cm⁻¹. The frequencies of ν_3 , ν_{10} , and ν_{11} are in accordance with high spin nature of cytochrome P-450_{scc} heme. When a 488.0 nm line from an Ar-ion laser was employed for the excitation, essentially the same spectra were obtained for cholesterol-free state and cholesterol and adrenodoxin-bound state, but with much reduced Raman intensities (data not shown). The decrease in

frequency of ν_4 line by 2 cm^{-1} in Figures D-3 upon spin conversion from low to high state was not consistent with the result observed by Shimizu et al. (20); in which they observed the frequency increase of ν_4 line by 2 cm^{-1} upon conversion from low to high spin state. However the decrease of the ν_4 frequency upon spin conversion from low to high is a right direction judged by the empirical relationship observed for other hemoproteins.

We could observe only two Raman lines at 346 and 380 cm^{-1} in lower frequency region spectrum of cholesterol-free form except for the lines from glycerol (Figure D-4). Since oxidized adrenodoxin itself has Raman lines at 289 , 346 and 391 cm^{-1} with almost the same intensities each other at this excitation wavelength (Tsubaki, unpublished observation; 21), the major part of Raman intensities at 348 cm^{-1} in the lower spectrum in Figure D-4 is expected to be due to adrenodoxin. Cholesterol-cytochrome P-450_{scc}-adrenodoxin complex stabilize cytochrome P-450_{scc} heme completely in high spin state and, thus, the Raman intensities of 346 and 380 cm^{-1} modes of cytochrome P-450_{scc} must be extremely weak in the Raman spectra of high spin state cytochrome P-450_{scc}.

2. Carbon Monoxide Reduced Form and Its Conversion to P-420 Form in the Absence of Cholesterol

The CO-complex of reduced cytochrome P-450_{scc} gave rise to ν_4 mode at 1368 cm^{-1} (Figure D-5, upper spectrum). This frequency is consistent with that reported by Shimizu et al. (20) and close to those of CO-complexes of other cytochromes P-450 (22). These slightly lower frequency of ν_4 mode in CO-complex of reduced cytochrome P-450 compared

to those of carbonmonoxy hemoglobin and myoglobin (1372 and 1370 cm^{-1} , respectively) was considered due to the strong π -donor retained in its CO-complex as the fifth ligand of heme iron.

During the laser illumination at room temperature (25° C), this CO-complex of reduced cytochrome P-450_{scc} (cholesterol-free) was converted to its denatured "P-420" form even the sample was kept in a spinning cell. Several hours of laser illumination caused an almost complete conversion of cytochrome P-450_{scc} to "P-420" form judged by visible absorption spectra. This conversion was clearly indicated in the Raman spectra by a significant broadening of the 1368 cm^{-1} line towards lower frequency, suggesting the photodissociation of CO-complex of reduced "P-420" (data not shown). It is well known that the bound carbon monoxide molecule of "CO-P-420" is easily photodissociated (20,23) and resulting photodissociated (or reduced) "P-420" is characterized by the appearance of ν_4 Raman line at 1357 cm^{-1} with a very strong intensity (Figure D-6, lower spectrum)(22,24).

In the lower frequency region spectra of CO-complex of reduced cytochrome P-450_{scc}, there is a strong Raman line at 477 cm^{-1} which was assigned to the Fe-CO stretching frequency on the basis of frequency shift by carbon monoxide isotope substitution (Figure D-7, upper spectrum). This 477 cm^{-1} line reduced its intensity upon conversion to "P-420" form. This intensity reduction was accompanied by the disappearance of 318 and 280 cm^{-1} lines. The Raman spectra of "P-420" form in lower frequency region were characterized by the appearance of 224 cm^{-1} line. This line may be due to photodissociated form of "P-420" because there was a relatively sharp Raman line at 225 cm^{-1} in the spectra of reduced "P-420" (data not shown).

3. Effect of Cholesterol and Adrenodoxin on the CO-Reduced Form

Although the presence of cholesterol showed no effect on the visible absorption spectra of CO-reduced form of cytochrome P-450_{scc}, there were some significant influences on the resonance Raman spectra. The most significant effect of cholesterol-binding on the spectra of CO-reduced form was an increase of photodissociability of bound carbon monoxide. This phenomenon is clearly seen in Figure D-5. The strong ν_4' line at 1368 cm^{-1} and several Raman lines around $1550\text{--}1650\text{ cm}^{-1}$ region reduced their intensities in the presence of cholesterol ($278.1\text{ }\mu\text{M}$) and the spectra in this higher frequency region became similar to that of reduced cytochrome P-450_{scc} (compare Figure D-5, middle spectrum with Figure D-6, upper spectrum). Since the spectrum of reduced "P-420" form or CO-photodissociated "P-420" form was completely different from these spectra, this effect could not be ascribed to the denaturation to "P-420". The effect of photodissociation in the Raman spectrum due to cholesterol-binding was clearly observed in lower frequency region also (Figure D-7, middle spectrum). The Fe-CO stretching frequency at 477 cm^{-1} lost its strong intensity slightly and showed a clear shift to 483 cm^{-1} even considering the effect of glycerol Raman lines at 484 and 420 cm^{-1} with almost the same intensities each other, the former overlapping with the Fe-CO stretching line.

On the other hand, the addition of adrenodoxin to cholesterol-bound CO-reduced form caused no additional effect on the resonance Raman spectra in both higher and lower frequency region as shown in Figures D-5 and 7, suggesting a weaker interaction between adrenodoxin and cholesterol-bound CO-reduced cytochrome P-450_{scc}. It must be noted that adrenodoxin was in reduced form in this condition.

We tried to see the effect of cholesterol and adrenodoxin on the bound C-O stretching frequency. In the absence of cholesterol the bound C-O stretching frequency could be observed at 1953 cm^{-1} by resonance Raman spectroscopy but with a much weak intensity compared to that of Fe-CO stretching frequency (10). However we could not detect any corresponding bound C-O stretching frequency around in this region in the presence of cholesterol alone or both cholesterol and adrenodoxin. This is presumably due to the strong photodissociability of carbon monoxide of CO-complex of cytochrome P-450_{scc} in the presence of cholesterol.

III. DISCUSSION

1. Oxidized Form

The optical spectral change of the oxidized cytochrome P-450_{scc} from low to high spin state upon cholesterol binding is considered to indicate directly the cholesterol binding to the substrate binding site. However it is known that the 1:1 molar complex of cholesterol and cytochrome P-450_{scc} displays a high to low spin transition upon temperature elevation; this is in an opposite direction observed for other cytochrome P-450 such as cytochrome P-450_{cam} and cytochrome P-450_{LM2} (25,26). Since the hydrophobic affinity of cholesterol for substrate-free cytochrome P-450_{scc} is enhanced with increasing temperature (19,27), the temperature-dependent high to low spin conversion of cholesterol-bound cytochrome P-450_{scc} appears to be related to unknown structural changes rather than the simple release of cholesterol from the enzyme. Thus, Hasumi et al.(17) speculated that temperature modulates specific interactions between the cytochrome

P-450_{scc} and bound cholesterol (such as a subtle movement of cholesterol in the vicinity of the heme) and that bound cholesterol is not released from the cytochrome P-450_{scc} by increasing temperature.

There is no suitable way to verify this hypothesis conclusively. However our observation during this study supports this hypothesis (data not shown); in which the rate of spin conversion from low to high spin upon decreasing temperature was much faster than that of corresponding spin change upon addition of cholesterol to substrate-free cytochrome P-450_{scc}; the latter is directly indicating the cholesterol-binding to the substrate binding site of cytochrome P-450_{scc}.

Whatever the true nature of this spin conversion is, the present study clearly indicates that cholesterol-binding can affect a configuration around the oxidized heme of cytochrome P-450_{scc} significantly. Adrenodoxin alone has no effect on the heme spin state, although there is a substantial interaction between adrenodoxin and substrate-free cytochrome P-450_{scc} as evidenced by a successful preparation of cholesterol-free cytochrome P-450_{scc} using an adrenodoxin-Sepharose 4B column chromatography in the present study. Thus adrenodoxin can affect the heme electronic structure only when cholesterol is bound to the substrate binding site. In the context of Hasumi et al. (17), binding of adrenodoxin to cholesterol-bound cytochrome P-450_{scc} can induce a subtle movement of bound cholesterol in the vicinity of the heme leading to the complete spin conversion to high spin.

The ν_{10} mode of oxidized cytochrome P-450_{scc} in high spin state observed at 1620 cm^{-1} , slightly higher than the value reported by Shimizu et al. (20), is still in the reported range of hexa-coordinated high-spin

complex ($1608-1623\text{ cm}^{-1}$) as suggested by Shimizu et al. (20). The ν_3 mode, which is overlapped with glycerol Raman line at 1470 cm^{-1} , is expected to locate around 1485 cm^{-1} as described in RESULTS. This frequency is also in the range of hexa-coordinated complex ($1475-1488\text{ cm}^{-1}$). On the basis of the empirical relationship between the ν_{10} frequency and the coordinated atom (28), Shimizu et al. (20) suggested that the sixth ligand of the heme iron of cytochrome P-450_{scc} in high spin state would be an oxygen atom, most likely oxygen from a water molecule.

The resonance Raman spectrum in the lower frequency region ($200-600\text{ cm}^{-1}$) is quite informative since the Fe-ligand stretching modes of hemoproteins usually appear in this region. Indeed Champion et al. (29) detected the Fe-S⁻ stretching frequency at 351 cm^{-1} by resonance Raman spectroscopy using isotopically labeled (^{54}Fe and ^{34}S) samples of the oxidized cytochrome P-450_{cam}-substrate complex. Moreover this $\nu(\text{Fe-S}^-)$ stretching band disappeared upon depletion of the substrate, indicating that the substrate-binding produces a significant change in the Fe-S⁻ interaction. The 346 cm^{-1} line in the Raman spectra of oxidized cytochrome P-450_{scc} may correspond to the 351 cm^{-1} Fe-S⁻ stretching line in cytochrome P-450_{cam}. But the 346 cm^{-1} line reduced its intensity upon depletion of cholesterol (substrate) contrary to the 351 cm^{-1} mode in cytochrome P-450_{cam}, using glycerol Raman lines at 420 and 484 cm^{-1} as internal standards. Because Champion et al. (29) used the laser wavelength at 363.8 nm , it must be very careful to compare directly our observation with them. As a plausible explanation, the $\nu(\text{Fe-S}^-)$ stretching mode appears only at near ultraviolet excitation and the 346 cm^{-1} mode in cytochrome P-450_{scc} may be a porphyrin ring mode.

2. CO-Reduced Form

We had assigned Fe-CO stretching frequency of the CO-complex of cytochrome P-450_{scc} at 477 cm⁻¹ in the previous paper on the basis of the frequency shift upon carbon monoxide isotope substitution; i.e., from 477 cm⁻¹ for ¹²C¹⁶O to 470 cm⁻¹ for ¹²C¹⁸O (10). This frequency is much lower than the corresponding frequencies in carbonmonoxy hemoglobin and myoglobin at 507 and 512 cm⁻¹, respectively (11). This unusually low frequency could be explained mainly in terms of d π (Fe)- π^* (CO) interaction which is weaker in cytochrome P-450_{scc} than in usual hemoproteins due to a strong π -interaction in Fe-S⁻ bond. Other factor which causes this unusually low Fe-CO stretching frequency is a linear and perpendicular bonding of carbon monoxide to the heme. It is known that the distorted Fe-C-O linkage with respect to the porphyrin ring causes the increase in ν (Fe-CO) stretching frequency with a concomitant decrease of bound C-O stretching frequency. X-ray diffraction studies revealed a distortion of Fe-C-O linkage in carbonmonoxy hemoglobin and myoglobin; this distortion causes the increase in ν (Fe-CO) frequency by 12-17 cm⁻¹ compared to that of ferrous-carbonyl complex of Heme 5 which is expected to have a linear and perpendicular Fe-C-O structure (30) and, therefore, to have a comparable Fe-C-O configuration with cytochrome P-450_{scc} in the absence of cholesterol (10).

Recently Uno et al.(31) reported that the Fe-CO stretching frequency in substrate-free cytochrome P-450_{cam}-CO-complex lies at 464 cm⁻¹. Upon addition of substrate, camphor, the Fe-CO stretching frequency shifted to 481 cm⁻¹ and to 483 cm⁻¹ upon forming a bimolecular complex with putidaredoxin and this frequency shift towards higher frequency was

accompanied by a concomitant decrease of bound C-O stretching frequency from 1963 cm^{-1} to 1940 and 1932 cm^{-1} , respectively.

As seen in Figure D-8, our previous data and those of Uno et al.(31) can be plotted along a line parallel to the one obtained for various ferrous heme-carbonyl complexes with nitrogen atom as a fifth ligand. The departure of these two lines are probably not due to the Fe-C-O configuration, but due to the differences in bonding nature between heme iron and fifth ligands (10).

From this parallelism we can speculate that substrate (camphor or cholesterol) binding causes a distortion of Fe-C-O linkage with respect to porphyrin ring on the basis of our previous proposal; i.e. as the distal steric hindrance increases, the $\nu(\text{Fe-CO})$ frequency increases with a concomitant decreasing of the bound $\nu(\text{C-O})$ frequency (10). It is very likely that almost the same mechanism is operative on Fe-C-O linkage in CO-complex of cytochrome P-450_{cam} as in cytochrome P-450_{scc} complex upon substrate-binding. Indeed the increase of Fe-CO stretching frequency by 6 cm^{-1} in the presence of cholesterol, as observed in the present study, is a right direction on the view of our previous proposal. It is known that cholesterol binding site is so close to the heme that C-22 of cholesterol side chain is at very vicinity of heme iron when cholesterol is bound, from a series of studies using synthesized steroid derivatives having the potential to interact with both the substrate binding site and the heme-iron catalytic site of the enzyme (32-34). Thus it is very likely that the side chain group of cholesterol opposes a linear and perpendicular binding of carbon monoxide to the heme iron of cytochrome P-450_{scc}.

Increased photodissociability of carbon monoxide from CO-complex of cytochrome P-450_{scc} upon addition of cholesterol can be easily understood in this context. It is known that the electronic excitation at the porphyrin ring by the illumination of laser light at the Soret or Q (α and β) bands can affect the $d_{\pi}(\text{Fe})-\pi^*(\text{CO})$ interaction indirectly through the $d_{\pi}(\text{Fe})-\pi^*(\text{porphyrin})$ orbital interaction, leading to the photodissociation of the sixth ligand, carbon monoxide (11). In the distorted Fe-C-O configuration, the contribution of σ -type ($d_{z^2}(\text{Fe})-\pi^*(\text{CO})$) interaction may decreased significantly in Fe-CO bond due to the bonding geometry, and the resulting increase of π -type ($d_{\pi}(\text{Fe})-\pi^*(\text{CO})$) interaction in Fe-CO bond may be the reason of the enhanced photodissociability upon cholesterol-binding.

Other aspect of the effect of cholesterol on CO-complex of cytochrome P-450_{scc} was the enhanced stability of native ("P-450") state. Without cholesterol the CO-complex of cytochrome P-450_{scc} became its denatured form (CO-complex of "P-420") steadily as described. To the contrary, in the presence of cholesterol, the CO-complex of cytochrome P-450_{scc} was extremely stable for more than several hours even kept irradiated by laser light at room temperature (data not shown). To reveal the nature of this effect is beyond our scope in the present study. We can only say at this stage that cholesterol bound to the substrate binding site may stabilize the tertiary structure around the heme.

The absence of the additional effect of adrenodoxin in the resonance Raman spectra of CO-reduced form of cytochrome P-450_{scc} is noteworthy. It must be noted that adrenodoxin is in reduced form in this experimental condition. However it is known that the reduction state

of adrenodoxin does not appear to have major effects on its association with cytochrome P-450_{scc}; reduction of adrenodoxin actually results in a slight weakening, by a factor of 2, of the interaction with both oxidized and reduced cytochrome P-450_{scc} (3).

There is no available data to estimate the interaction between adrenodoxin and cholesterol-bound CO-reduced cytochrome P-450_{scc} other than present study. However, from the view point of a physiological mechanism of steroidogenic electron transport, stronger interaction between adrenodoxin and cholesterol-bound CO-reduced form must be favored, because cholesterol-bound CO-reduced form can be considered as a nice model for an oxygenated intermediate complex during the initial phase of the side chain cleavage reaction.

References

1. Stone, D. and Hechter, O. (1954) Arch. Biochem. Biophys. 51, 457.
2. Lambeth, J.D., Seybert, D.W., Lancaster, J.R., Jr., Salerno, J.C. and Kamin, H. (1982) Mol. Cell. Biochem. 45, 13.
3. Lambeth, J.D. and Pember, S.O. (1983) J. Biol. Chem. 258, 5596.
4. Kido, T. and Kimura, T. (1979) J. Biol. Chem. 254, 11806.
5. Tsubaki, M., Srivastava, R.B. and Yu, N.-T. (1981) Biochemistry 20, 946.
6. Tsubaki, M. and Yu, N.-T. (1981) Proc. Natl. Acad. Sci. USA 78, 3581.
7. Tsubaki, M. and Yu, N.-T. (1982) Biochemistry 21, 1140.
8. Spiro, T.G. (1982) in "Iron Porphyrins, Part II" (Lever, A.B.P. and Gray, H.B., eds) p.89. Addison-Wesley Publishing Company, Massachusetts, USA.
9. Tsubaki, M., Matsusaka, K., and Ichikawa, Y. (1984) in "Proceedings of the IXth International Conference on Raman Spectroscopy" p.752, Organizing Committee for the IXth International Conference on Raman Spectroscopy, c/o The Chemical Society of Japan, Tokyo, Japan.
10. Tsubaki, M. and Ichikawa, Y. (1985) Biochim. Biophys. Acta 827, 268.
11. Tsubaki, M., Srivastava, R.B. and Yu, N.-T. (1982) Biochemistry 21, 1132.
12. Hiwatashi, A., Ichikawa, Y., Maruya, N., Yamano, T. and Aki, K. (1976) Biochemistry 15, 3082.
13. Laemmli, U.K. (1970) Nature 227, 680.
14. Sugiyama, T., Miura, R. and Yamano, T. (1976) in "Iron and Copper Proteins" (Yasunobu, K., Mower, H.F. and Hayaishi, O., eds), p.290, Academic Press, New York.
15. Chashchin, V.L., Vasilevsky, V.I., Shkumatov, V.M. and Akhrem, A.A. (1984) Biochim. Biophys. Acta 787, 27.

16. Kido,T., Arakawa,M. and Kimura,T.(1979) J. Biol. Chem. 254, 8377.
17. Hasumi,H., Yamakura,F., Nakamura,S., Suzuki,K. and Kimura,T.(1984)
Biochim. Biophys. Acta 787, 152.
18. Katagiri,M., Takikawa,O., Sato,H. and Suhara,K.(1977) Biochem.
Biophys. Res. Commun. 77, 804.
19. Hanukoglu,I., Spitesberg,V., Bumpus,J.A., Dus,K.M. and
Jefcoate,C.R. (1981) J. Biol. Chem. 256, 4321.
20. Shimizu,T., Kitagawa,T., Mitani,F., Iizuka,T. and Ishimura,Y.(1981)
Biochim. Biophys. Acta 670, 236.
21. Adar,F., Blum,H., Leigh,J.S.,Jr., Ohnishi,T., Salerno,J.C., and
Kimura,T. (1977) FEBS Lett. 84, 214.
22. Ozaki,Y., Kitagawa,T., Kyogoku,Y., Imai,Y., Hashimoto-Yutsudo,C. and
Sato,R.(1978) Biochemistry 17, 5826.
23. Shimada,H., Iizuka,T., Ueno,R. and Ishimura,Y.(1979) FEBS Lett. 98,
290.
24. Champion,P.M., Gunsalus,I.C. and Wagner,G.C.(1978) J. Am. Chem. Soc.
100, 3743.
25. Sligar,S.G.(1976) Biochemistry 15, 5399.
26. Ristau,O., Rein,H., Janig,G.-R. and Ruckpaul,K.(1978) Biochim.
Biophys. Acta 536, 226.
27. Kido,T., Yamakura,F. and Kimura,T. (1981) Biochim. Biophys. Acta
666, 370.
28. Teraoka,J. and Kitagawa,T.(1980) J. Phys. Chem. 84, 1928.
29. Champion,P.M., Stallard,B.R., Wagner,G.C. and Gunsalus,I.C.(1982)
J. Am. Chem. Soc. 104, 5469.
30. Yu,N.-T., Kerr,E.A., Ward,B. and Chang,C.K.(1983) Biochemistry 22,
4534.

31. Uno, T., Nishimura, Y., Makino, R., Iizuka, T., Ishimura, Y., and Tsuboi, M. (1985) J. Biol. Chem. 260, 2023.
32. Sheets, J.J. and Vickery, L.E. (1982) Proc. Natl. Acad. Sci. USA 79, 5773.
33. Sheets, J.J. and Vickery, L.E. (1983) J. Biol. Chem. 258, 1720.
34. Sheets, J.J. and Vickery, L.E. (1983) J. Biol. Chem. 258, 11446.
35. Kitagawa, T., Abe, M., and Ogoshi, H. (1978) J. Chem. Phys. 69, 4516.
36. Abe, M., Kitagawa, T., and Kyogoku, Y. (1978) J. Chem. Phys. 69, 4526.
37. Carson, S.D., Constantinidis, I., Satterlee, J.D., and Ondrias, M.R. (1985) J. Biol. Chem. 260, 8741.
38. Uno, T., Nishimura, Y., Tsuboi, M., Kita, K., and Anraku, Y. (1985) J. Biol. Chem. 260, 6755.
39. Argade, P.V., Ching, Y.C., and Rousseau, D.L. (1984) Science 225, 329.
40. Kerr, E.A., Yu, N.-T., Bartnicki, D.E., Mizukami, H. (1985) J. Biol. Chem. 260, 8360.

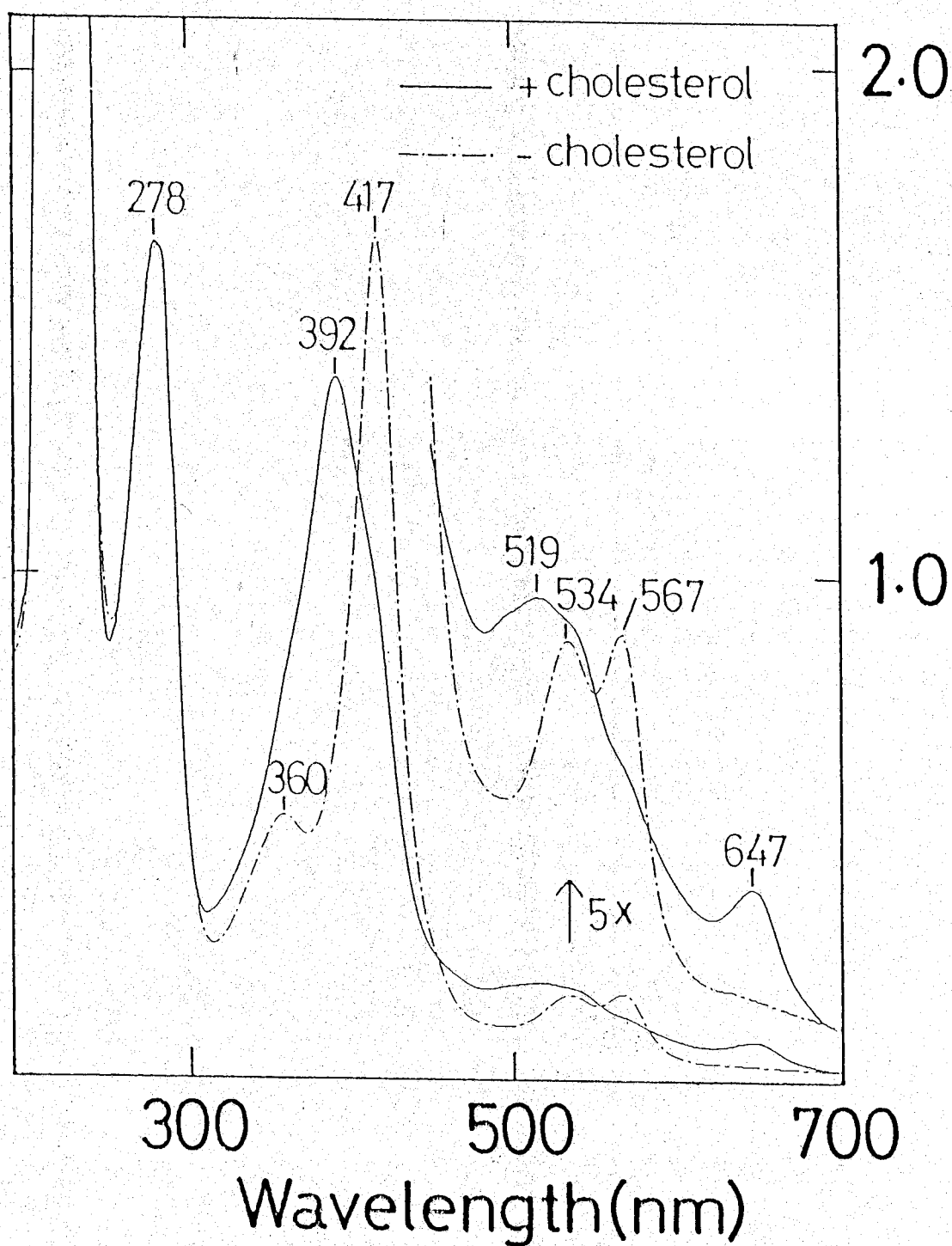


Figure D-1. U.V.-visible absorption spectra of Emulgen 913-depleted cytochrome P-450_{SCC} after adrenodoxin-Sepharose 4B column chromatography. One dotted line, cholesterol-free form; solid line, cholesterol-bound form (28.6 μ M cholesterol). Cytochrome P-450_{SCC} concentration, 12.6 μ M; temperature 10°C.

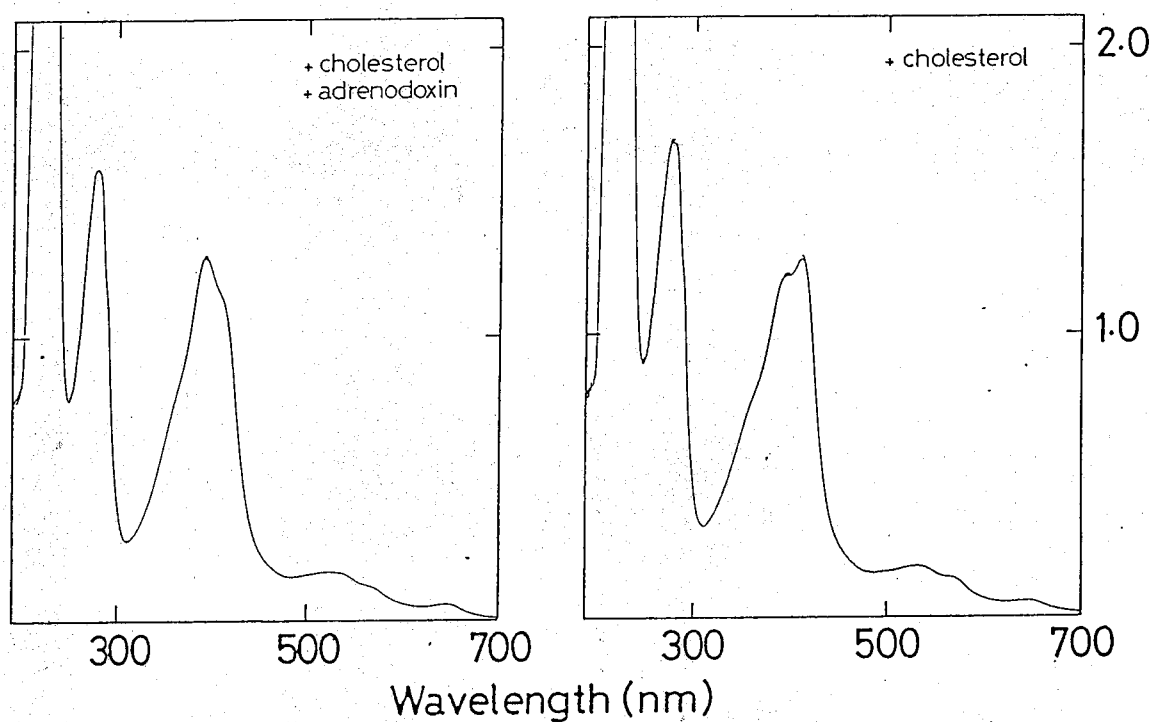


Figure D-2. Effect of cholesterol and adrenodoxin on the ultraviolet-visible absorption spectra of cytochrome P-450_{scc} (Emulgen 913-depleted form). Right panel, cytochrome P-450_{scc} in the presence of cholesterol (28.6 μ M); left panel, cytochrome P-450_{scc} in the presence of both cholesterol and adrenodoxin (2.3 μ M). Temperature, 25°C. Other conditions are the same as in Figure D-1.

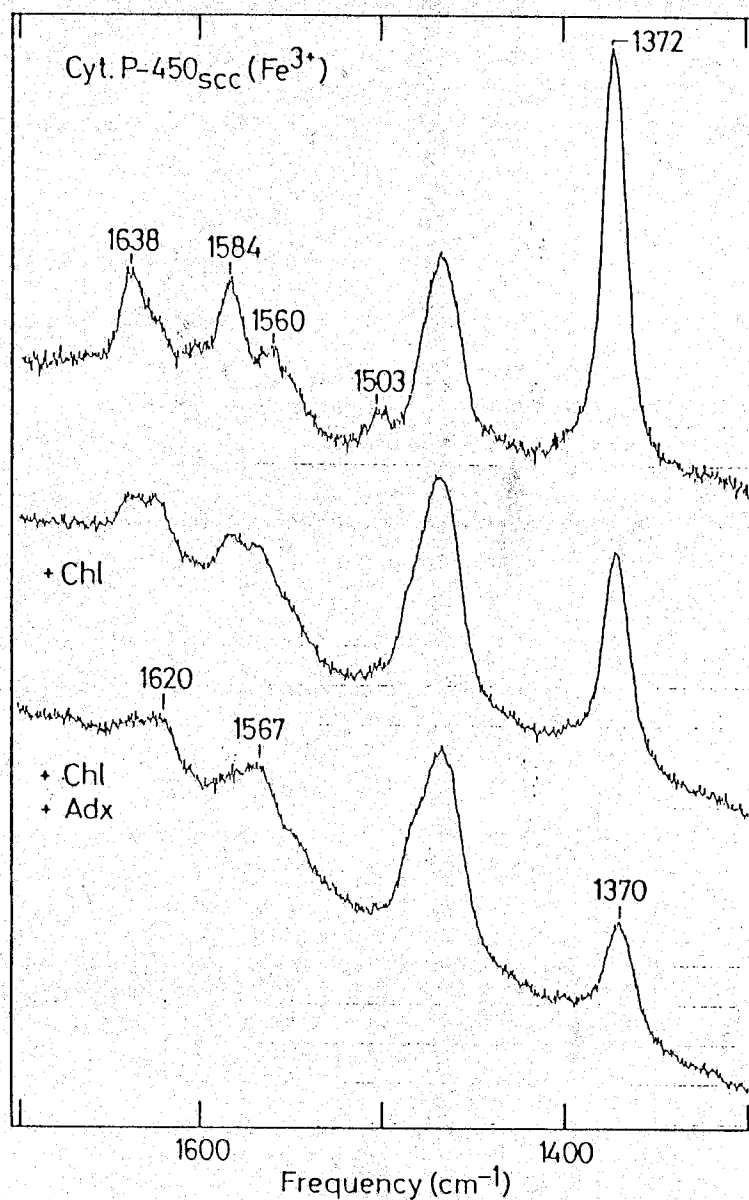


Figure D-3. Effect of cholesterol and adrenodoxin on the higher frequency region resonance Raman spectra of oxidized cytochrome P-450_{scc} in the absence of cholesterol (upper), in the presence of cholesterol (278.1 μM) (middle), and in the presence of both cholesterol (278.1 μM) and adrenodoxin (36.3 μM) (lower). Temperature of sample, 10°C. Cytochrome P-450_{scc} concentration, 47.5 μM ; excitation wavelength, 441.6 nm; laser power, 18 mW at sample point; entrance slit width and height, 250 μm and 12 mm, respectively.

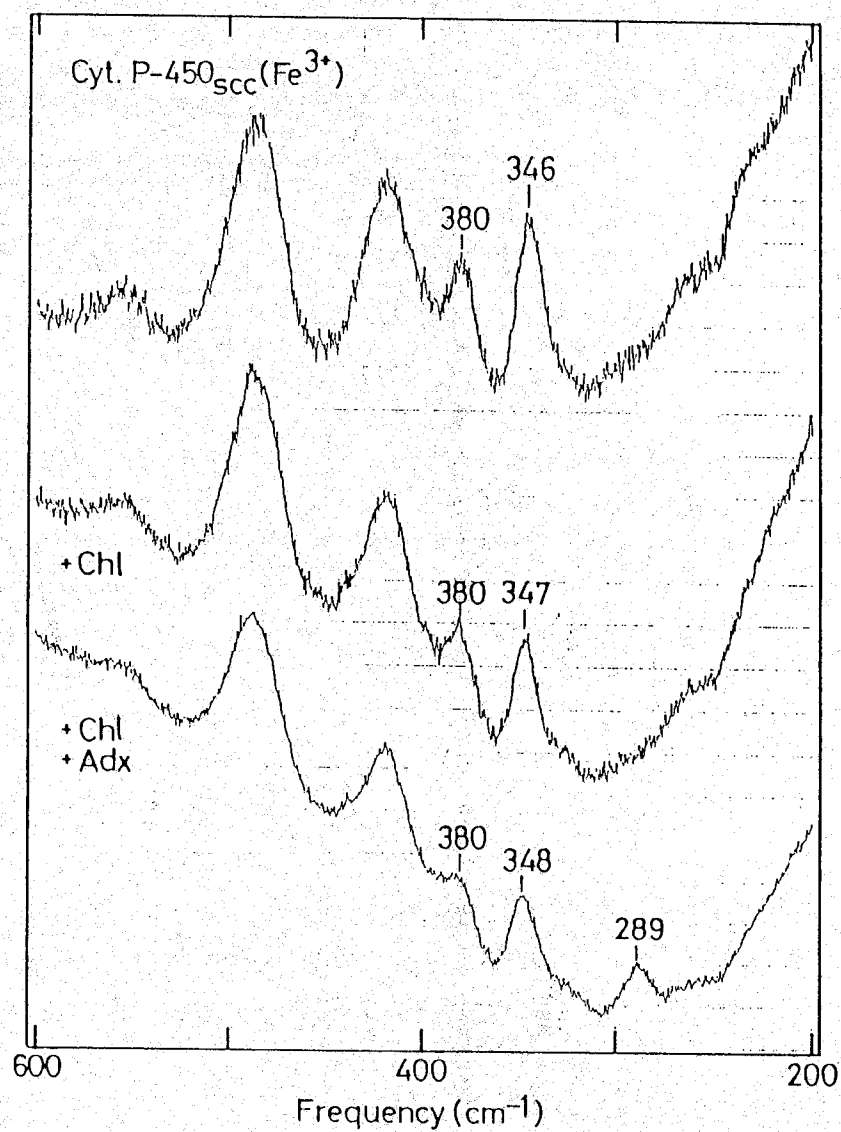


Figure D-4. Effect of cholesterol and adrenodoxin on the lower frequency region resonance Raman spectra of oxidized cytochrome P-450_{scc}. Upper, in the absence of cholesterol; middle, in the presence of cholesterol; lower, in the presence of both cholesterol and adrenodoxin. Other conditions are the same as in Figure D-3.

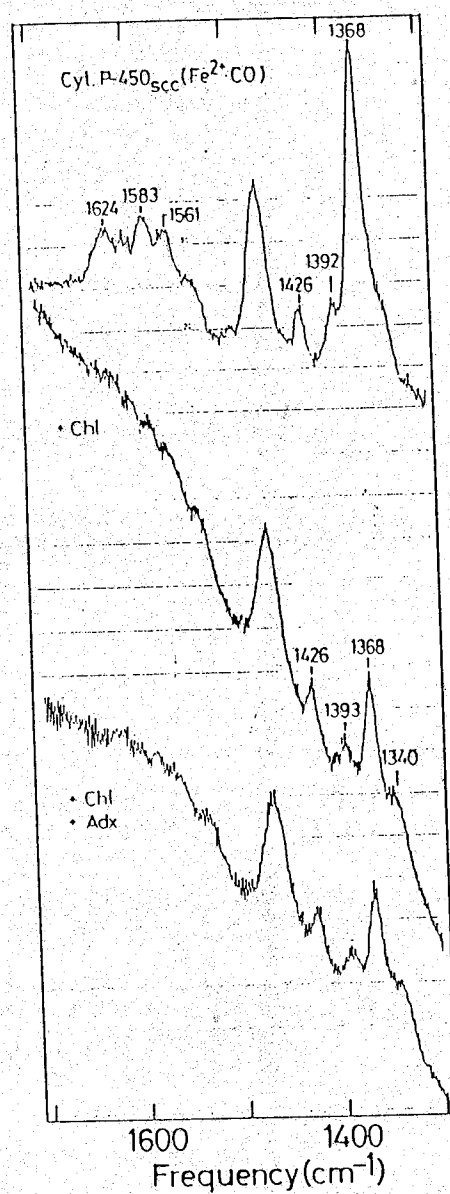


Figure D-5. Effect of cholesterol and adrenodoxin on the higher frequency region spectra of cytochrome P-450_{scc}(Fe²⁺-CO). Upper, in the absence of cholesterol; middle, in the presence of cholesterol; lower, in the presence of both cholesterol and adrenodoxin. Other conditions are the same as in Figure D-3.

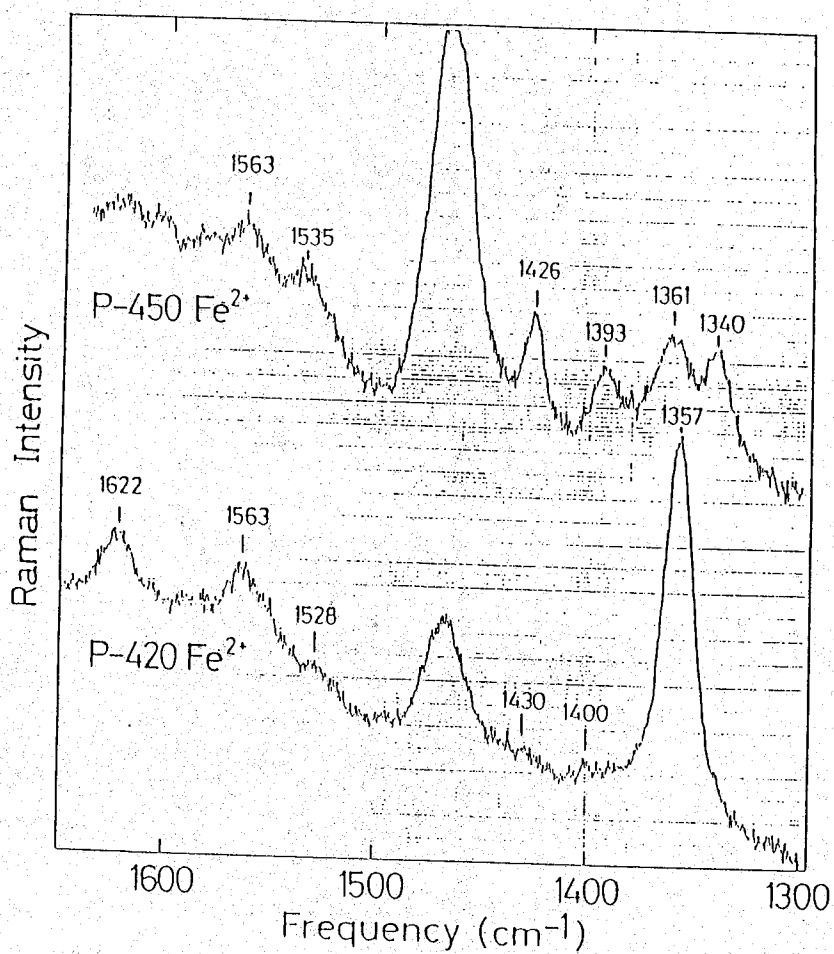


Figure D-6. The resonance Raman spectra of cytochrome P-450_{scc} in the native ("P-450") reduced state (upper spectrum), and in the denatured ("P-420") reduced state (lower spectrum). Both spectra were measured in the absence of cholesterol. Other conditions are the same as in Figure D-3.

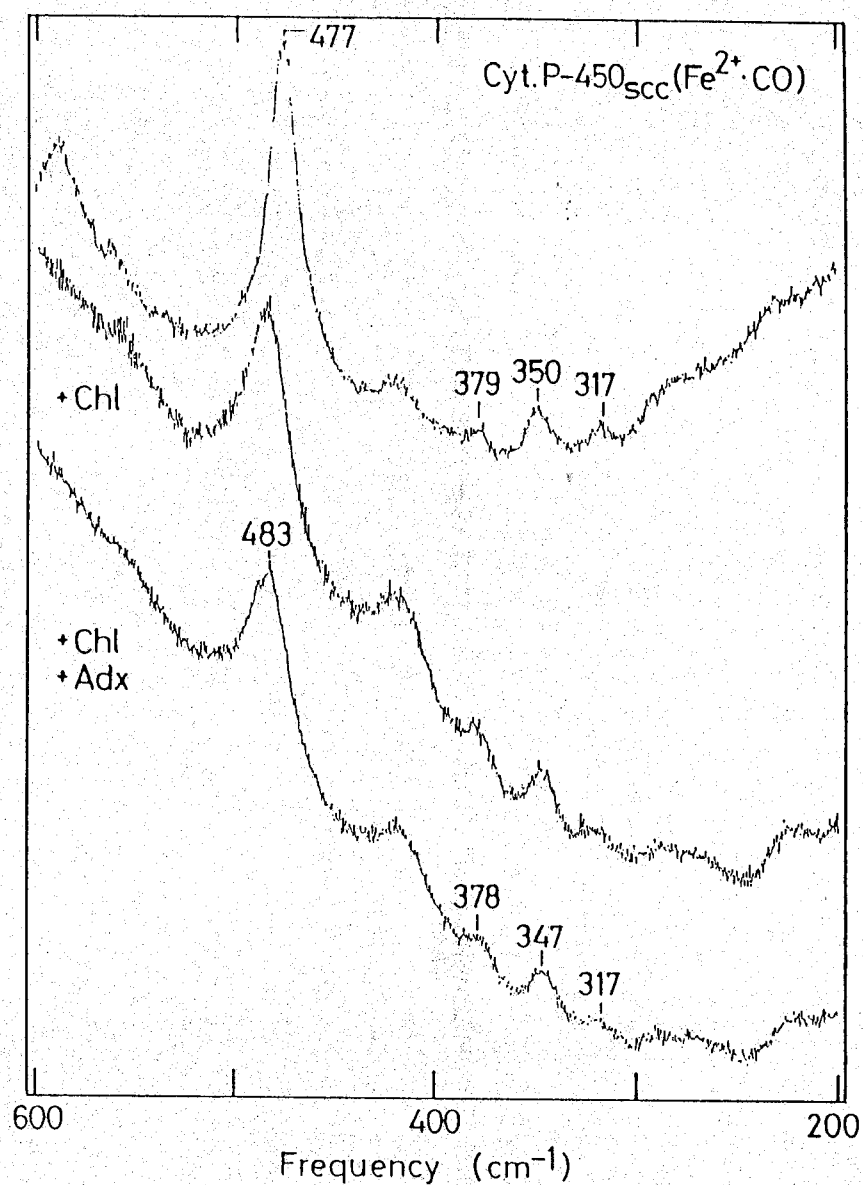


Figure D-7. Effect of cholesterol and adrenodoxin on the lower frequency region Raman spectra of cytochrome P-450_{scc}(Fe²⁺-CO). Upper, in the absence of cholesterol; middle, in the presence of cholesterol; lower, in the presence of both cholesterol and adrenodoxin. Other conditions are the same as in Figure D-3.

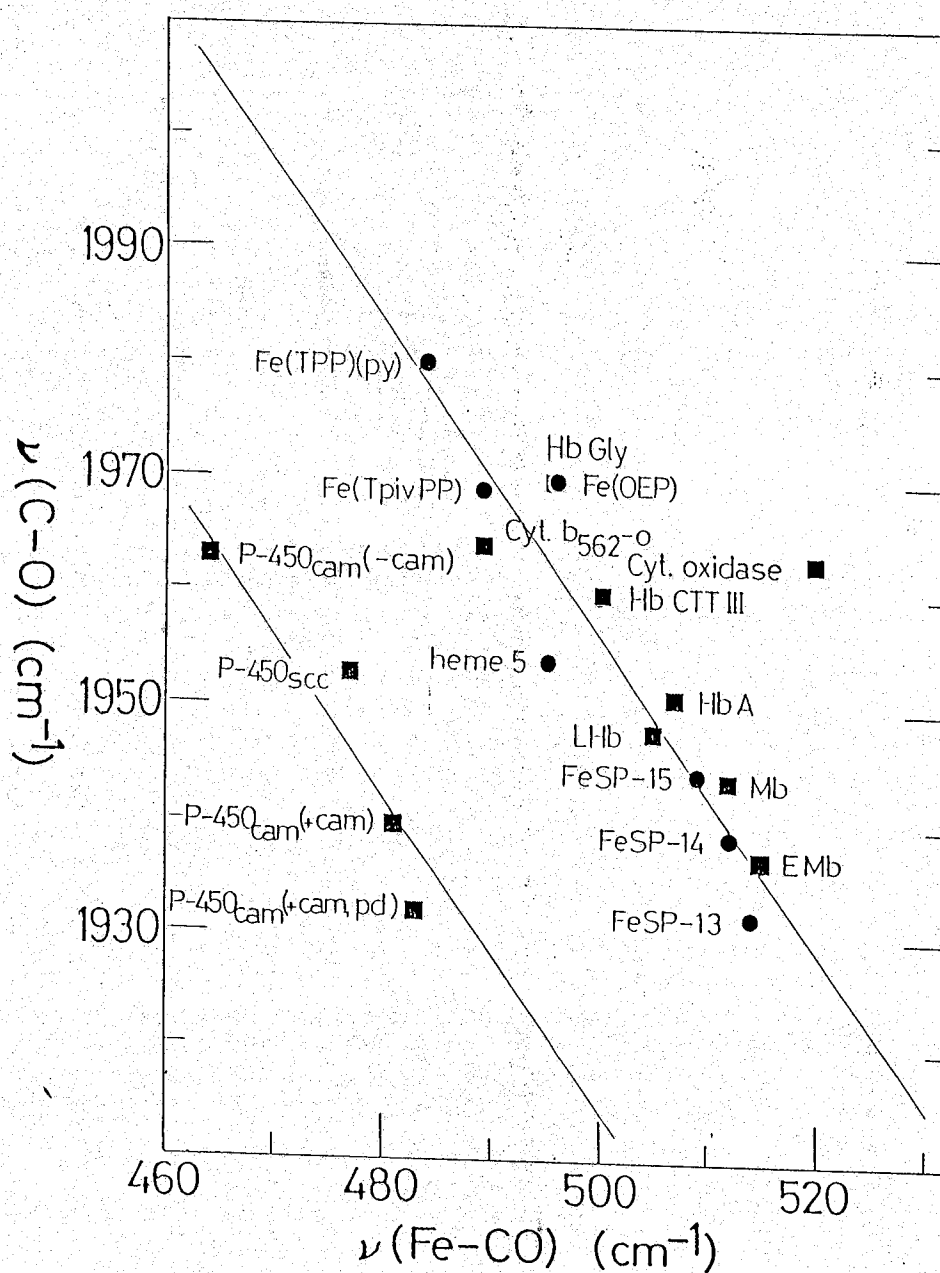


Figure D-8. Fe-CO stretching frequency vs. C-O stretching frequency plots for various ferrous-heme-carbonyl complexes. Solid square (■), data points for native heme proteins: Glycra hemoglobin (Hb Gly), cytochrome b_{562-o} complex (Cyt. b_{562-o}), cytochrome oxidase (Cyt. oxidase), elephant myoglobin (EMb), cytochrome P-450_{cam} (P-450_{cam}); data taken from Carson et al.(37), Uno et al.(38), Argade et al.(39), Kerr et al.(40), Uno et al.(31), respectively. Solid circles (●), data points for various heme model complexes. Other data points were cited previously in Tsubaki & Ichikawa (10).

Conclusions

(1) For the first time, the direct identification of the iron-carbon bond in (carbonmonoxy)hemoglobin (HbCO) and -myoglobin (MbCO) by resonance Raman spectroscopy was made. The Fe-CO stretching, Fe-C-O bending, and bound C-O stretching vibrations have been detected at 507(512), 578(577), and 1951(1944) cm^{-1} , respectively, in human (carbon monoxy)HbA (sperm whale MbCO) upon excitation at 406.7 nm within the Soret band. These assignments were made on the basis of frequency shifts with the isotopes $^{13}\text{C}^{16}\text{O}$, $^{12}\text{C}^{18}\text{O}$, and $^{13}\text{C}^{18}\text{O}$. Calculated isotope shifts according to the model Im-Fe-C-O (but not Im-Fe-O-C) agree well with the observed data. The possible mechanism of resonance Raman enhancement of these vibrations are discussed in terms of the $d\pi(\text{Fe})-\pi^*(\text{CO})$ interaction. Careful examination of the Fe-CO stretching mode at 507 cm^{-1} in both (carbon monoxy) HbA and (carbon monoxy) Hb Kansas with and without inositol hexaphosphate (IHP) reveals no changes in frequency and intensity. This implies that no significant change in the Fe-C bond energy is induced by switching the quaternary structure from the R to T form in ligated (carbon monoxy)Hb Kansas. The absence of bound tension between the iron atom and the proximal histidine is suggested. However, the resonance Raman spectrum of carp (carbon monoxy)Hb exhibits a broadening of the Fe-CO stretching mode on the lower energy side upon R - T conversion with IHP, suggesting the presence of a new conformer (or conformers) with a weaker Fe-CO bond or a somewhat different CO distortion.

(2) Resonance Raman scattering experiments on CO-complexed cytochrome P-450_{scc} from bovine adrenocortical mitochondria demonstrate the simultaneous enhancement of the $\nu(\text{Fe-CO})$ stretching and bound $\nu(\text{C-O})$ stretching frequencies at 477 and 1953 cm^{-1} , respectively. These assignments were made on the basis of frequency shifts with the isotope $^{12}\text{C}^{18}\text{O}$. This unusually low $\nu(\text{Fe-CO})$ stretching frequency in cytochrome P-450_{scc}, compared with other CO-complexed hemoproteins such as CO-hemoglobin and -myoglobin, is presumably due to the thiolate ligation to the heme iron trans to CO and due to the linear and perpendicular configuration of CO binding to the heme.

(3) The effects of cholesterol- and adrenodoxin-binding on resonance Raman spectra of cytochrome P-450_{scc} in both oxidized and CO-reduced states were examined. Upon cholesterol-binding, oxidized cytochrome P-450_{scc} showed a significant shift of spin equilibrium from low spin to high spin state. Addition of adrenodoxin caused a complete conversion of cholesterol-bound oxidized cytochrome P-450_{scc} to a pure high spin state which was considered to be in hexa-coordinated state as judged by the ν_{10} mode at 1620 cm^{-1} and ν_3 mode around 1485 cm^{-1} . Cholesterol in substrate binding site may oppose a linear and perpendicular binding of carbon monoxide to the reduced heme iron leading to the distorted Fe-C-O linkage. This is based on the following observations: (a) increase of the Fe-CO stretching frequency to 483 cm^{-1} from 477 cm^{-1} upon addition of cholesterol; (b) enhanced photodissociability of bound carbon monoxide of CO-complex of cytochrome P-450_{scc} in the presence of cholesterol. As another aspect of the effect of cholesterol on CO-complex form of cytochrome P-450_{scc}, the enhanced stability of native

form ("P-450" form) was observed. There was no additional effect of reduced adrenodoxin on the spectra of CO-reduced form of cytochrome P-450_{scc}.

Acknowledgements

I would like to express my thanks to Drs. Hideki Morimoto, Hiroshi Hori, Gentaro Miyazaki, Kiyoshi Nagai, Teizo Kitagawa for leading me to the exciting world of hemoproteins; Drs. Nai-Teng Yu, Raja B. Srivastava, Helen C. Mackin, Yoshiyuki Ichikawa, Atsuo Hiwatashi, and Akira Miyatake were greatly acknowledged for providing me occasions to begin and continue this study and for many helpful discussions. Dr. Yoshimasa Kyogoku was greatly acknowledged for kindful discussions and suggestions.

Part of this investigation was supported by Grants for Scientific Reserch from Ministry of Education, Science, and Culture, Japan and grants-in-aids from The Shimabara Science Promotion Foundation and The Naito Foundation.

